University of Nebraska - Lincoln

DigitalCommons@University of Nebraska - Lincoln

U.S. Navy Research

U.S. Department of Defense

2012

Review of fracture toughness (G, K, J, CTOD, CTOA) testing and standardization

Xian-Kui Zhu
Battelle Memorial Institute, zhux@battelle.org

James A. Joyce
U.S. Naval Academy, jaj@usna.edu
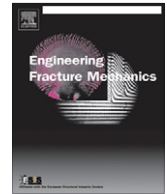
Review of fracture toughness (G, K, J, CTOD, CTOA) testing and standardization

Xian-Kui Zhu [a,*], James A. Joyce [b]

[a] *Battelle Memorial Institute, 505 King Avenue, Columbus, OH 43201, USA*
[b] *Mechanical Engineering Department, US Naval Academy, 590 Holloway Road, Annapolis, MD 21402, USA*

ARTICLE INFO

ABSTRACT

The present paper gives a technical review of fracture toughness testing, evaluation and standardization for metallic materials in terms of the linear elastic fracture mechanics as well as the elastic–plastic fracture mechanics. This includes the early investigations and recent advances of fracture toughness test methods and practices developed by American Society for Testing and Materials (ASTM). The review describes the most important fracture mechanics parameters: the elastic energy release rate G, the stress intensity factor K, the J-integral, the crack-tip opening displacement (CTOD) and the crack-tip opening angle (CTOA) from the basic concept, definition, to experimental estimation, test methods and ASTM standardizing practices. Attention is paid to guidelines on how to choose an appropriate fracture parameter to characterize fracture toughness for the material of interest, and how to measure the fracture toughness value defined either at a critical point or in a resistance curve format using laboratory specimens. The relevant ASTM fracture toughness test standards considered in this paper are E399 for K_{Ic} testing, E561 for $K–R$ curve testing, E813 for J_{Ic} testing, E1152 for $J–R$ curve testing, E1737 for J_{Ic} and $J–R$ curve testing, E1290 for CTOD (δ) testing, a combined common test standard E1820 for measuring the three parameters of K, J and δ, E1921 for the transition reference temperature T_0 testing and the master curve of cleavage toughness K_{Jc} testing, and E2472 for CTOA testing. The effects of loading rate, temperature and crack-tip constraint on fracture toughness as well as fracture instability analysis are also reviewed.

© 2012 Elsevier Ltd. All rights reserved.

1. Introduction

Fracture toughness is usually used as a generic term for measures of material resistance to extension of a crack. It is restricted to results of fracture mechanics tests in this work, which are directly applicable to fracture control and to fracture test in describing the material property for a crack to resist fracture. The experimental measurement and standardization of fracture toughness play an imperative role in application of fracture mechanics methods to structural integrity assessment, damage tolerance design, fitness-for-service evaluation, and residual strength analysis for different engineering components and structures. The fracture toughness values may also serve as a basis in material characterization, performance evaluation, and quality assurance for typical engineering structures, including nuclear pressure vessels and piping, petrochemical vessels and tanks, oil and gas pipelines, and automotive, ship and aircraft structures. Therefore, fracture toughness testing and evaluation has been a very important subject in development of fracture mechanics method and its engineering applications.

* Corresponding author. Tel.: +1 614 424 4387; fax: +1 614 458 4387.
E-mail addresses: zhux@battelle.org (X.-K. Zhu), jaj@usna.edu (J.A. Joyce).

Nomenclature

Latin characters

a	crack length
a_0	original crack length
a_b	blunting corrected crack length
A_2	a constraint parameter used in $J - A_2$ three-term solution
A_{pl}	area under a load–plastic displacement curve
A_{tot}	total area under a load–displacement curve
A_{CMOD}^{pl}, A_{Vpl}	plastic area under load–plastic CMOD curve
A(B)	arc-shaped bending specimen
A(T)	arc-shaped tension specimen
b	crack remaining ligament
b_0	original crack ligament
B	specimen thickness
B_N	specimen net-section thickness
C	specimen load-line compliance
C(T)	compact tension specimen
CTOD	crack-tip opening displacement
CTOA	crack-tip opening angle
CMOD	crack-mouth opening displacement
DC(T)	disk-shaped compact tension specimen
E	Young's modulus
$f_{ij}(\theta)$	angular functions of crack-tip stress field
G	elastic energy release rate
G_c	critical elastic energy release rate
G_{Ic}	plane strain fracture toughness characterized by G
G_R	G-based crack extension resistance
I_n	an integration constant
J	J-integral
J_c	critical J-integral at fracture instability
J_{Ic}	plane strain fracture toughness characterized by J-integral
J_{el}	elastic component of J-integral
J_i	crack initiation toughness characterized by J-integral
J_{pl}	plastic component of J-integral
J_{max}	the maximum J-integral allowable in a valid J–R curve test
J_R	J-based crack extension resistance
J_{Rc}	point-value fracture toughness at fracture instability
K, K_I	stress intensity factor for model-I crack
K_{eff}	effective stress intensity factor
K_{Ic}	plane strain fracture toughness characterized by K-factor
K_{max}	the maximum stress intensity factor
K_Q	conditional fracture toughness at a critical point
K_R	K-based crack extension resistance
K_{Jc}	critical K value converted from J_c or J_{Ic}
K_0	a scale parameter equal to the fracture toughness corresponding to 63.2% failure probability
K_{min}	the lower bound (threshold) fracture toughness
$K_{Jc(1T)}$	the equivalent toughness of the 1 T specimen
$K_{Jc(med)1T}$	an equivalent median toughness for the test specimens other than 1 T size
L	specimen length of middle-cracked panel
LLD	load-line displacement
M	applied bending moment
M(T)	middle-cracked tension panel
m	a conversion factor between J-integral and CTOD or an exponential parameter
n	strain hardening exponent
N	total number of fracture tests
P	applied load
P_{max}	the maximum applied load or force
P_Q	a critical load used to determine the conditional fracture toughness K_Q
P_5	a load determined by the 5% secant method
P_N	normalized load

P_f	cumulative probability of failure
Q	a triaxial stress parameter representing the second term of elastic–plastic crack-tip field
R-curve	crack extension resistance curve
r	radial coordinate in the polar system
r_y	first-order plastic zone size
r_p	second-order plastic zone size or plastic rotation factor
S	beam span of single-edge notched specimen
SE(B)	single-edge notched specimen in three-opine bending
T	T-stress representing the second term of elastic crack-tip stress field or temperature
T_0	a reference temperature
T_{app}	applied tearing modulus
T_i	traction components
T_R	material tearing resistance
U	strain energy
V	total crack-mouth opening displacement (CMOD)
V_{el}	elastic component of CMOD
V_{pl}	plastic component of CMOD
w	strain energy density
W	specimen width

Greek characters

α	geometric parameter or strain hardening parameter
δ	crack-tip opening displacement (CTOD)
δ_5	crack-opening displacement measured at the original crack size location over a gage length of 5 mm
Δ	total load-line displacement (LLD)
Δ_{el}	elastic component of LLD
Δ_{pl}	plastic component of LLD
$\overline{\Delta_{pl}}$	normalized plastic component of LLD
Δa	crack extension equal to $a - a_0$
Δa_{eff}	inferred effective crack extension
Δa_{max}	the maximum crack extension allowable in a valid J–R curve test
Δa_p	measured effective crack extension
η, γ	LLD-based geometric factors
η_{el}	elastic η-factor
η_{pl}	plastic η-facotr
$\eta_{CMOD}, \gamma_{CMOD}$	CMOD-based geometric factors
v	Poisson's ratio
Γ	the integration path around the crack tip
θ	angular coordinate in the polar system
σ_{ij}	stress components
σ_0	a reference stress or the yield stress
σ_{ys}	the 0.2% offset yield stress
σ_Y	effective yield stress equal to the average of yield stress and tensile stress
ε_{ij}	strain components

The stress intensity factor K (or its equivalent partner – the elastic energy release rate G), the J-integral, the crack-tip opening displacement (CTOD), and the crack-tip opening angle (CTOA) are the most important parameters used in fracture mechanics. The K factor was proposed in 1957 by Irwin [1] to describe the intensity of elastic crack-tip fields, and symbolizes the linear elastic fracture mechanics. The J-integral was proposed in 1968 by Rice [2] to characterize the intensity of elastic–plastic crack-tip fields, and symbolizes the elastic–plastic fracture mechanics. The CTOD concept was proposed in 1963 by Wells [3] to serve as an engineering fracture parameter, and can be equivalently used as K or J in practical applications. The CTOA parameter was used in the recent decade to describe fracture behavior of stable crack extension for thin-walled materials. Different experimental methods have been developed for measuring these parameters to describe fracture toughness of materials. The detailed descriptions of these fracture mechanics parameters and their applications can be found in the textbooks of fracture mechanics, such as those by Broek [4], Kanninen and Popelar [5], Hertzberg [6], Anderson [7] and others. The basic fracture mechanics concepts were summarized by Irwin and Dewit [8]. Recently, Erdogan [9] and Cotterell [10] reviewed the history and development of fracture mechanics. Extensive applications of fracture mechanics methods via fracture toughness in structural integrity and assessment were documented in a set of 11-volume comprehensive books compiled by Milne et al. [11]. Standard terminology relating to fracture toughness testing and evaluation has been defined in E1823 [12] by the American Society for Testing and Materials (ASTM) in the United States. All terms and concepts pertaining to fracture tests used in this work are consistent with those defined by ASTM E1823.

The behavior of a metallic material during a fracture toughness test can be described by three aspects: the fracture behavior of the material, the strength and deformation behavior of the material, and the constraint effect of the geometry. Understanding these three aspects can help in the successful conduct of the fracture toughness test. However, in the early days of fracture toughness test method standardization, these three considerations tended to be confused. Thus, care should be taken to distinguish their differences so that the proper fracture parameters and characterization procedures are used in the fracture toughness test for the material of interest. Basically, the fracture behavior relates to the micro-mechanism of fracture, and is usually described as being ductile or brittle. Brittle fracture behavior results in the development of rapid and unstable crack extension and can correspond to micro-ductile void growth fracture or to cleavage fracture. Macroscopically, a test specimen demonstrating this mode of fracture has a unique and well-defined point of crack initiation, corresponding to a sudden drop in load, characterizing fracture failure, and provides a measurement of a point value of fracture toughness.

Due to crack extension by micro ductile void growth and coalescence which tends to absorb more energy, ductile fracture behavior results in slow and stable crack extension. This macro mode of fracture has a continuous process of ductile tearing rather than a point fracture, and requires a crack extension resistance curve, labeled an R-curve, to be measured for characterizing ductile fracture. The R-curve behavior can cause some uncertainty as to where to specify the fracture point since crack extension can occur under increasing load conditions due to material strain hardening. The entire R-curve can be used to describe the ductile fracture. However, many methods that use fracture toughness for structural integrity assessment require a single-point value of toughness. A typical point value of ductile fracture toughness is usually defined near the onset of stable crack tearing and deduced from the R-curve near the transition from initial crack blunting to crack tearing which is usually characterized by a distinct change in slope of the R-curve. This result is referred to as fracture initiation toughness. A typical example is to estimate the ductile fracture toughness as the toughness demonstrated by a deeply cracked bend type specimen at 0.2 mm of crack extension beyond initial crack tip blunting.

The material deformation behavior can be characterized as being linear elastic, nonlinear elastic, or elastic–plastic. In general, the deformation behavior of a material determines which fracture parameter to be used for describing fracture toughness and which fracture test method to be adopted for measuring the toughness value for the material. For brittle fracture, an annular zone of linear elastic deformation surrounds and dominates the crack tip and the initiation toughness dominates the material fracture resistance with only slight additional resistance to crack extension beyond crack initiation. Often the energy required to extend the crack beyond initiation is small in comparison with the energy stored in the test machine, the specimen fails unstably, and no measurement of the fracture resistance beyond initiation is possible. Thus the toughness is often measured as a point value and characterized by the stress intensity factor K or the energy release rate G at crack initiation. The first fracture toughness test standard ASTM E399 [13] was developed to determine the point value of plane strain fracture toughness at or near to the onset of crack initiation, K_{Ic}.

When tougher materials are tested, the tearing resistance to grow the crack a small increment can be significant. In some cases predominantly elastic conditions can continue to exist throughout the test piece, stable crack growth conditions can be maintained, and a K-based R-curve can be developed which includes both crack initiation and crack extension resistance information. ASTM E561 [14] was developed for measuring the K–R curve of relatively tough thin sheet materials, where the measured R-curve is a plot of crack-extension resistance as a function of either stable crack extension, Δa_p (a visually measured physical crack extension) or Δa_e (an inferred effective crack extension).

For ductile fracture, the plastic deformation dominates at the crack tip and the material resistance against fracture increases as the crack grows, and thus the toughness is often described in a resistance curve format using the J-integral or CTOD (δ). The J-integral is a nonlinear elastic quantity rather than being a true plastic quantity and this requires care in its application to elastic–plastic fracture toughness measurement and application. Extensive experimental and computational work has been devoted to demonstrating the applicability of the J-integral as a useful measure of fracture toughness for applications using elastic–plastic metallic materials. A J–R (or δ–R) curve is a plot of resistance to stable crack extension, measured in terms of J (or δ), plotted versus ductile crack extension, usually taken as Δa_p, the measured physical crack extension, though in many cases only estimates of this crack extension are available. ASTM E1820 [15] was developed for measuring the elastic–plastic initiation toughness J_{Ic} and J–R curves or the corresponding δ_{Ic} and δ–R curves in plane strain conditions, whereas ASTM E1290 [16] was developed essentially to evaluate CTOD at the onset of cleavage, δ_c. For thin-walled materials in low constraint conditions, the CTOA parameter is also being used to describe the stable crack extension, and ASTM 2472 [17] was developed for the CTOA testing. For ductile–brittle transition fracture, the toughness demonstrates much greater variability due to the "weakest link" failure mechanism that initiates cleavage in these materials. In some cases the cleavage initiation toughness can be defined in terms of a critical elastic K_c, but other tests at the same temperature likely require the use of the elastic–plastic J-integral to accurately define the cleavage initiation. ASTM E1921 [18] was developed to define the ductile–brittle transition in terms of a master curve and a reference temperature, T_o, obtained from a minimum of six repeat tests determining, for each specimen, first measured as J_c, the J-integral at the onset of cleavage, and subsequently converted to K_{Jc}.

Use of fracture mechanics methods in engineering design and structural analysis requires fracture toughness to serve as a material property that can be transferred from the laboratory test to a structural application. However, the crack-tip constraint caused by thickness, size and configuration of fracture test specimens can have a strong effect on the laboratory measured values of fracture toughness (K, J and δ). In general, high constraint results in higher crack-tip stresses with less crack-tip yielding and promotes a more brittle fracture or reduces the resistance curve toughness for ductile fracture; while low constraint results in lower crack-tip stresses with more crack-tip yielding and tends to reduce the possibility of brittle frac-

ture and to raise the resistance curve toughness for ductile fracture. The thickness constraint is usually specified as being plane stress and/or plane strain, with plane strain fracture toughness being regarded as the lower bound value. In plane strain conditions, the specimen configuration, loading mode and crack depth can cause an in-plane constraint effect on fracture toughness. For example, a deeply cracked bend dominated specimen will demonstrate higher in-plane constraint at the crack tip than that shown by a shallow cracked, tensile specimen. To reduce the effects of specimen configuration and thickness on the measured toughness results, ASTM standards require use bending dominated specimens with a fixed range of crack depth to width ratios, set limits on remaining ligament to thickness ratios, require a minimum size, and in many cases require side grooves along the crack ligament. When side grooves are present and the specimen meets the other ASTM requirements the specimen can be predominantly in plane strain conditions so that the plane strain fracture toughness is measured. However, the transferability problem remains from the laboratory specimen, basically a deep crack bending dominated geometry, to an application which is likely to be shallow cracked, tension loaded, and loaded more slowly or more rapidly than the laboratory sample. In order to obtain conservative, constraint-independent fracture toughness measurements, all ASTM fracture test standards prescribe strict specimen geometry requirements. These are targeted to produce a lower bound of fracture toughness in most cases, though the degree of conservatism is not defined. Conservative specimens, deep cracks, side grooves, conservative evaluation of K, J or CTOD all contribute to conservative results. In addition, the loading rate, temperature, environment, etc., all have effects on fracture toughness measurements and need to be understood in the measurement of and the application of fracture toughness.

Fracture toughness testing has been recognized as the key to provide accurate toughness values needed in the linear elastic fracture mechanics and in the elastic–plastic fracture mechanics. Since the 1950s, extensive analytical, numerical and experimental investigations have been conducted worldwide in technical development of effective test methodology and test techniques for measuring the critical values of the parameters G and K, then J and δ, and more recently CTOA, and for determining the relevant crack growth resistance curves, including K–R curve, J–R curve and δ–R curve. Different experimental techniques and test procedures for measuring these fracture parameters were developed and maintained by ASTM in the United States, and significant progresses have been achieved over the years. Heyer [19] presented an early literature review of K-based fracture test approaches developed by ASTM before 1973. In the 1987 edition of ASTM retrospective publication series, Barsom [20] collected the early classic papers on fracture analysis and testing from 1913 to 1965 that laid the technical foundation and presented a historic progress in the field of fracture mechanics. In an ASTM manual published in 1996, Joyce [21] gave a brief review of fracture toughness test methods and experimental techniques for the critical J-integral and J–R curve testing. In 2000, Landes [22] presented an interesting historical review of the development of J-based elastic–plastic fracture mechanics and experimental testing that involved events, places, people in addition to the important concepts and methods developed by ASTM. Recently, Landes [23] offered a general review of fracture toughness testing and estimation, Schwalbe et al. [24] presented an updating review of classic fracture mechanics methods involving fracture test techniques and experimental analysis, and Zhu [25,26] reviewed the state-of-the-arts advances of J-integral resistance curve testing and evaluation. However, a systematic review of fracture toughness test methods and standardization developed by ASTM for all parameters of G, K, J, δ, and CTOA is not available, and such work is definitely beneficial to the community of fracture mechanics and engineering applications. Note that in this review the standardization is central to ASTM fracture toughness test standards, and there are not many discussions on the standards developed by other organizations, such as the International Organization for Standardization (ISO), the British Standard Institution (BSI), the European Society of Structural Integrity (ESIS) and the Japanese Standard Association (JSA). All international fracture test standards were primarily developed from the lead of ASTM standards, as discussed by Landes [23] and Schwalbe et al. [24].

This paper reviews the historical investigation and state-of-the-art development of fracture toughness testing, evaluation and standardization for structural metallic materials in terms of the linear elastic fracture mechanics and the elastic–plastic
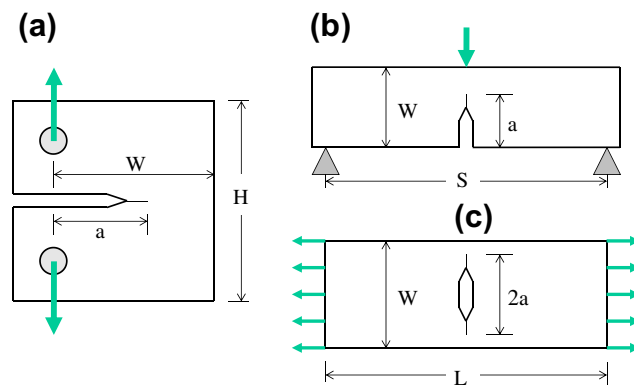
Fig. 1. The conventional fracture test specimens. (a) Compact tension (C(T)) specimen, (b) single edge-notched bend specimen (SE(B)) in three-point bending, and (c) middle-cracked tension (M(T)) specimen.

fracture mechanics. Particular attention is paid to the practices of fracture toughness test methods developed by ASTM for measuring the fracture mechanics parameters of the stress intensity factor K (or the elastic energy release rate G), the J-integral, the crack-tip opening displacement and the crack-tip opening angle. The effects of loading rate, temperature and crack-tip constraint on fracture toughness measurements as well as fracture instability analysis are also reviewed. Six types of conventional fracture test specimens are permitted in ASTM fracture test standards, but no single standard allows all six configurations. These include compact tension (C(T)) specimen, single edge-notched bend (SE(B)) specimen in three-point bending, middle-cracked tension (M(T)) panel, disk-shaped compact tension (DC(T)) specimen, arc-shaped tension (A(T)) specimen and arc-shaped bend (A(B)) specimen. This paper focuses on the mostly often used C(T), SE(B) and M(T) specimens containing a through-thickness tensile crack, i.e., mode-I crack, as illustrated in Fig. 1. In this figure, W is the specimen width, B is the specimen thickness, H is the height of C(T) specimen, S is the span of SE(B) specimen, L is the length of M(T) specimen, a is the crack length of the two bending specimens and $2a$ is the crack length of the tensile specimen. In most cases, $W = 2B$, $H = 1.2W$, $S = 4W$, $L \geqslant 3W$ and $a/W \approx 0.5$. However, different specimen size requirements are prescribed in different fracture test standards in order to obtain valid fracture toughness and to limit the effects of crack-tip constraint on that fracture toughness parameter.

2. K-based fracture testing

2.1. K-factor concept and elastic crack-tip field

For a through-thickness mode-I crack of length $2a$ in an infinite plate subjected to a remote tensile stress σ, Irwin [1] at the US Naval Research Laboratory and Williams [27] at the California Institute of Technology independently obtained the asymptotic crack-tip stress field with the same leading term:

$$\sigma_{ij} = \frac{K_I}{\sqrt{2\pi r}} f_{ij}(\theta) \tag{1}$$

where the subscripts i, j denote the rectangular coordinates x and y or the polar coordinates r and θ with the origin at the crack tip, $f_{ij}(\theta)$ are the angular stress functions, and $K_I = \sigma\sqrt{\pi a}$. While Irwin's solution is the leading term, Williams' solution is a series expansion that includes the leading term as Eq. (1) and other higher-order terms. The second term was later denoted as a "T-stress", and the T-stress has been used to quantify the fracture constraint effect, as detailed in Section 6. Eq. (1) indicates that the elastic crack-tip field is singular because the stresses become infinite as $r \to 0$. The parameter K_I describes the intensity of stress singularity at the crack tip, and thus is called as "stress intensity factor" for the mode-I crack. In reality, infinite stresses do not exist, and plastic deformation generated at the crack tip keeps the stresses finite. For plane stress mode-I cracks, Irwin and co-workers [28,29] obtained a first-order estimate of the plastic zone size r_y ahead of the crack tip as:

$$r_y = \frac{1}{2\pi} \left(\frac{K_I}{\sigma_{ys}} \right)^2 \tag{2}$$

where σ_{ys} is the 0.2% offset yield stress. Eq. (2) is strictly correct only for perfectly elastic materials. If plastic yielding and the resulting stress redistribution at the crack tip are allowed, the plastic zone would be larger, and a second-order estimate of the plastic zone size r_p can be as twice as the first-order estimate of the plastic zone size, i.e., $r_p = 2r_y$. A similar result to r_p was obtained by Dugdale [30] using a strip-yield model.

If two differently configured and loaded cracks in an elastic material have the same K_I, then it follows from Eqs. (1) and (2) that both the leading stress field and the plastic zone size at their crack tips are the same. As such, the stress intensity factor K_I is a unique measure of stresses and strains at the elastic crack tip. When the stresses or strains at its tip reach a critical value, a crack may grow. This means that one can expect fracture to occur when K_I reaches a critical value, K_{Ic}, i.e., $K_I = K_{Ic}$. In this elastic fracture criterion, K_{Ic} is a material parameter known as fracture toughness to describe the resistance of the material against fracture.

Using the elastic crack-tip solution and the energy theory of Griffith [31], Irwin [1] established a simple relationship between the factor K_I and the elastic energy release rate G as:

$$\frac{K_I^2}{E'} = G \tag{3}$$

where $E' = E$ for plane stress conditions, and $E' = E/(1 - v^2)$ for plane strain conditions with E being Young's modulus and v Poisson's ratio. Note that Eq. (3) was obtained from, and thus is strictly valid for a through crack in an infinite plate in tension. As a result, the Griffith energy criterion, i.e. $G = G_c$, is equivalent to the K-based stress criterion for an elastic crack, and the two material resistance parameters G_c and K_{Ic} are related by Eq. (3). Because of its dual roles in describing the crack-tip conditions and in measuring fracture resistance, K has become a notable parameter of elastic fracture mechanics. Owing to his many theoretical and experimental contributions to fracture mechanics, Dr. George Irwin is called the father of fracture mechanics [22].
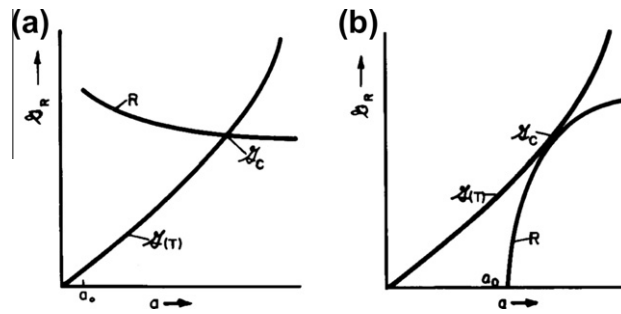
Fig. 2. The early definition of fracture resistance R of materials. (a) The 1954 concept proposed by Irwin and Kies [39], (b) the 1960 concept proposed by Irwin [40].

Many analytical and computational solutions for stress intensity factors have been developed for a variety of geometry and loading configurations and the K solutions are compiled in the stress intensity factor handbooks of Tada et al. [32], Murakami [33], and Rooke and Cartwright [34]. Presently, most commercial finite element analysis software has the capacity to numerically calculate the K factor for any adequately modeled crack. In parallel, extensive experimental investigations were conducted to measure the fracture toughness K_{Ic} for a wide range of materials, which are reported, for instance in Ref. [35].

2.2. Early fracture testing

Early fracture testing and analysis was based on the energy approach that described the occurrence of fracture when the energy available for crack growth is sufficient to overcome the resistance of the material. Griffith [31] at the British Royal Aircraft Establishment was the first to propose the fundamental energy theory for brittle materials like glass, where the resistance was assumed to come exclusively from the surface formation energy of the material. For metallic materials, plastic deformation generated at the crack tip absorbs much more applied energy than the surface energy, and thus Griffith's energy theory underestimates severely the fracture strength of metals. Irwin [36] and Orowan [37] modified Griffith's theory by including the local plastic dissipation energy for its application to metals. Irwin [38] further modified this theory using the energy release rate G as a measure of the energy available for an increment of crack extension. On these bases, Irwin [1] obtained the simple relationship of Eq. (3) between G and K for the infinite plate in tension. This relationship is significant to connect the global energy concept of Griffith to a more readily calculable crack-tip parameter. Because of the leading roles they played in its development, the linear elastic fracture mechanics is often known as Griffith–Irwin theory.

The concept of fracture resistance was first introduced by Irwin and Kies [39] using the energy approach. As illustrated in Fig. 2a, the 1954 concept regards the fracture resistance R of the material as a constant or slightly decreasing value, when plotted against the crack length, whereas the driving force G was an increasing function of crack length. Fracture instability was defined by a critical value G_c at the intersection of these two curves. However, experimental data showed that wider specimens produced higher values of G_c. Irwin [40] noticed the increase of fracture resistance and introduced a rising crack growth resistance curve (R-curve) that resulted from the plastic zone growth as the crack extended. This concept was mentioned in the first report of the ASTM Special Committee on Fracture Testing in January 1960 [41]. As illustrated in Fig. 2b, the 1960 concept defines fracture instability by the critical G_c at the tangency of the R-curve and the driving force G-curve. This fracture instability condition can be expressed as:

$$\begin{cases} G = R \\ \frac{dG}{da} = \frac{dR}{da} \end{cases} \tag{4}$$

Since the G-curve is geometry dependent, the tangent point G_c obtained from Eq. (4) is geometry dependent and increases with increase in specimen width. Based on these energy concepts, Krafft et al. [42] at the US Naval Research Laboratory gave the most extensive discussions on the growth of resistance to crack extension during a test. With a hypothesis that for a given material and thickness there was a unique relationship between the amount of crack growth and the applied stress intensity factor, they determined the earliest R-curves using a set of center-cracked thin plates for 7075-T6 aluminum alloy in terms of G (calculated from $G = \pi\sigma^2 a/E$) and absolute crack extension Δa, as shown in Fig. 3. These results showed that the R-curves were nearly independent of the initial crack length, but G_c was apparently dependent on the initial crack length. The R-curve concept has been thus accepted to describe the resistance increase with crack length rather than remaining constant or decreasing as previously supposed.

For a given material, experimental analysis showed that both the appearance of the facture surface and the critical energy release rate G_c depend on specimen thickness, as shown in Fig. 4 with data obtained by Irwin et al. [28] for a 7075-T6 aluminum alloy. From this figure, it is observed that G_c decreases with increasing thickness and reaches a lower bound value denoted by G_{Ic} for large thickness where plane strain deformation prevails. On the other hand, the percentage square (or flat) fracture indicates that the appearance of crack surface changed from slant or V-slant to fully flat as the thickness increases
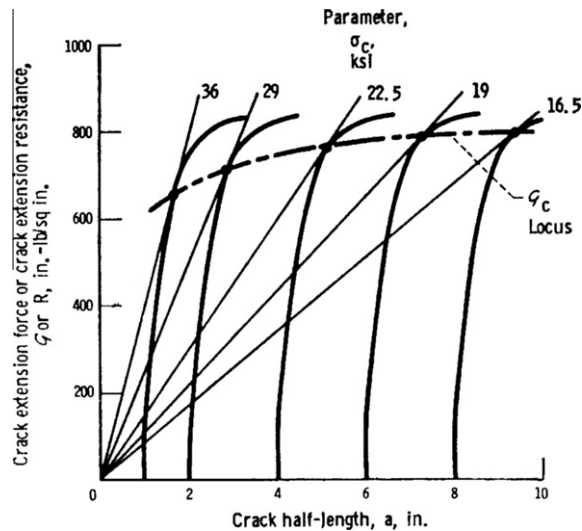
Fig. 3. The earliest crack extension resistance curves obtained by Krafft et al. [42] for 7075-T6 aluminum alloy.
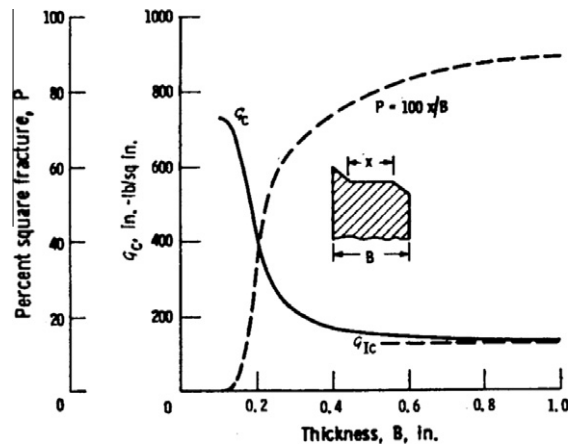

Fig. 4. Variations of the critical energy release rate G_c and the fracture surface appearance with the specimen thickness, obtained by Irwin et al. [28] for 7075-T6 aluminum alloy.

from thin to thick. The characteristics are qualitatively typical of many high strength structural metals, and the change of fracture behavior from thin to thick sections are regarded as those from plane stress to plane strain conditions. The quantitative aspects, such as the peak value of G_c, the lower bound value G_{Ic}, the thickness at which G_c is greatest, and the range of thickness over which the major part of the fracture mode transition occurs, are all dependent on the material and the test temperature. Detailed discussions were given by Srawley and Brown [43] on the R-curve characteristics in terms of G, including the effect of specimen geometry and plastic zone size on G_c at fracture instability. They also described experimental methods and techniques for testing G_c and G–R curves with use of different fracture specimens, including the center-cracked plate, double edge-cracked plate, single edge-notched plate in tension, three-point bend specimen, four-point bend specimen, surface-cracked plate, and circumferentially notched round bar.

In the 1960s, R-curves were developed first in terms of the energy release rate G, and later the stress intensity factor K was often used. Basically, a K–R curve is equivalent to a G–R curve for an elastic material due to Eq. (3). The thickness dependence of the critical K_c was observed to be similar to the critical G_c, as shown in Fig. 4. This means that with increase in thickness from thin to thick, the apparent fracture toughness K_c decreases until a lower bound value K_{Ic} is reached at the large thickness where plane strain deformation predominates. Thus K_{Ic} is called "*plane strain fracture toughness*" for the mode-I crack, representing the minimum value of fracture toughness of the material. In general, it was postulated that plane stress fracture occurred in thin sections, and plane strain fracture occurred in thick sections. Extensive test programs were then undertaken in attempt to develop experimental procedures and test methods for measuring fracture toughness in high strength materials for both plane stress and plane strain crack problems [43,44].

2.3. K_{Ic} testing and ASTM E399 development

As defined in ASTM E1823, the plane strain fracture toughness, K_{Ic}, is the crack-extension resistance under conditions of crack-tip plane strain in mode I for slow rates of loading under predominantly linear-elastic conditions and negligible plastic-zone adjustment. K_{Ic} provides for the measurement of crack-extension resistance at the onset (2% or less) of crack extension. This section discusses the K_{Ic} test standard ASTM E399 and its development history.

The test procedures for measuring fracture toughness of materials have been developed and standardized by the American Society for Testing and Materials (ASTM) in the United States. In 1958, a special ASTM Technical Committee E24 on Fracture Testing of Metals was established for the purpose to develop and write test methods for determination of fracture properties. Kaufman [44] reviewed the progress of the committee effort over the early 10 years. Note that ASTM Technical Committees E09 on fatigue and E24 on fracture merged 25 years later in 1993 as the present ASTM Technical Committee E08 on Fatigue and Fracture Mechanics.

Much of the early fracture toughness testing was directed at relatively thin sections and the procedures prescribed in the first and second ASTM E24 committee reports [45,46] dealt almost entirely with thin-section problems. It was indicated that thickness-dependent apparent toughness K_c might not be a single-value property, and thickness-independent plane strain toughness K_{Ic} might be a more fundamental property of materials. Thus the committee effort shifted from the thin-section problem to concentration on the thick-section problem to develop test methods for determining K_{Ic}. It was anticipated that once the plane strain problem was solved, attention would return to the thin-section (or plane stress) problem.

When a material behaves in a linear elastic manner prior to failure, the plastic zone at the crack tip can be very small compared to the specimen size, and brittle fracture behavior results even with ductile micromechanisms predominating on the fracture surface. In this case, the critical K_{Ic} is an appropriate fracture parameter. Srawley and Brown [43,47] at the NASA Lewis Research Center in Cleveland contributed much to establish a standard for the K_{Ic} testing, including the details of specimen design, specimen size requirement, fatigue precracking, specimen fixturing, load transducer, crack opening displacement gage, test procedure, data instrumentation, K calibration and calculation method. On these bases, the ASTM Technical Committee E24 proposed a draft of test method for plane strain fracture toughness K_{Ic} testing in 1966 [47], and then standardized it tentatively with designation E399–70T. This tentative standard was published in ASTM STP 463 in 1970 [48], and officially balloted into a standard in 1972. Thus, it took about 10 years to establish the first ASTM fracture test standard, E399–72, that became the model for all subsequent ASTM fracture test standards and all international standards for fracture testing. Since ASTM requires updating and improving its test methods periodically, this standard has undergone a number of revisions over the years though the key provisions have remained largely unchanged to the present version, ASTM E399–09e2 [13].

The recommended specimens for the plane strain fracture toughness K_{Ic} testing are the three-point bend SE(B) specimen, compact C(T) specimen, disk-shaped compact DC(T) specimen, arc-shaped tension A(T) specimen and arc-shaped bend A(B) specimen. The frequently used specimens are the first two: SE(B) and C(T). Fatigue precracking is required for producing a sharp crack for all specimens. The initial crack size a_0 (i.e., total size of crack starter notch plus the fatigue crack) allowed in ASTM E399 is between 0.45 W and 0.55 W. When a precracked specimen is tested according to E399, load and crack opening displacement are required recording. Fig. 5 shows three typical types of load–displacement curves with the critical load P_Q defined for each type curve. A 5% secant method was proposed to determine P_Q and then K_{Ic} with an intention to define the K_{Ic} at the 2% or less crack extension. In the 5% secant method [41], the 5% secant line with a slope equal to 95% of the initial elastic loading slope of the tangent line is constructed to determine P_5. For the Type I case, where the load–displacement curve is smooth and deviates only slightly from linearity before reaching the maximum load (P_{max}), $P_Q = P_5$. The nonlinearity can be caused by plasticity, subcritical crack growth or both. For the Type II case, where a small amount of unstable crack growth (i.e., a pop-in) initiates before the applied load reaches P_5 and continues beyond the 5% secant line, P_Q takes the load value at the pop-in initiation (note that if the pop-in is so small the jump does not cross the 5% secant line, it is ignored). For the Type III case, where a specimen fails completely before achieving 5% nonlinearity, $P_Q = P_{max}$. From the P_Q value and the measured crack length for each test, conditional fracture toughness K_Q is calculated using the equation:
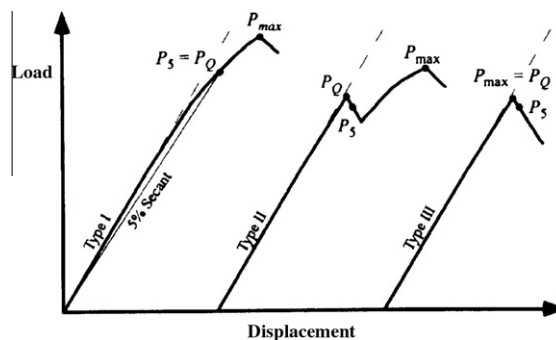

Fig. 5. Three typical types of load–displacement curves with the critical load P_Q defined for each type.

$$K_Q = \frac{P_Q}{B\sqrt{W}f(a/W)} \tag{5}$$

where $f(a/W)$ is a geometry function that depends on the crack size to specimen width ratio a/W only. For SE(B) specimens,

$$f\left(\frac{a}{W}\right) = \frac{3\frac{S}{W}\sqrt{\frac{a}{W}}}{2\left(1+2\frac{a}{W}\right)\left(1-\frac{a}{W}\right)^{3/2}}\left[1.99 - \frac{a}{W}\left(1-\frac{a}{W}\right)\left\{2.15 - 3.93\left(\frac{a}{W}\right) + 2.7\left(\frac{a}{W}\right)^2\right\}\right] \tag{6}$$

and for C(T) specimens,

$$f\left(\frac{a}{W}\right) = \frac{\left(2+\frac{a}{W}\right)}{\left(1-\frac{a}{W}\right)^{3/2}}\left[0.886 + 4.64\left(\frac{a}{W}\right) - 13.32\left(\frac{a}{W}\right)^2 + 14.72\left(\frac{a}{W}\right)^3 - 5.60\left(\frac{a}{W}\right)^4\right] \tag{7}$$

Eqs. (6) and (7) are adopted by ASTM E399. Further analyses of these geometry functions were given by Newman [49] and Srawley [50] for the C(T) specimen and by Freese and Baratta [51] for the SE(B) specimen.

Since the apparent toughness K_c decreases with increasing specimen size until a plateau is reached, specimen size requirements are imposed in ASTM E399 with an intention to ensure that a K_{Ic} measurement corresponds to the lower bound at the plane strain plateau. In addition to the initial crack size requirement of $0.45 \leqslant a_0/W \leqslant 0.55$, the following two validity requirements proposed by Brown and Srawley [47] and Srawley et al. [52] must be met so that the conditional toughness K_Q value calculated from Eq. (5) is a valid K_{Ic} result:

$$B, a \geqslant 2.5\left(\frac{K_Q}{\sigma_{ys}}\right)^2 \tag{8a}$$

$$P_{\max} \leqslant 1.1 P_Q \tag{8b}$$

Eqs. (5)–(8) are adopted in the present ASTM E399–09e2, except to accommodate side grooves the thickness B in Eq. (5) is replaced by $\sqrt{BB_N}$, where B_N denotes the net specimen thickness for side-grooved alternative specimens.

A large test program was often required to arrive at useful criteria to guarantee a consistent outcome of the test standard. The K_{Ic} test method in ASTM E399 has been evaluated in several inter-laboratory round-robin studies. Selected high strength alloys were tested using standard three-point bend SE(B) specimens [53], compact C(T) specimens [54] and Arc- (or C-) shaped A (T) specimens [55].

The combination of the 95% secant offset procedure and strict limits on specimen size and geometry is an attempt by the authors of E399 to obtain a P_Q value and hence K_{Ic} close to the point of crack initiation or a 2% crack extension, without measuring the crack initiation point directly. This procedure is effective for the Type II or Type III behaviors, but is strongly specimen size dependent in the Type I case, or if the Type I behavior transitions to Type II or III behavior as the specimen size is increased. More consistent results of initiation toughness are obtained using ASTM E1820 procedures, as described later in this review, in which a direct measurement is made at the point of crack initiation.

The size requirements in Eq. (8a) make it difficult to measure K_{Ic}, since, as shown by Anderson [7], the material must be relatively brittle or the test specimen must be very large with the specimen width W exceeding 1 m for the 95% secant offset procedure in E399 to accurately estimate the load at crack initiation. The second requirement, Eq. (8b) is an attempt to assure that the nonlinearity observed in the load–displacement record relates to crack initiation and not just to the growth of a large plastic zone or plastic hinge across the specimen ligament. However, this load requirement mostly invalidates good experimental results. Recently, Wallin [56] has outlined a proposed framework for improving the ASTM E399 test method, and suggested determining K_Q at a fixed amount of crack growth like 0.5 mm or 2% ligament of the 1T size to eliminate the size effect. In this case, the restriction on the load ratio in Eq. (8b) would no longer be necessary. If so, the users can use the unloading compliance method to obtain the value of K_Q at the 2% crack extension, and many tests determined to be "invalid" by the criteria in Eq. (8) would be valid. In addition, Joyce and Smudz [57,58] demonstrated that the J-integral specimens (to be discussed in Section 3) can be used to evaluate K near crack initiation (denoted K_{Jc}) in an accurate and size insensitive fashion, and thus a recent ASTM standard E1820–11 [15] provides an alternative test method that permits valid fracture toughness estimates from invalid K_{Ic} tests.

The plane strain fracture toughness of certain metallic materials may be sensitive to loading rate, and a decreased toughness may be noted as loading rate increases. To obtain a conservative toughness value, a plane strain facture toughness test should consider the loading rate effect. Irwin [59,60] and Madison and Irwin [61] conducted a series of dynamic fracture tests and developed basic concepts for dynamic K_c testing at different loading rates. On this basis, Shoemaker and Seeley [62] developed a test procedure for rapid load, plane strain facture toughness testing in a round-robin study. Their recommendations served as a guideline that was added to Annex A10 of ASTM E399–84 and all later versions to provide special requirements and test method for determining rapid load, plane strain fracture toughness $K_{Ic}(t)$ at loading rate exceeding those for conventional or quasi-static testing (that is, rates exceeding 2.65 MPa$\sqrt{m}$/s). If the static analysis equations of E399 are used, the time to P_Q should not be less than 1 ms, and thus ASTM E399 does not apply to impact or quasi-impact testing.

2.4. K–R curve testing and ASTM E561 development

After a substantial amount of progress was made on the K_{Ic} testing of thick-section test geometries, the attention was refocused in the 1970s on the K_c testing for thin-sections where plane stress prevails. Feddersen [63] showed that the apparent toughness K_c at fracture instability can accurately predict the residual strength of center-cracked panels in tension for different materials. However, the point-value toughness K_c method is not applicable when slow stable crack growth occurs, an essential plane stress behavior of structural metals. Experiments indicated that the stable crack growth frequently resulted in a rising resistance curve (R-curve) for thin-section materials that can serve as a fracture property to describe the stable crack growth.

To measure R-curves for the thin-section material, fracture test method was developed using large in-plane specimens with highly confined plastic deformation. A favorite specimen in early R-curve testing was the center-cracked wide panel or large middle-cracked tension specimen, as used by Feddersen et al. [64] and Orange et al. [65]. In the aerospace industry, full-section fracture tests are conducted by use of large wide panels with a specimen width of up to 2 m for aluminum alloys typical of airframe materials in order to determine valid K–R curves [66]. An early literature review of K-based resistance curve test methods that were developed before 1973 was presented by Heyer [19]. To obtain a valid K–R curve, an effective crack length concept was introduced to approximately account for plastic deformation. The effective crack length was defined as that obtained by adding the Irwin plastic zone size to the physical crack length [67], or inferred from a compliance procedure [68]. Various experiments [67–74] showed that for a specific material, R-curves obtained using different specimen geometries were similar. Thus, the R-curve was regarded as a material property, independent of in-plane specimen size and specimen type. Observed effects were dependent on the specimen thickness and test temperature. In-plane geometry independence of resistance curves was later verified by the theoretical work of Chao [75] and the numerical work of Yan and Mai [76] who showed that fracture constraint has no noticeable effect on the crack-tip field under plane stress conditions.

Experimental investigations also showed that small-sized test specimens can obtain R curve data comparable to those generated with large wide panels. A small C(T) specimen has a typical width less 125 mm, and a small M(T) specimen has a typical width less 305 mm. Use of such small specimens can significantly reduce material costs, and lower the test machine load requirement. The K–R curve test method using the small test geometries was standardized and approved in 1974 by ASTM with designation E561–74. This standard has undergone several revisions over the years, and the present version is ASTM E561–10 [14]. The recommended specimens are the C(T) and M(T) specimens. A crack-line-wedge-loaded [C(W)] specimen was adopted in the older versions of E561 for the K–R curve testing, but was removed in the present version of this standard. In ASTM E561, a general equation for calculating the stress intensity factor K is given as:

$$K = \frac{P}{B\sqrt{W}} f\left(\frac{a}{W}\right) \tag{9}$$

where P is the applied load, B is the specimen thickness, W is the specimen width, a is the crack length for the C(T) specimen and a half crack length for the M(T) specimen. For the C(T) specimen, the geometry function $f(a/W)$ is the same as Eq. (7). For the M(T) specimen, $f(a/W)$ used in the present ASTM E561–10 was obtained by Feddersen [77] as:

$$f\left(\frac{a}{W}\right) = \sqrt{\frac{\pi a}{W} \sec\left(\frac{\pi a}{W}\right)} \tag{10a}$$

A more accurate expression than Eq. (10a) was given by Tada et al. [32]:

$$f\left(\frac{a}{W}\right) = \sqrt{\frac{\pi a}{W} \sec\left(\frac{\pi a}{W}\right)} \left[1 - 0.025\left(\frac{2a}{W}\right)^2 + 0.06\left(\frac{2a}{W}\right)^4\right] \tag{10b}$$

Newman and Haines [78] showed that Eq. (10a) has an accuracy of 2% when compared with numerical results for the M(T) specimen with 0 < 2a/W < 0.9, while Eq. (10b) has an accuracy of 0.5% for a wider range of 0 < 2a/W < 0.95.

In ASTM E561, a K–R curve is defined as an effective stress intensity factor (K_{eff}) versus effective crack extension (Δa_{eff}) curve or physical crack extension. K_{eff} is calculated using Eq. (9) with the effective crack size a_{eff}, a plastic zone corrected crack length. The value of a_{eff} can be estimated as the physical crack size adding the Irwin plastic zone size in Eq. (2), or determined using a secant compliance technique. In the latter approach, the specimen loading compliance is inferred from the secant slope of a measured load–displacement curve, and is calculated as the ratio ($\Delta V/\Delta P$) of specimen displacement to the load carried by the specimen during the test, as shown in Fig. 6. The secant compliance value and an appropriate calibration equation are used at each loading point to determine a_{eff}, and then to compute K_{eff} in a K–R curve evaluation.

Buckling may be developed in laterally unsupported specimens in a K–R curve test, which depends on the sheet thickness, material toughness, crack size and specimen size. Buckling can seriously affect the validity of a K-test analysis, and is particularly troublesome when the compliance technique is used to determine crack size [79]. It is therefore required that anti-buckling guides be applied to the thin-sheet specimens in critical regions when conditions for buckling are anticipated in a fracture test. A procedure for detection of possible buckling is described in Section 9.8.3 of ASTM E561.
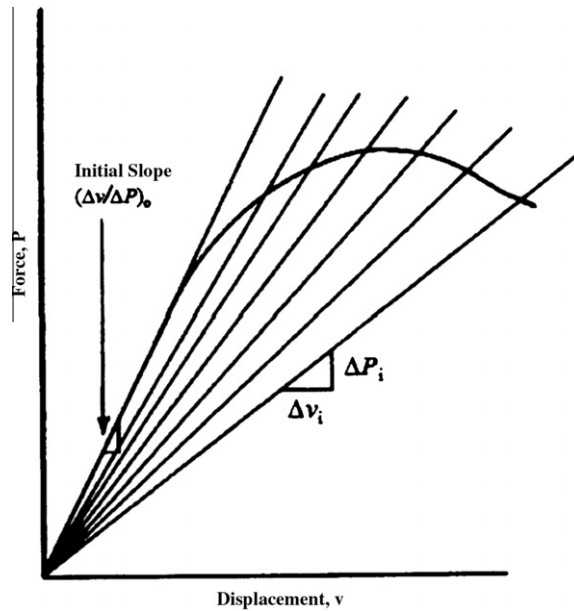
Fig. 6. A load–displacement curve and its secant slopes used for inferring the specimen compliance in a K–R curve test.

In order to validate a calculated K_R (=K_{eff}) value, the remaining ligament must be predominately elastic at the applied load corresponding to the value of effective crack extension. ASTM E561 provides methods for estimating allowed specimen sizes for each specimen type. For the M(T) specimen, the length between the loading pins shall be at least three specimen widths, i.e. $L = 3W$, when single-pin grips are used. The initial crack size $2a_0$ shall be within the range of 0.25–0.40W. The net-section stress due to the physical crack size must be less than the yield strength of the material. For the C(T) specimen, the initial crack size a_0 shall be between 0.35W and 0.55W, and the following validity criterion is enforced:

$$(W - a_{phy}) \geqslant 8r_y = \frac{4}{\pi} \left(\frac{K_{max}}{\sigma_{ys}} \right)^2 \tag{11}$$

where the maximum plastic zone size r_y is estimated at the maximum expected toughness K_{max} and σ_{ys} is the 0.2% offset yield strength. In general, a wider specimen with larger W will provide more valid data to a larger value of a_{eff} than a narrow specimen with small W.

A round-robin study reported by Pearson and McCabe [80] verified the guidelines for K–R curve testing specified in the standard ASTM E561. McCabe and Ernst [81], Newman [82] and Reynolds [83] showed that R-curves for 2024-T351 aluminum alloy were correlated very well for different C(T) specimens. Pearson [84] further showed a good agreement of valid R-curves obtained using C(T) and M(T) specimens for two materials of 7075-T561 aluminum alloy and 4340 steel. Based on the K–R curve, fracture instability analysis can be performed using an instability criterion similar to Eq. (4), as done by McCabe and Schwalbe [85] for both load control and displacement control conditions.

When plastic deformation predominates in a small specimen, the linear elastic fracture mechanics (LEFM) or the K-factor theory becomes invalid, and the elastic–plastic fracture mechanics (EPFM) or the J-integral theory must be used to characterize ductile crack growth resistance. McCabe and Ernst [81], Newman [82], Reynolds [83], McCabe and Landes [86], and Haynes and Gangloff [87] developed crack growth resistance curves using C(T) specimens for different materials in terms of both parameters K and J. These investigators found that a K–R curve can be similar to a J–R curve for high strength aluminum alloys, and J–R curves could be developed for different metals. Recently, Zhu and Leis [88] showed that ASTM E1820 can be equivalent to ASTM E561 in determination of size-independent R curves for thin-section, low toughness 7075-T561 aluminum alloy, and ASTM E1820 would be applicable to different thin-sheet ductile materials if the specimen thickness requirement in E1820 is disregarded. Thus, an E1820 J–R curve is more general and useful than an E561 K–R curve. It was also found that the validity criterion in Eq. (11) for the C(T) specimen is overly stringent for 2024-T351 aluminum alloy, but is not stringent enough for 7075-T561 aluminum alloy. An alternative validity criterion was thus suggested by Zhu and Leis [88] in a valid K–R curve evaluation for thin-walled materials. Note that ASTM E399 and ASTM E1820 were developed for plane strain fracture toughness testing, a minimum specimen thickness is required. In contrast, ASTM E561 does not contain any minimum thickness criteria, which makes it more suitable for thin-section R-curve testing in the thickness of application, including the transition thickness from flat to shear fracture.

3. *J*-based fracture testing

3.1. J-integral concept and HRR field

For structural steels in the presence of large-scale plasticity, linear elastic fracture mechanics cannot accurately characterize the fracture behavior, and thus an alternative nonlinear fracture mechanics model is needed. Based on the deformation theory of plasticity, Rice [2] at Brown University (now at Harvard University) proposed a new fracture parameter that was called *J* integral and defined as:

$$J = \oint_{\Gamma} \left(w\,dy - T_i \frac{\partial u_i}{\partial x}\,ds \right)$$

(11)

where Γ is an arbitrary curve around the tip of a crack, as shown in Fig. 7, w is the strain energy density, T_i is the components of the traction vector, u_i is the displacement vector components, ds is the length increment along the contour, x and y are the rectangular coordinates with the y direction taken normal to the crack line and the origin at the crack tip. Rice [2] showed that for deformation plasticity (i.e., nonlinear elasticity) the *J*-integral is independent of the path of integration around the crack tip. This path independence was first verified by Kobayashi et al. [89] using the finite element analysis (FEA). Thus, *J* is called a path-independent integral.

With the *J*-integral, Hutchinson [90] at Harvard University and Rice and Rosengren [91] at Brown University independently evaluated the character of crack-tip stress fields for power-law hardening materials. Hutchinson considered both plane stress and plane strain conditions, while Rice and Rosengren considered only plane strain conditions. These two papers revealed that for the material model they adopted the product of stress and strain varies as $1/r$ near the crack tip, and Hutchinson further provided a mathematical proof of this relationship. For a power-law hardening material, as pointed out by McClintock [92], Hutchinson obtained the following asymptotic solutions of crack-tip stress and strain fields:

$$\sigma_{ij} = \sigma_0 \left(\frac{J}{\alpha \sigma_0 \varepsilon_0 I_n r} \right)^{\frac{1}{n+1}} \tilde{\sigma}_{ij}(n, \theta)$$

(12a)

$$\varepsilon_{ij} = \alpha \varepsilon_0 \left(\frac{J}{\alpha \sigma_0 \varepsilon_0 I_n r} \right)^{\frac{n}{n+1}} \tilde{\varepsilon}_{ij}(n, \theta)$$

(12b)

where $\varepsilon_0 = \sigma_0/E$, σ_0 is a reference stress, n is the strain hardening exponent, I_n is an integration constant that depends on n, $\tilde{\sigma}_{ij}$ and $\tilde{\varepsilon}_{ij}$ are the dimensionless functions of n and θ. Rice and Rosengren obtained essentially identical results to Hutchinson's solutions for plane strain in a different format. Eq. (12) is thus referred to as HRR field, and the *J*-integral is used to describe the singularity intensity of the crack-tip stress field for elastic–plastic hardening materials, just as the stress intensity factor K is used to characterize the intensity of singularity of the linear elastic stress field. The *J*-integral and HRR field laid a solid foundation of EPFM theory. For a linear elastic material, $n = 1$, and Eq. (12) predicts $1/r^{1/2}$ singularity, which is consistent with Eq. (1) for LEFM theory. Note that for perfectly plastic materials McClintock [92] at the Massachusetts Institute of Technology presented the slip-line field solutions without singularity at the crack-tip for bending and tension geometries. When $n \to \infty$, the singularity of HRR field disappears and the crack-tip stress state approaches to the Prandtl slip-line field as for a deeply-cracked bending specimen, but the deformation concentrates along a single slip line emanating from the crack tip [92,95]. As the leading term of an elastic–plastic crack-tip field with stress varying as $1/r^{1/(n+1)}$, the HRR field dominates only near the crack tip and well within the plastic zone. For very small r values, however, the HRR solution is invalid because it neglects finite geometry changes (e.g. crack tip blunting) at the crack tip, as shown by McMeeking and Parks [93]. As a result, the HRR singularity is accurate in an annular region within the elastic–plastic deformation zone. When the HRR singularity dominates, the loading is proportional, which implies the adequacy of a single-parameter description of the crack-tip field. When the higher-order terms in the asymptotic solutions are significant, the loading is often non-proportional and two-parameter solutions are required to describe the elastic–plastic crack-tip behavior and to quantify the crack-tip constraint effect that is discussed in Section 6.
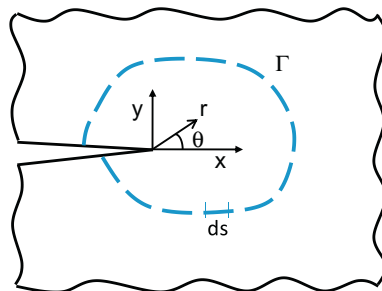

Fig. 7. An arbitrary contour around the crack tip used in the definition of *J*-integral.

Broad finite element analyses [93–97] verified that the HRR solution matches actual crack-tip fields for deeply cracked bending specimens, and that a single J-integral parameter can accurately describe the intensity of the crack-tip stress field. In the late 1970s and the early 1980s, Electric Power Research Institute (EPRI) in the United States sponsored a series of major projects for establishing a J-integral handbook. An engineering estimation scheme for elastic–plastic fracture analysis was thus developed, and the J-integral solutions for many specimens and simple geometries in plane stress and plane strain conditions were obtained by Kumar et al. [98] using finite element numerical calculations. Today, most commercial finite element analysis software has the capacity to calculate the J-integral at a two-dimensional crack tip or along a three-dimensional crack front for actual structures containing a crack.

Rice [2] showed that the J-integral is essentially equal to the energy release rate or work done on a nonlinear elastic body containing a crack per unit fracture surface area, which can be expressed in displacement control conditions as:

$$J = -\left(\frac{dU}{Bda}\right)_\Delta \tag{13}$$

where U is the strain energy stored in the body, a is the crack length, B is the thickness and the subscript Δ follows the partial derivative convention indicating the displacement variable that is held constant during partial differentiation. The definition of J in Eq. (13) is similar to the elastic energy release rate G, but J is a more general function of nonlinear elastic energy release rate. The original energy release rate is defined as the potential energy that is released from an elastic structure when the crack grows. However, much of the strain energy absorbed by an elastic–plastic material does not recover when the crack grows or the specimen is unloaded. Therefore, rather than defining the energy released from the body when crack grows, Eq. (13) relates J to the difference in energy absorbed during loading by specimens with incrementally different crack sizes. This is the basis of early experimental evaluations of the J-integral.

For the special case of a linear elastic material, $J_{el} = G$. From Eq. (3), the relationship between the elastic J and the K factor is obtained as:

$$J_{el} = \frac{K_I^2}{E'} \tag{14}$$

Therefore, from both energy and field theories of view, the J-integral is an extension of the K approach that Irwin [1] proposed more than a decade earlier. As similar to the K-factor fracture criterion, the J-integral fracture criterion was then developed and J-based fracture toughness was measured, as discussed in the following subsections. Owing to its dual roles in describing the crack-tip mechanics behaviors and in measuring fracture resistance, J has become a notable symbol and parameter of elastic–plastic fracture mechanics.

3.2. Early J estimation and η-factor equations

In order to define a J fracture criterion of $J = J_{Ic}$, where J_{Ic} can be considered a material parameter, extensive experimental investigations on the J-integral testing were conducted with a target to develop effective test methods for evaluating the critical value J_{Ic} for plane strain opening cracks, where the applied fracture work is predominantly in mode-I loading and elastic–plastic conditions. Among the pioneers, Begley and Landes [99] and Landes and Begley [100] at the Westinghouse R&D Center first successfully measured the J-integral and its critical value J_{Ic} at crack initiation using the energy principle and multiple compact specimens with mode-I tensile cracks. Kobayashi et al. [89] also obtained approximate J_{Ic} values from a set of center-cracked specimen tests through using the Dugdale model [30] with a plasticity modification factor. These experiments showed that the J_{Ic} can be used as a fracture criterion for ductile materials. Consequently, the J-integral was recognized as a measurable material parameter for characterizing fracture toughness of ductile materials. In the experimental evaluation, Begley and Landes [99] tested a series of compact specimens with the same geometry but different crack sizes. From the measured load–displacement data, they determined the energy absorbed by each specimen and then calculated the J using Eq. (13). This J testing technique has the disadvantages that the experimental procedure is complicated and multiple specimen tests are required to obtain a single experimental result of J. Even so, their early work encouraged a broad effort in the J-integral fracture mechanics. The first major forward step was the development of a simple analysis for estimating J as a function of crack length at a point on the load–displacement record from a single specimen test.

In the analytical work, Rice et al. [101] presented the most notable approach for evaluating the J-integral directly using the load–displacement curve obtained from a single specimen test. Since strain energy U can be determined from the area under a load versus displacement curve, two equivalent expressions of Eq. (13) were developed to express the J-integral as:

$$J = -\frac{1}{B}\int_0^\Delta \left(\frac{\partial P}{\partial a}\right)_\Delta d\Delta \tag{15}$$

for displacement control conditions and

$$J = \frac{1}{B}\int_0^P \left(\frac{\partial \Delta}{\partial a}\right)_P dP \tag{16}$$

for load control conditions. In Eqs. (15) and (16), P is the total generalized load and Δ is the associated load-point. Using Eq. (15), Rice et al. [101] obtained different J estimation equations for conventional fracture specimens. For pure bending specimens with deep cracks, the J-integral was approximated as:

$$J = \frac{2}{Bb} \int_0^\Omega M \, d\Omega \tag{17}$$

where $b = W - a$ is the remaining ligament, W is the specimen width, M is the bending moment, and Ω is the angular rotation of the specimen ends. If the remaining ligament supported primarily a bending moment due to the applied load P, like three-point bend or compact specimens, the J-integral estimation was similar to Eq. (17):

$$J = \frac{2}{Bb} \int_0^\Delta P \, d\Delta = \frac{2A_{tot}}{Bb} \tag{18}$$

where A_{tot} is the total area under a load–displacement (P–Δ) curve and represents the energy absorbed by the specimen. Landes et al. [102] showed that Eq. (18) was applicable with reasonable accuracy to ASTM E399 three-point bend and compact specimens with deep cracks, even when the load-line displacement (LLD) was substituted for the actual load-point displacement for the evaluation of A_{tot}. The simple relationship in Eq. (18) marks a major step forward in the development history of a practical test method for J-integral testing.

For C(T) specimens, Merkle and Corten [103] showed that Eq. (18) gives a J value that is slightly less than the G value in an elastic condition. They suggested the addition of a multiplier to take into account the tensile component of the applied load on the C(T) specimen for accurately estimating J. Since the total displacement can be separated into an elastic and a plastic component, i.e., $\Delta = \Delta_{el} + \Delta_{pl}$, the total J-integral was separated correspondingly into two parts:

$$J = J_{el} + J_{pl} \tag{19}$$

in which the elastic component, J_{el}, can be regarded to the elastic strain energy release rate G, and calculated directly from the stress intensity factor K using Eq. (14). The solutions of the stress intensity factor were compiled in the handbook of Tada et al. [32] for various fracture specimens. The plastic component, J_{pl}, was expressed similarly to Eqs. (15) and (16) as:

$$J_{pl} = -\frac{1}{B} \int_0^{\Delta_{pl}} \left(\frac{\partial P}{\partial a}\right)_{\Delta_{pl}} d\Delta_{pl} = \frac{1}{B} \int_0^P \left(\frac{\partial \Delta_{pl}}{\partial a}\right)_P dP \tag{20}$$

Through plastic limit analysis, Merkle and Corten [103] obtained a more accurate J estimate for C(T) specimens:

$$J_{pl} = \frac{2}{b} \frac{(1+\alpha)}{(1+\alpha^2)} \int_0^{\Delta_{pl}} \left(\frac{P}{B}\right) d\Delta_{pl} + \frac{2}{b} \frac{\alpha(1-2\alpha-\alpha^2)}{(1+\alpha^2)^2} \int_0^{\frac{P}{B}} \Delta_{pl} \, d\left(\frac{P}{B}\right) \tag{21}$$

where the parameter α is defined as:

$$\alpha = 2\sqrt{\left(\frac{a}{b}\right)^2 + \frac{a}{b} + \frac{1}{2}} - 2\left(\frac{a}{b} + \frac{1}{2}\right) \tag{22}$$

It was shown that the J-integral may be computed accurately from Eq. (21), based on the total displacement, for a linear or nonlinear load–deflection curve if $a/W \geqslant 0.5$. Otherwise, the elastic and plastic components of J should be calculated separately using Eqs. (14), (21) and (19). Since Eq. (21) is complicated in practical application, Landes et al. [102] simplified this Merkle–Corten equation in terms of the total displacement as:

$$J = \left(\frac{1+\alpha}{1+\alpha^2}\right) \frac{2A_{tot}}{Bb} \tag{23}$$

Eq. (23) indicates that the J-integral for C(T) specimens can be estimated from the energy absorbed by the specimen that is quantified by the total area under the load–displacement curve. Through experimental comparisons, Landes et al. [102] concluded that the total energy-based expressions in Eqs. (18) and (23) should be used to estimate J, respectively for three-point bend and compact tension specimens with deep cracks. A similar suggestion to use the total energy was given by Srawley [104] for three-point bend specimens.

A more general relationship for estimating the J-integral was proposed by Sumpter and Turner [105] at the Naval Construction Research Establishment in Scotland and at the Imperial College in London as a sum of elastic and plastic components:

$$J = \frac{\eta_{el} A_{el}}{Bb} + \frac{\eta_{pl} A_{pl}}{Bb} \tag{24}$$

where A_{el} is the elastic area under the load–displacement curve, A_{pl} is the plastic area under the load–displacement curve, η_{el} and η_{pl} are two geometry factors dependent on a/W but independent of material properties. In this equation, the η-factor concept was first introduced in J estimation. In general, the elastic and plastic η-factors are not equal, and should be calculated separately for a specimen, as shown by Turner [106] and Roos et al. [107]. The elastic η_{el} factor can be determined from

the elastic compliance of a specimen, as discussed in Turner [108], and thus it always exists for converting the elastic work into the elastic J-integral. In the special case where $\eta_{el} \approx \eta_{pl}$, Eq. (24) reduces to Eqs. (18) and (23), respectively for SE(B) and C(T) specimens. Since the elastic J_{el} can be calculated directly from the K-factor solution using Eq. (14), the η_{el} factor determination becomes redundant. Thus, Eq. (24) is equivalent to:

$$J = J_{el} + J_{pl} = \frac{K_I^2}{E'} + \frac{\eta_{pl} A_{pl}}{Bb} \tag{25}$$

As a result, the determination of the plastic η_{pl} factor becomes the key in the experimental estimation of J-integral. The laboratory work of Sumpter and Turner [105] showed evidence that the J-based fracture toughness testing was feasible using the η-factor method.

The early approaches to determine the plastic η_{pl} factor were based on the plastic limit analysis. For C(T) specimens with deep cracks, Clarke and Landes [109] obtained an approximate fitted function of the η_{pl} factor as:

$$\eta_{pl} = 2 + 0.522(b/W) \tag{26}$$

For SE(B) specimens in pure bending, Sumpter [110] obtained the η_{pl} factor for a complete range of crack sizes as:

$$\eta_{pl} = \begin{cases} 2, & a/W > 0.282 \\ 0.32 + 12\left(\frac{a}{W}\right) - 49.5\left(\frac{a}{W}\right)^2 + 99.8\left(\frac{a}{W}\right)^3, & a/W \leqslant 0.282 \end{cases} \tag{27}$$

More accurate values of η_{pl} can be determined from finite element calculations, as done by Kirk and Dodds [111] and Nevalainen and Dodds [112].

The use of the η-factor considerably simplifies the task of J-integral determination, and Eq. (25) gives a very convenient way for experimental evaluation of J for any fracture specimen from a single load–displacement record, provided that the K_I and the η_{pl} factor is determined a priori for that specimen. Detailed discussions on the plastic η_{pl} factor were given by Paris et al. [113], who pointed out that expressing J as a function of A_{pl} and plastic η_{pl} factor is rigorous only when the variables of geometry and deformation are separable, that is $F(\Delta_{pl}/W, a/W) = G(\Delta_{pl}/W) * H(a/W)$. The early load separation analysis was performed by Ernst et al. [114]. About 10 years later, Sharobeam and Landes [115,116] strictly verified the existence of load separation relationship for ductile materials using detailed experimental investigations and numerical finite element analyses. This laid a solid foundation for the simple J estimation procedure using the η-factor equation approach. Eq. (25) taken together with (26) and (27) are utilized in the basic procedure in ASTM E1820 for the evaluation of initiation toughness J_{Ic} near the onset of stable crack growth. Note that early J_{Ic} evaluations were conducted using the "maximum load"-based J_{Ic} estimates, as done by Joyce [117] and Towers and Garwood [118]. Clearly, since the hardening masked crack initiation and growth in high strain hardening materials, the maximum load toughness did not give accurate J_{Ic} results for these materials.

Landes and Begley [119] published the first J_{Ic} tests for A216 steel using the η-factor Eq. (18) and the multiple specimen technique, where loading was stopped and the cracks marked, broken open and measured visually. A resistance curve technique was then developed, in which J values from bend-type specimens were plotted as a function of crack extension measured from the specimen fracture surfaces. A single J resistance curve was assembled and a J_{Ic} value was then estimated from the resistance curve. At this point a multiple specimen technique was not needed to obtain an individual J value, but it was required to determine J_{Ic}, thus requiring the tests of several specimens to obtain a resistance curve and then one material toughness value.

3.3. Incremental J-integral equations

Hutchinson and Paris [120] showed that the J-integral can be used to characterize the crack growth process, provided that the remaining ligament is large enough and the applied deformation is small enough so that a region of proportional strain field easily encompasses the local crack-tip non-proportional strain field. This is the so-called J-controlled crack growth regime. To obtain a J resistance curve from a single specimen test, Clarke et al. [121] proposed an elastic unloading compliance technology to determine the amount of crack extension present at a specific location on an experimental load versus load-line displacement record. In this procedure small elastic unloadings were applied periodically during the experimental test procedure and the change in compliance of these unloadings was used to estimate the crack extension. Combined with J calculated using the total η Eq. (18) and the initial crack length, an early J–R curve was constructed. The results were accurate only for small amounts of crack growth, but nonetheless provide a limited, single specimen J–R curve from which J_{Ic} could be evaluated. The basic procedure presented in the first J-based fracture toughness standard, introduced in the ASTM book of standards in 1982 as E813–81, was the multi-specimen procedure, and a rudimentary unloading compliance technique was included as an appendix. The unloading compliance technique became a standard procedure in ASTM E813–88.

For more extensive crack growth it was realized that the additional crack growth corrections would be necessary because the η-factor based J-integral equations described above are valid only for non-growing cracks. The early incremental unloading experimental techniques, in turn, gave impetus to develop incremental procedures to evaluate the J-integral for specimens with growing cracks. For a growing crack, accurate J-integral evaluation requires the use of the current crack size and the evaluation of a crack growth correction. Eq. (25) was modified in different manners to consider the crack growth

effect in a J–R curve evaluation. Two examples are incremental equations, where test data are spaced at small intervals of crack extension and the J-integral is evaluated always from the previous step. The first incremental equation of the J estimate was proposed by Garwood et al. [122] at the British Welding Institute for a single edge bend specimen with a deep crack. At the nth step of crack growth, the total J was determined in terms of the previous value as:

$$J_n = J_{n-1}\left(\frac{W - a_n}{W - a_{n-1}}\right) + \frac{2U_4}{B(W - a_{n-1})} \tag{28}$$

where the variable U_4 refers to the increment of the total area under an actual load–displacement record from step $n - 1$ to n. Etemad et al. [123,124] generalized Eq. (28) for an arbitrary fracture specimen as:

$$J_n = J_{n-1}\left(1 + \frac{g(\eta)}{(W - a_n)}(a_n - a_{n-1})\right) + \frac{\eta \Delta U_{n,(n-1)}}{B(W - a_n)} \tag{29}$$

where $\Delta U_{n,(n-1)} = U_4$, as used in Eq. (28); η is the plastic geometry factor, as used in Eq. (25); $g(\eta)$ is another geometry factor related to η by $g(\eta) = 1 + (b/\eta)(d\eta/da) - \eta$. An incremental equation similar to Eq. (29) was given by Anderson [7].

The second incremental equation to estimate J was obtained by Ernst et al. [125] at the Westinghouse R&D Center based on the principle of load separation. Under the J-controlled crack growth conditions, the deformation theory based J-integral is independent of the loading path leading to the current displacement and crack size. Thus, the J-integral is a unique function of two independent variables: load-line displacement, Δ, and crack length, a. From the total η-factor equation, Ernst et al. derived a complete differential of the total J-integral in a form of:

$$dJ = \frac{\eta}{bB}Pd\Delta - \frac{\gamma}{b}Jda \tag{30}$$

where both η and γ are two geometry factors and related by the relationship $\gamma = \eta - 1 - (b/W\eta)(d\eta/d(a/W))$. Integrating Eq. (30), one has:

$$J = \int_0^\Delta \frac{\eta}{bB}Pd\Delta - \int_{a_0}^a \frac{\gamma}{b}Jda \tag{31}$$

This equation holds true for any loading path leading to the current values of Δ and a, including the actual loading path for a growing crack. Fig. 8 illustrates a typical P–Δ curve for a growing crack. This figure includes three deformation paths: one is for the original crack length a_0, and the other two are for arbitrarily fixed crack lengths a_{i-1} and a_i. Since the J in Eq. (31) is valid for any loading path leading to the current values of Δ_i and a_i, the integration path AC can be approximated by the deformation segment AB with the fixed crack length a_{i-1} and the segment BC where the displacement Δ_i remains constant, but the crack size increases from a_{i-1} to a_i. Along the segments AB and BC, the total J at the ith step of crack growth was determined as:

$$J_i = \left[J_{i-1} + \frac{\eta_{i-1}}{Bb_{i-1}}A_{i-1,i}\right]\left(1 - \frac{\gamma_{i-1}}{b_{i-1}}(a_i - a_{i-1})\right) \tag{32}$$

where $A_{i-1,i}$ is the incremental area under an actual load–displacement record from step $i - 1$ to i. Both the incremental equations in Eqs. (29) and (32) consider the crack growth correction on the J-integral from the preceding step. Eq. (32) also makes a correction to the incremental work done on the specimen, while Eq. (29) does not. As a result, a larger J estimate is obtained from Eq. (29) than from Eq. (32), as shown by Joyce [126]. A recent study of Zhu and Joyce [127] showed that Eq.
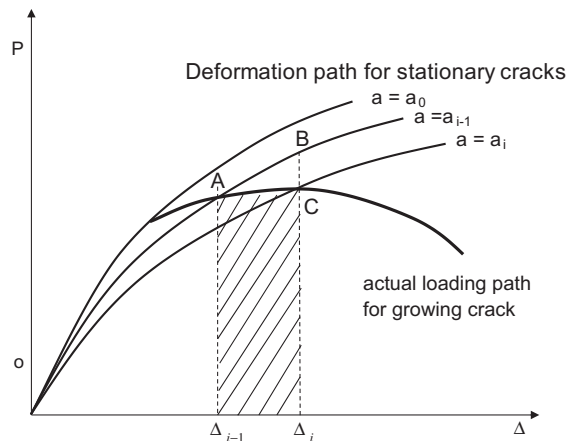

Fig. 8. An actual load–displacement curve for a growing crack and three deformation paths for stationary cracks.

(32) can always provide conservative results, while Eq. (29) may give non-conservative results for larger crack growth increments. In general, these two incremental formations of the J-integral equation are applicable to any specimen geometry, provided that the two geometry factors are known for the specimen.

The development of computerized laboratory data acquisition methods by Joyce and Gudas [128] allowed the accurate evaluation of crack growth increments and also allowed the application of the more complex incremental J-integral equations. The development of these incremental J-integral equations moved the emphasis of elastic–plastic fracture testing from crack initiation at J_{Ic} to crack growth where J resistance curves became the principal focus of research. Research sponsors in the nuclear, offshore, and defense industries generally had small laboratory specimens, large structures for application and little desire to be strictly limited to design against crack initiation.

The first J–R curve standard ASTM E1152 in 1987 separated the total J-integral into elastic and plastic parts, as shown in Eq. (19), with the two parts determined separately. This separation improves the accuracy of J estimates near linear elastic conditions. The elastic component of J is obtained directly from the stress intensity factor using Eq. (14), and the plastic component of J is obtained from the Ernst-type incremental J-integral Eq. (32), namely:

$$J_{pl(i)} = \left[J_{pl(i-1)} + \frac{\eta_{i-1}}{Bb_{i-1}} A_{pl}^{i-1,i} \right] \left(1 - \frac{\gamma_{i-1}}{b_{i-1}} (a_i - a_{i-1}) \right) \qquad (33)$$

where $A_{pl}^{i-1,i}$ is the increment of plastic area under a load–displacement record from step $i-1$ to i:

$$A_{pl}^{i-1,i} = \frac{1}{2} (P_i + P_{i-1})(\Delta_{pl(i)} - \Delta_{pl(i-1)}) \qquad (34)$$

Until 2008, the two geometry factors used for deep-cracked SE(B) specimens in ASTM E1820 were the constant values of $\eta_{i-1} = 2.0$ and $\gamma_{i-1} = 1.0$, but changed in the current ASTM E1820–11 to:

$$\eta_{i-1} = 1.9 \quad \text{and} \quad \gamma_{i-1} = 0.9 \qquad (35)$$

to accommodate 3D finite element results of Nevalainen and Dodds [112]. While for the SE(B) specimen these factors are independent of crack length, for C(T) and DC(T) specimens these factors are functions of b/W:

$$\eta_{i-1} = 2.0 + 0.522(b_{i-1}/W) \quad \text{and} \quad \gamma_{i-1} = 1.0 + 0.76(b_{i-1}/W) \qquad (36)$$

The four equations from Eqs. (33)–(36) are adopted by ASTM E1820–11, with the net thickness B_N being used for side-grooved specimens in place of the full thickness B. Small and uniform crack growth increments are required in Eq. (33) for accurate estimates of $J_{pl(i)}$. With the calculated J_i and measured crack extension $(a_i - a_0)$, where a_0 is the original crack
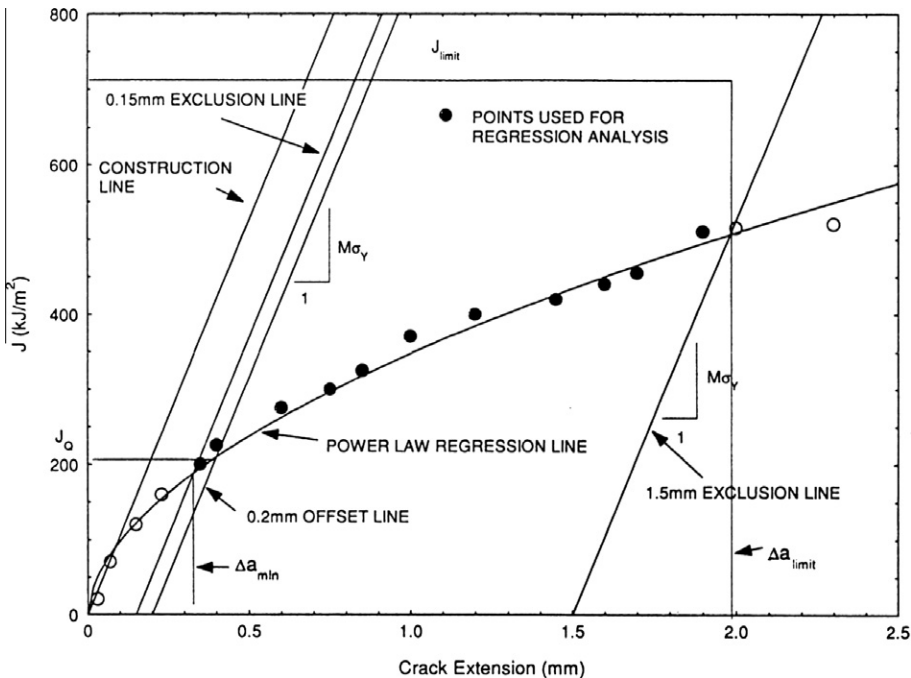

Fig. 9. A typical J–R curve with test data points, construction lines and limitation bounds required by ASTM E1820.

length, a J–R curve is obtained by applying Eqs. (14), (19) and (33) to successive increments of crack growth from a single test. Fig. 9 shows a typical J–R curve with measured data points and an associated power-law regression curve of the test data.

Recently, Neimitz [129] and Kroon et al. [130] presented two different approximations of the J-integral equation, which they proposed as more accurate than the Ernst-type Eq. (33). However, Zhu and Joyce [127] showed that these two "new" incremental J-integral equations are actually alternative forms of Garwood-type Eq. (29), and are not recommended for use due to its non-conservative nature. In contrast, the Ernst-type Eq. (33) is preferred by ASTM standards since it obtains a conservative measurement of J. A more accurate J approximation than Eq. (33) was then proposed by the present authors in [127] in a slightly more complicated incremental form:

$$J_{pl(i)} = J_{pl(i-1)} \left(1 - \frac{\gamma_{i-1}}{b_{i-1}}(a_i - a_{i-1})\right) + \left[\frac{1}{2B}\left(\frac{\eta_{i-1}}{b_{i-1}} + \frac{\eta_i}{b_i}\right)A_{pl}^{i-1,i}\right]\left(1 - \frac{\gamma_{i-1}}{2b_{i-1}}(a_i - a_{i-1})\right) \tag{37}$$

For sufficiently small increments of crack growth, e.g., $da_i = a_i - a_{i-1} < 0.01b_0$, where b_0 is the original crack ligament, the results indicated that all three types of incremental J-integral equations (Eqs. (29), (33) and (37)) determine essentially equivalent J–R curves for the same test.

3.4. Experimental methods for determining J–R curves

Like the K testing, the J testing requires a measurement of load and displacement on the load line (or a displacement measurement that can be related to the load-line displacement). With the J-integral experimental estimation described previously, a J–R curve can be determined if the crack length is known. This requires that the crack length must be monitored during the test. For the multiple specimen test method, the crack lengths are usually measured visually on the fracture surface. The visual method was the first and the most used one. It uses one specimen to generate one single point on the resistance curve by loading the specimen until some ductile crack extension occurred. The specimen is then unloaded, broken open, and the crack length measured visually on the fracture surface. It requires a number of specimens to generate a resistance curve. In ASTM E1820, the multiple specimen test method is valid only for the basic procedure, where the R-curve is used to determine J_{Ic} at the onset of ductile crack tearing and a full-range J–R curve is not needed. In contrast, to obtain a full-range J–R curve from only one specimen test, two single-specimen test methods were developed with the crack lengths being monitored during the test. One is the elastic unloading compliance method that is the most often used of the single specimen methods. Another is the electrical potential drop method.

The elastic unloading compliance method uses the elastic properties of the specimen geometry to evaluate crack length. It was first proposed by Clarke et al. [121] and originally standardized in ASTM E813–81. This rudimentary single specimen test method used a complex system of laboratory-built apparatus and enlarged pen-plot graphs to evaluate specimen compliance. This elastic compliance method was improved dramatically by Joyce and Gudas [128] when they developed a computer-enhanced, interactive system for digital data acquisition and test control to the fracture mechanics test in laboratory. The improved elastic compliance method became the basis of the first ASTM J–R curve standard E1152–87, and now E1820 for the measurement of the instantaneous physical crack length from a single specimen test. It actually measures the displacement compliance at regular intervals during the test by partially unloading the specimen, and then infers the crack length. As the crack grows, the specimen becomes less stiff and the compliance increases. The unloading compliance method cannot be used under rapid-loading conditions or for materials that do not have a strictly linear-elastic loading character.

Another method used to monitor crack length in a single specimen test is the electrical potential drop method proposed by Johnson [131] and used by Schwalbe and Hellmann [132] and Bakker [133], for example. This method monitors crack growth and infers crack length through measuring the change of electrical resistance which accompanies in the cross section area. When a constant current is applied to a specimen, the electrical potential across calibration points on the specimen increases as the crack grows. It requires a material that is an electrical conductor and has a measurable electrical resistance, so it is used mostly for metallic materials. The potential drop method can yield a higher density of points to define a J–R curve than is typically achievable using the elastic unloading compliance method. The procedures and guidelines of the direct current electrical potential determination of crack size were detailed in Annex A5 in ASTM 1737–96. For a ductile crack growth, the specimen usually has extensive plastic deformation and this sometimes influences the potential drop signal so that it is difficult to distinguish the crack extension part of the voltage change from that caused by plasticity. As a result, this potential drop method has been used less frequently for J–R curve testing than the elastic compliance method that is based on deformation properties of the specimen, and thus is not included in ASTM E1820. An alternative method for direct determination of crack length is a key curve method or a normalization method that is discussed later in Section 3.9.

3.5. Crack initiation and fracture instability

From a J–R curve, the characteristic values of elastic–plastic fracture mechanics are deduced generally. One of significant parameters is the *plane strain initiation toughness* J_{Ic} that provides a measure of crack growth resistance near the onset of stable crack growth for mode-I cracks. Since it is difficult to define the instant of crack initiation in ductile metals, different def-

initions of initiation toughness were used in different test standards, as discussed by Roos and Eisele [134,135]. ASTM E1820 adopts an engineering definition of J_{Ic} at the intersection of a 0.2-mm offset construction line and the J–R curve, as shown by J_Q in Fig. 9. This figure illustrates a typical construction procedure used to evaluate J_{Ic} as specified in ASTM E1820. At first, the J–R curve is defined as the test data in the region bounded by the coordinate axes and the J_{max} and Δa_{max} limits, where $J_{max} = b_0\sigma_Y/10$ or $J_{max} = B\sigma_Y/10$ and $\Delta a_{max} = 0.25b_0$, see Section 3.10 for discussion on these two limits. To develop the construction lines, a blunting construction line is defined as $J = M\sigma_Y\Delta a$, where the slope $M = 2$ or a larger M can be determined from the fit of the initial test data. Plot this blunting line, then draw an exclusion line parallel to the blunting line intersecting the abscissa at 0.15 mm. Draw a second exclusion line parallel to the blunting line intersecting the abscissa at 1.5 mm. Also draw a line parallel to the construction and exclusion lines at an offset value of 0.2 mm. The $J - \Delta a$ data points that fall inside the region between the 0.15-mm and 1.5-mm exclusion lines are valid data that are used for fitting a power-law regression curve. The intersection of the power-law regression curve with the 0.2-mm offset line defines the provisional point-value J_Q that is subject to qualification criteria to see if it is an acceptable value. The basic one is to guarantee a sufficient specimen size: $b, B \geqslant 25J_Q/\sigma_Y$. If this qualification requirement and others defined in Section A9.8 of E1820 are met, the J_Q is J_{Ic}. Experiments showed that J_{Ic} is nearly a geometry-independent fracture parameter over the range of C(T) and SE(B) specimen sizes allowed by E1820.

Because the J concept applies equally well to structures failing in elastic conditions and in fully-plastic conditions, K_{Jc} is related to J_{Ic} in the following relationship, similar to Eq. (3):

$$K_{Jc} = \sqrt{J_{Ic}E/(1 - v^2)} \tag{38}$$

Note that Begley and Landes [99] related J_{Ic} to K_{Ic} via CTOD and G_{Ic} in a similar relation to Eq. (38), recognizing that linear elastic fracture mechanics is a special case of non-linear elastic fracture mechanics. However, since J_{Ic} and K_{Ic} are defined differently by ASTM E1820 and E399, respectively, a relationship between them is not possible. Accordingly, as is done in E1820, we use K_{Jc} here when the initiation fracture toughness is measured using J_{Ic} and the E1820 method, and K_{Ic} when the initiation fracture toughness is measured using the E399 method.

Another parameter is *fracture instability toughness*, J_{Rc}, a measure of fracture resistance at the onset of ductile fracture instability. The instability conditions for a growing crack under elastic–plastic conditions are similar to those in Eq. (4) for the elastic case in terms of G or K. As illustrated in Fig. 10a, fracture instability is expected when the crack driving force J curve is tangent to the J–R curve at J_{Rc}, which is expressed mathematically by:

$$\begin{cases} J = J_R \\ \frac{dJ}{da} = \frac{dJ_R}{da} \end{cases} \tag{39}$$

When the fracture is cleavage, the resistance to crack extension can be almost zero, i.e., $dJ/da \sim 0$, and the J_R at onset of cleavage is generally referred to as J_c. When the fracture process is ductile hole growth with significant plastic ductility, at least local to the crack process, the slope of the J–R curve at a given amount of crack extension is indicative of the relative stability of the crack growth. A material with a steep R curve is less likely to experience unstable crack propagation. To describe the onset of tearing instability of ductile crack growth, Paris et al. [136] defined a dimensionless applied and a material *tearing modulus*:

$$T_{app} = \frac{E}{\sigma_{ys}^2} \frac{dJ}{da} \quad \text{and} \quad T_R = \frac{E}{\sigma_{ys}^2} \frac{dJ_R}{da} \tag{40}$$

where dJ/da is the driving tearing force obtained from an analysis of the cracked structure, and dJ_R/da is the material tearing resistance obtained from the J–R curve of the material. Using Eq. (40), the fracture instability conditions, Eq. (39), become $J_{app} = J_R$ and $T_{app} = T_R$. This corresponds the intersection of the applied J_{app}–T_{app} curve and the material J_R–T_R curve, and the intersection point determines the J_{Rc} value at the instability point of ductile crack growth. Fig. 10b shows schematically
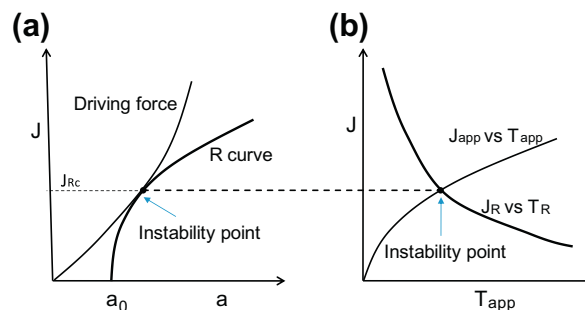
Fig. 10. The J-integral defined crack instability: (a) At the tangent point of the driving force and the J–R curve, (b) at the intersection point of the applied J_{app}–T_{app} curve and the material J_R–T_R curve.

an applied tearing force curve (J_{app}–T_{app} curve), a material tearing resistance curve (J_R–T_R curve), and their intersection point where J_{Rc} is defined.

Use of the ASTM E1820 J–R curve for the evaluation of J_R at the onset of ductile tearing instability is possible – but this is not sanctioned by E1820 because very few people are interested in the onset of ductile tearing instability or the fracture instability toughness J_{Rc} in specimen geometry in a test machine environment. The primary reason is that J_{Rc} is a geometry and size dependent value. Therefore, the tearing instability of interest is strictly in the structural application by combining the material J–R curve and the structure loading and compliance environment.

In an elastic–plastic fracture test, when cleavage fracture instability occurs prior to the onset of significant stable tearing crack extension, the single-point toughness value is labeled J_c. When fracture instability occurs after the onset of significant stable tearing crack growth, a single-point toughness value is labeled J_u, as suggested in ASTM E1820. Both J_c and J_u are calculated using Eq. (25) at the final point where instability occurs. In general, J_c is insensitive to the in-plane sizes of the specimen, but J_u is not. J_c values are highly variable and the Master Curve Standard E1921 [18] has been developed specifically to analyze sets of these values to evaluate the reference temperature, T_0, defining the onset of lower shelf cleavage behavior in ferritic structural steels (see Section 4 below).

3.6. CMOD-based η factor equations

Compact C(T) specimen geometries were modified for a J-integral evaluation by adding cut-outs that allow the direct measurement of LLD using clip-on transducers. This allows the J-integral and sensitive compliance measurements to be made using one transducer. For SE(B) specimens two transducers have been required, a CMOD transducer for crack length measurements and a LLD transducer to measure the J-integral. Since CMOD gage mounting is easier than LLD gage and the use of one transducer is clearly better than two, CMOD-based J estimates have been proposed for SE(B) specimens. Sumpter [110] first used load–CMOD data directly in the evaluation of the J-integral for the three-point bend specimens in order to analyze surface cracks occurred in regions of welds. Following Sumpter's basic ideas and using elastic–plastic finite element analyses (FEA), Kirk and Dodds [111] at the University of Illinois – Urbana Champaign investigated several J estimations for SE(B) specimens with a/W ratios ranging from 0.1 to 0.8. Their results showed that the LLD-based J estimation equation gives accurate results for $a/W > 0.3$, but inaccurate results were observed for hardening materials with $a/W < 0.3$, because the corresponding plastic η factor is very sensitive to the strain hardening exponent for SE(B) specimens with a shallow crack. In contrast, for the same geometries, the CMOD-based plastic η-factor is insensitive to the strain hardening for $a/W > 0.05$. As a result, Kirk and Dodds concluded that the CMOD-based J estimation is the preferred method for the case of shallow cracks and they suggested the following η-factor equation to estimate the J-integral for SE(B) specimens:

$$J = \frac{K^2(1 - v^2)}{E} + \frac{\eta_{CMOD}A^{pl}_{CMOD}}{Bb}$$ (41)

where A^{pl}_{CMOD} is the plastic area under the load–CMOD curve, and η_{CMOD} is the CMOD-based plastic geometry factor that was determined by curve-fitting their FEA results [111] as:

$$\eta_{CMOD} = 3.785 - 3.101(a/W) + 2.018(a/W)^2, \quad 0.05 \leqslant a/W \leqslant 0.7$$ (42)

Morrison and Karisallen [137] and Wang et al. [138] applied Eqs. (41) and (42) to their experimental evaluations of J-integral and its critical value at the onset of crack initiation for SE(B) specimens in different steels. The results showed that the LLD- and CMOD-based J-integral Eqs. (33) and (41) determined similar results, and the CMOD approach was more efficient. The CMOD approach was readily adopted for the ductile-to-brittle transition test which was being developed using the master curve approach, see Section 4 below, since this test required only the onset of crack extension. It was not adopted for J–R curve methods, in spite of its obvious advantages, because there was no corresponding incremental formation at that time. In 2005, 10 years later, ASTM E1820–05a adopted the CMOD-based η-factor Eqs. (41) and (42) in the basic procedure for J_{Ic}, J_c and J_u evaluation, but this was done principally to provide experimental input values for the latter two parameters for the recently adopted E1921 master curve standard.

3.7. Improved crack growth correction procedure

In order to unify the different fracture test standards in Europe and the USA, Wallin and Laukkanen [139] at the Technical Research Center of Finland (VTT) proposed a new ductile crack growth correction procedure to obtain a valid J–R curve when the J–R curve is being developed using a multi-specimen method, for example in the case of elevated rate testing, or when a J–R curve is being assembled from a set of J_u measurements. The procedure is used particularly to determine crack growth corrected J-integral values, which can be regarded as an improved basic method of ASTM E1820 or in the case where a J–R curve could only be obtained using the multi-specimen procedure. To obtain crack growth corrected J-integral values, the following four steps are suggested:

Step 1. Calculate the $J_{el(i)}(a_0)$ and $J_{pl(i)}(a_0)$ at a loading point i for each SE(B) specimen using Eq. (25) if LLD data are used or Eq. (41) if CMOD data are used. For the latter case, the η^i_{CMOD} factor should take values in reference to the current crack length a_i, rather than the original crack length a_0.

Step 2. Obtain initial crack growth corrected *J*-integral values for all loading points using the following equation:

$$J_i(\Delta a) = J_{el(i)}(a_0) + \frac{J_{pl(i)}(a_0)}{1 + \left(\frac{\alpha - 0.5}{\alpha + 0.5}\right) \cdot \frac{\Delta a}{b_0}} \tag{43}$$

with $\alpha = 1$ for SE(B) specimens and $\alpha = 0.9$ for C(T) specimens.

Step 3. Fit a power-law expression $J = J_{1mm}\Delta a^m$ to the initial crack growth corrected *J–R* curve obtained in Step 2 for crack extension with $\Delta a \geqslant 0.05b_0$, where $\Delta a = a_i - a_0$, J_{1mm} is the *J*-integral value at 1 mm crack extension and m is an unknown curve-fit parameter.

Step 4. Calculate final crack growth corrected *J*-integral values using the following equation with the curve-fitted m value obtained in Step 3:

$$J_i(\Delta a) = J_{el(i)}(a_0) + \frac{J_{pl(i)}(a_0)}{1 + \left(\frac{\alpha - m}{\alpha + m}\right) \cdot \frac{\Delta a}{b_0}} \tag{44}$$

where m is in the range of $0 < m < \alpha$ for most ductile metals. Eq. (44) reduces to Eq. (18) when $m = \alpha$. This procedure allows the use of either C(T) and SE(B) specimens as well as LLD and CMOD data, and is applicable for the single and multiple
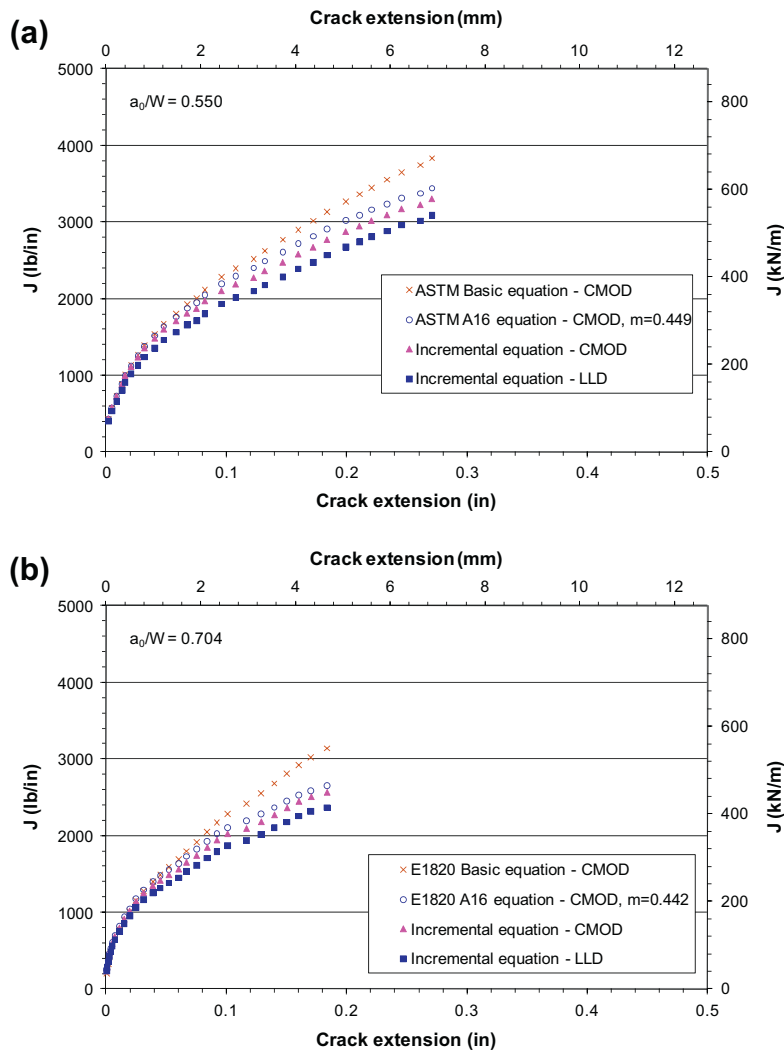

Fig. 11. The experimental *J–R* curves of HY80 steel obtained using different evaluation equations as indicated and SE(B) specimens of deep cracks: (a) $a_0/W = 0.55$, and (b) $a_0/W = 0.704$.

specimen tests with reasonable accuracy. This improved procedure was adopted by ASTM E1820–05 and its latter versions as Annex A16 for obtaining crack growth corrected J-integral values whenever incremental J integral evaluations were not possible.

3.8. CMOD-based incremental J-integral equations

Using CMOD data in the improved crack growth correction procedure outlined above, an accurate J–R curve can be determined from a single specimen test. However, the crack growth correction is indirect and complicated, with multiple analysis steps involved. Recently, Zhu et al. [140] at Battelle Memorial Institute and at the US Naval Academy obtained a functional relationship between LLD and CMOD, and developed a long overdue CMOD method for the direct evaluation of crack growth corrected J–R curves. Based on the deformation theory of plasticity and following the ideas of Ernst et al. [125], Zhu et al. [140] obtained a CMOD-based incremental J-integral equation in a form similar to Eq. (33) as:

$$J_{pl(i)} = \left(J_{pl(i-1)} + \frac{\eta_{CMOD}^{i-1}}{b_{i-1}B_N}A_{V_{pl}}^{i-1,i}\right)\left(1 - \frac{\gamma_{CMOD}^{i-1}}{b_{i-1}}(a_i - a_{i-1})\right) \tag{45}$$

for plastic J_{pl} calculations. In this equation, η_{CMOD} and γ_{CMOD} are two CMOD-based plastic geometry factors, $A_{V_{pl}}^{i-1,i}$ denotes the incremental area under the P–V_{pl} curve (where V_{pl} is the plastic component of measured CMOD), and is calculated by:

$$A_{V_{pl}}^{i-1,i} = \frac{1}{2}(P_i + P_{i-1})\left(V_{pl}^i - V_{pl}^{i-1}\right) \tag{46}$$

The elastic J_{el} and the total J-integral at each load step are computed by Eqs. (14) and (19), respectively. As in Eq. (33), the γ_{CMOD} term in Eq. (45) is used to correct J to account for crack growth. Note that an equation similar to Eq. (45) was recently proposed by Cravero and Ruggieri [141], using a different analysis for a single edge-notched tension (SE(T)) specimen. For center-cracked tension and compact tension specimens, the LLD data could be estimated directly from the CMOD gages, and thus the two incremental J-integral Eqs. (33) and (45) become identical. In general, Eq. (45) can be used for any specimen, provided that the geometry factors η_{CMOD} and γ_{CMOD} are known a priori for that specimen. These geometry factors can be determined using the accurate finite element analysis. For three-point bend SE(B) specimens, Zhu et al. [140] proposed the following expressions for the two geometry factors:

$$\eta_{CMOD} = 3.667 - 2.199(a/W) + 0.437(a/W)^2 \tag{47a}$$
$$\gamma_{CMOD} = 0.131 + 2.131(a/W) - 1.465(a/W)^2 \tag{47b}$$

These two functions for the geometry factors were obtained from curve-fitting of the available, valid finite element results, and are accurate for a wide range of crack sizes of interest: $0.25 \leqslant a/W \leqslant 0.7$. Thus recently, ASTM E1820–11 replaced the η_{CMOD} expression of Eq. (42) with Eq. (47a). Note that the CMOD-based γ factor is essentially equal to its LLD-based partner. As a result, a constant value of $\gamma_{CMOD} = \gamma_{LLD} = 0.9$ can be used for the standard SE(B) specimen with $0.45 \leqslant a/W \leqslant 0.7$.

Fig. 11 shows two examples of the J–R curves obtained by Zhu and Joyce [142] for HY80 steel using SE(B) specimens with deep cracks of $a/W = 0.5$ and 0.7. In this figure four different J estimation methods are used: E1820 CMOD basic Eq. (41), E1820 A16 CMOD Eq. (44), LLD-based incremental J-integral Eqs. (14), (19) and (33), CMOD-based incremental J-integral Eqs. (14), (19) and (45). As shown in Fig. 11, the basic equation obtained an elevated J–R curve because crack growth correction is not considered, the CMOD direct and indirect methods obtained consistent J–R curves that are slightly higher than the conventional LLD incremental method. This indicates that the newly proposed CMOD direct method is simple, reliable, and somewhat less conservative than the LLD incremental method.

Once the CMOD-based incremental J-integral Eq. (45) was developed, it was added to ASTM E1820 for balloting. In 2009, ASTM E1820 has officially adopted the CMOD direct method and the incremental Eq. (45) for a J–R curve evaluation. As such, the standard test procedures in E1820 are simplified significantly, because only load–CMOD data are needed to record in the fracture test when the elastic unloading compliance method is employed. As a result, the J–R curve testing becomes simpler and more cost-effective, and the results would be more accurate. In addition to this direct CMOD method, Zhu and Leis [143] proposed another indirect CMOD method to evaluate a J–R curve using load–CMOD data for SE(B) specimens. A conversion technique was developed to infer LLD data from CMOD measurements, and the J-integral calculation still uses the LLD-based incremental Eq. (33) in the J–R curve evaluation.

3.9. Normalization data reduction technique

The conventional elastic unloading compliance method and electric potential drop method are difficult or impractical to be implemented in a fracture test under severe test conditions such as high loading rate, high temperature, or aggressive environments. An alternative technique named normalization method was developed to estimate instantaneous crack length directly from the load versus LLD data record. The basis is the principle of load separation [114–116] and the key curve method [126,144]. This technique does not require any devices for online monitoring of crack growth, but suggests an individual calibration curve to be used to determine instantaneous crack size. Different calibration functions were proposed, including a power-law function by Herrera and Landes [145] and Joyce [146], a combined function of power law and straight line by

Herrera and Landes [147], and a three-parameter LMN function by Orange [148] and Landes et al. [149]. The LMN function was improved to be a four-parameter normalization function by Joyce [150] and it is this form that is presently used in E1820.

Basically, the normalization method infers crack length change by comparing the measured and normalized load versus LLD data with the following analytical normalization function:

$$P_N = \frac{c_1 + c_2 \overline{\Delta}_{pl} + c_3 \overline{\Delta}_{pl}^2}{c_4 + \overline{\Delta}_{pl}},$$

(48)

where c_1, c_2, c_3 and c_4 are the curve-fitting coefficients that are determined by the least squares regression method from the normalized load versus plastic displacement curve on which each point ($\overline{\Delta}_{pli}$, P_{Ni}) is calculated from the measured load and displacement data. To obtain a crack-tip blunting corrected normalization function, the measured load data are normalized by:

$$P_{Ni} = \frac{P_i}{WB[1 - a_{bi}/W]^{\eta}},$$

(49)

where i refers the ith loading point, P_{Ni} is a normalized load and a_{bi} is the blunting corrected crack length. From a measured total LLD datum, Δ_i, a normalized plastic LLD, $\overline{\Delta}_{pli}$, is given by:

$$\overline{\Delta}_{pli} = \frac{\Delta_{pli}}{W} = \frac{\Delta_i - P_i C_i}{W},$$

(50)

where C_i is the specimen load-line compliance in reference to the blunting corrected crack length a_{bi}. Using Eqs. (49) and (50), load–displacement data up to, but not including the maximum load, are normalized. The final load–displacement pair is normalized using the same equations except that the final crack length is used without blunting correction. From the normalized points, the normalization function (48) can be determined by curve-fitting. An iterative procedure is then used, adjusting each a_i so that $\overline{\Delta}_{pli}$, P_{Ni} data pairs at each loading point lie on the normalization function of Eq. (48). In this way, crack length at each data point is determined.

Two round-robin test programs were organized by ASTM E08.08 Task Group for validating the normalization method in J–R curve testing for high-rate loading conditions [150] and for static loading conditions [151] using C(T) specimens. Further investigations and applications of normalization method were performed by Dzugan and Viehrig [152], Zhu and Joyce [153], Zhu and Leis [154], and Zhu et al. [155] using SE(B) specimens for different metallic materials. The results showed that the normalization method can be equivalent to the elastic unloading compliance method and the electric potential drop method under quasi-static and dynamic loading conditions. The normalization method was accepted by ASTM E1820–01 and its later versions in Annex A15 "Normalization Data Reduction Technique".

3.10. ASTM E813, E1152, E1737, and E1820 development

As defined by ASTM E1823, the plane strain fracture toughness, J_{Ic}, is the crack-extension resistance under conditions of crack-tip plane strain in mode I for slow rates of loading or substantial plastic deformation. J_{Ic} provides for the measurement of crack-extension resistance near the onset of stable crack extension. A J–R curve is a plot of resistance to stable crack extension, Δa_p (physical crack extension) for ductile materials. This section discusses the J_{Ic} and J–R curve test standard methods and their development history.

A procedure to determine the plane strain fracture toughness J_{Ic} near the onset of ductile crack growth was proposed initially by Clarke et al. [156]. Pin-loaded compact specimens and three-point bend specimens with $a/W = 0.5$ or greater were recommended for use in a fracture test. The J-integral was calculated from the total J estimate using Eq. (18) or (23) with the initial crack size and without consideration of crack growth correction, and the procedure was valid only for small amounts of crack extension, say 2 mm. A partial J–R curve was constructed from data points obtained using five or more specimens if multiple specimen technique was employed or using four crack length measurements within the specified range if the elastic compliance single specimen test was conducted. The J_{Ic} value was defined at the intersection of a linear fit to the $(J, \Delta a)$ pairs in an "inclusion zone" between crack extension limits and a blunting line defined by $J = 2\sigma_{ys}\Delta a$, if all required test criteria were met. This is the so-called bi-linear evaluation of J_{Ic}. In order to ensure the plane strain conditions prevail along the crack front, the minimum specimen thickness and remaining ligament were required for each specimen:

$$B, b > 25(J_{Ic}/\sigma_{ys})$$

(51)

Note that the factor "25" in the above inequity is based on experience. Paris [157] suggested a value of the factor ranging from 25 to 40 to require that CTOD $\approx J_{Ic}/\sigma_{ys}$ as CTOD $\leqslant b_o/(25–40)$ in a valid J_{Ic} test using bending specimens. Others suggested that the multiplier might need to be as large as 50 for various materials [156]. Landes and Begley [158] showed experimentally that the factor of 25 is appropriate for fracture tests of A533B steels. Using rudimentary 2D finite element analysis, Shih and German [94] showed that a factor ranging from 25 to 50 is required to ensure a path independent J characterization of an annular region surrounding the crack-tip in predominantly bending specimens. However, experience indicated that the size criterion in Eq. (51) is sufficient for deep cracked bending specimens.

In terms of this procedure, two round robin programs were conducted on determination of J_{Ic} values for ductile materials of A533B steel [159] and of HY130 steel [160]. The results indicated that the J_{Ic} value obtained using the single specimen test via unloading compliance technique closely agrees with that obtained by the multiple specimen test technique. This J_{Ic} test method became the first ASTM standard for the J-integral testing that was accepted in 1981 and published in 1982 with designation E813–81 [161]. As was the case with ASTM E399 for the K_{Ic} testing, this J_{Ic} standard took nearly 10 years to develop and ballot into a standard. In ASTM E813–81, the J was calculated using the total η-factor Eqs. (18) and (23), respectively for SE(B) and C(T) specimens, and the J_{Ic} was defined as the intersection of the blunting line and a linearly fitted R curve as used in the bi-linear evaluation of initiation toughness. The multiple specimen technique was the recommended standard procedure, but the unloading compliance technique was included in an annex as an option.

Using the unloading compliance technique in a single specimen test, Joyce and Gudas [128] showed from detailed computerized compliance data that the J–R curve is not a straight line as suggested in ASTM E813–81, but is in fact a curve. This conclusion was supported by the experimental observations of Hiser et al. [162] and Jablonski [163]. Moreover, Hiser et al. first suggested the power-law shape of a J–R curve. Thus, J_{Ic} was not clearly defined in E813–81. It was desired that the J_{Ic} offset be an interpolation rather than an extrapolation, and so 0.008 inches (or 0.2 mm) was selected by ASTM to define an offset line parallel to the blunting line, and then to define an engineering approximation of initiation fracture toughness, as shown by J_Q in Fig. 9. Note that the blunting construction line, the 0.15-mm exclusion line, the 0.2-mm offset line, the 1.5-mm exclusive line, the power-law regression curve, the J_{max} limit and the Δa_{max} limit are all included in Fig. 9 to illustrate their definitions used by ASTM E1820. As a result, the J_Q or J_{Ic} was defined as the value of J at the intersection of the 0.2-mm offset line and a power-law fitted J–R curve. This power-law curve fit definition of J_{Ic} was adopted first by ASTM E1152–82 [164] and then by ASTM E813–87. In these two earlier ASTM standards, the J was separated into the elastic and plastic parts, and computed using Eq. (25). Since then, both the multiple specimen test and the single specimen test, side grooves and the unloading compliance technique were allowed as standard procedures.

A tentative test procedure for determining the plane strain J–R curve was presented in 1982 by Albrecht et al. [165], and evaluated by Gudas and Davis [166] in a round-robin program. This tentative test procedure became the ASTM test method for determining J–R curves in 1982 with designation E1152–82 [164]. It is similar in many ways to E813–87, but using crack growth corrected J-integral evaluation and rotation corrected C(T) compliance equation. This standard method was intended to characterize the slow stable crack growth resistance of bend-type specimens in such a manner that it is geometry independent under plane strain conditions. The recommended specimens were the C(T) and SE(B) specimens with deep cracks of $0.5 \leqslant a_0/W \leqslant 0.75$, and the limit allowed on crack extension was $0.06b_o$. The recommended test method was the elastic unloading compliance technique to measure crack length and crack extension from a single specimen test, though the multi-specimen procedure of E813 was allowed. For a growing crack, the crack growth corrected J-integral was calculated incrementally using the total J-integral Eq. (32) in ASTM E1152–82, with an essential assumption of $\eta_{el} = \eta_{pl}$.

In the revisions of ASTM E1152–87 and ASTM E399–89, the J-integral was evaluated in the separate elastic and plastic parts using the relationship in Eq. (25) for J_{el} and Eqs. (33)–(36) for J_{pl}. The objective was to improve the accuracy of J estimates, and to obtain consistency of J when near linear elastic conditions predominate. A valid J–R curve is consisted of the measured data points in a region bounded by the coordinate axis and the J_{max} and Δa_{max} limits, as illustrated in Fig. 9. These two limits describe the measurement capacity of test specimen. The maximum J-integral capacity for a specimen was given by the smaller of:

$$J_{max} = b\sigma_Y/20 \quad \text{or} \quad J_{max} = B\sigma_Y/20 \tag{52}$$

where σ_Y is an effective yield strength assumed as the average of the 0.2% offset yield strength σ_{ys} and the ultimate tensile strength σ_{ts}. The maximum crack extension capacity for a specimen was modified as:

$$\Delta a_{max} = 0.1b_0 \tag{53}$$

where b_0 is the initial crack ligament. These criteria in Eqs. (52) and (53) were all relaxations of the earlier version requirements, relaxing the J_{max} requirement from 25 to 20 and the crack extension limit from 6% to 10% of b_0.

In 1996, the last versions of ASTM E813–89 and E1152–95 were merged into a single standard with the designation E1737–96 [167], and were withdrawn in 1997. In this combined standard E1737, the test procedures, specimen requirements and validity criteria are essentially the same as the previous two standards. For instance, the recommended specimens included C(T), SE(B) and DC(T) specimens with deep cracks of $0.45 \leqslant a_0/W \leqslant 0.70$. The recommended test methods included the elastic unloading compliance technique and the electrical potential drop technique for a single specimen test. The multi-specimen test method was allowed to be used to evaluate the single value of J_{Ic}. If a single specimen technique was used, the crack growth corrected J values were obtained from Eqs. (14), (33) and (19) with the measured crack length. If multi-specimen procedure was used, the J value was calculated for each specimen from Eq. (25) with the original fatigue precracked length. The plane strain specimen size requirements in Eq. (51) and the specimen capacity requirements in Eqs. (52) and (53) remained the same as ASTM E1152–87, however, the J_{Ic} definition was changed to the intersection point of the J–R curve and the 0.2 mm offset blunting line expressed by $J = M\sigma_Y(\Delta a - 0.2$ mm$)$ with $M \geqslant 2$. The default value of M was 2, but a procedure was allowed to evaluate a larger value of M in those cases, like some stainless steels, where a larger value of M seemed appropriate.

In parallel to the development of combined fracture toughness test standard ASTM E1737–96 for J_{Ic} and J–R curve testing, a more general and flexible fracture toughness test standard was in progress due to the major efforts of Profes-

sor John Landes at the University of Tennessee. In the 1990s, different ASTM standard procedures and methods were available for determining different fracture parameters, i.e., E399 for the K_{Ic} testing [13], E813 for the J_{Ic} testing [161], E1152 for the J–R curve testing [164], and E1290 for the crack-tip opening displacement (CTOD or δ) testing [168]. If a test was attempted and the test produced an invalid result, a different standard procedure usually could not be applied to the available data to give valid measure of toughness using one of the other standards. The difference between these standards was usually not based on technical requirements but were more often on test procedure preferences of the laboratories or authors represented in the individual standard writing groups, as pointed out by Landes [22]. Since all of the different toughness tests used the same basic specimen types, the same equipment, and basically the same test procedure, more flexible toughness tests were desired at that time. This prompted the formation of a unified or common test standard ASTM E1820–96 [169] for measurement of different fracture toughness parameters using one common test procedure that was published in 1997 as a combination of ASTM E399, E813, E1152, E1737 and E1290. Landes and Brown [170,171] presented the evaluation results of a round robin test program conducted between February 1991 and June 1992 for this combined standard E1820 of its tenth draft [172]. Note that after ASTM E1820–96 was published, ASTM E1737–96 was withdrawn in 1998.

The combined standard ASTM E1820–96 provided test methods to develop a set of multi-specimen data or continuous load–displacement record that can be used to evaluate initiation toughness values or resistance curves in terms of the fracture toughness parameters K, J and δ. The J-integral procedures were nearly identical to E1737 with the DC potential drop Annex removed. The E1290 δ and δ–R curve procedures were included. The E399 equivalent K_{Ic} procedures were included, but allowed side grooves and high rate tests. The recommended specimens in ASTM E1820 were SE(B), C(T) and DC(T) specimens with deep cracks of $0.45 \leqslant a_0/W \leqslant 0.70$ for J and δ determinations, but the crack length was restricted to the range of $0.45 \leqslant a_0/W \leqslant 0.55$ for K_{Ic} determination. However, experimental results of Joyce and Smudz [57,58] showed that the standard J-integral specimens with deep cracks of $0.45 \leqslant a_0/W \leqslant 0.70$, incorporating CMOD measurements and side grooves, can be used to obtain K_{Ic} as defined by ASTM E399.

Both the multiple specimen technique and the single specimen technique via the elastic unloading compliance method were allowed by ASTM E1820. Two test procedures were developed in E1820: a basic procedure directed toward evaluation of a single value of K_{Ic}, J_{Ic} or δ_{Ic} without use of crack extension measurement equipment, and a resistance curve procedure directed toward evaluation of a complete fracture toughness resistance curve using crack extension measurement equipment. The later procedure also included the evaluation of single-point toughness values. The basic procedure allowed multi-specimen tests and the toughness evaluations used the original crack sizes. However, the resistance curve procedure required only single specimen tests and the toughness evaluation used the unloading compliance measured crack sizes. The K_{Ic} definition was the same as in ASTM E399, the J_{Ic} definition was the same as ASTM E1737, and the δ_{Ic} definition was the same as ASTM E1290. In the present ASTM E1820–11, the CTOD evaluation uses the J-integral conversion procedures. The plane strain specimen size requirements remain the same as those in E399 and E1737, but the maximum Δa criterion in Eq. (53) was changed, based on experimental work of Joyce et al. [173,174], for a valid J–R curve or δ–R curve as:

$$\Delta a_{max} = 0.25 b_0 \tag{54}$$

This crack growth limit was recently confirmed by Landes [175] and Wallin [176] using statistical analyses for different databases obtained from the single specimen test and the multiple specimen test. These authors further pointed out that if the maximum crack extension criterion in Eq. (54) is satisfied, the J_{max} criterion may be not needed. Thus recently, ASTM E1820–11 has relaxed the J_{max} criterion by increasing the J_{max} value in Eq. (52) through use of 10 rather than 20 in the denominator, i.e., $J_{max} = b\sigma_Y/10$ and $J_{max} = B\sigma_Y/10$. Zhu and Leis [88] showed that Eq. (54) can also be used as the validity criterion for C(T) specimens in the E561 K–R curve test.

Over the years, ASTM E1820 has undergone a series of revisions, while the standards, E813, E1152, and E1737 have been allowed to lapse. In parallel, significant improvements have been added in the annexes of the present E1820–11. In particular, Annex A4 describes the methods for evaluating fracture instability and pop-in results; Annex A5 describes the methods for determining K_{Ic} similar to ASTM E399; Annex A6 describes fracture instability toughness determination using J and the basic procedure; Annex A7 describes fracture instability toughness determination using CTOD (δ); Annex A13 describes the methods for rapid loading K_{Ic} determination that is similar to Annex A10 of ASTM E399; Annex A14 describes special requirements for J-integral fracture toughness and J–$R(t)$ curve testing under rapid-load or drop weight conditions. Annex A15 describes the normalization method as an alternative to determine crack length directly for high loading rate and other aggressive test conditions, while Annex A16 presents a procedure to evaluate a crack growth correction procedure for a J–R curve evaluated using the basic multi-specimen procedure.

Other changes in ASTM E1820–11 include adoption of the more accurate expression for the η_{CMOD} factor in Eq. (47a) and the CMOD-based incremental J-integral Eq. (45) for SE(B) specimens. Presently in ballot is an Annex prescribing a test procedure for precracked Charpy size SE(B) specimens tested at elevated loading rates, an Annex providing procedures on testing shallow crack specimens to evaluate the effect of this contribution of low constraint on the material resistance curves defined by J or δ, and an Annex to include E1921 or the procedures made E1921 friendly for calculation of J_c at the onset of cleavage for the master curve calculations. Further improvements and fulfillments will continue to be made so that ASTM E1820 remains the most comprehensive tool for fracture toughness testing.

4. Cleavage toughness K_{Jc} testing and reference temperature T_0 determination

4.1. K_{Jc} concept and cleavage fracture

Fracture behavior of metallic materials relates to the micromechanism of fracture and to the stability of the fracture process. It is usually characterized as being ductile or brittle. Ductile fracture occurs by the formation, growth and coalescence of voids and microcracks, and results in slow, stable crack growth. This process is relatively insensitive to temperature and loading rate, and results in the dissipation of large amounts of energy per unit crack growth. Brittle fracture is most dramatic when it occurs by transgranular cleavage, and results in rapid, unstable crack growth. This cleavage process is initiated at a small number of initiation sites that are exposed to the elevated stress and strain field in the vicinity of the crack tip, and the fracture process absorbs very little energy per unit of crack growth. As the case of ductile fracture, the mechanism of brittle fracture, when the amount of energy released by the structure exceeds the amount of energy absorbed by the crack extension, can be insensitive to the temperature or loading rate over the range typical of engineering structural applications. However, if the load environment is predominantly load controlled and macroscopically unstable, fracture can occur even when the micromechanism of fracture is characterized by the growth and coalescence of voids and microcracks.

Fracture behavior of ferritic steels whether of carbon, low alloy, or high alloy grades can demonstrate ductile fracture at elevated temperatures, but can transition from stable ductile fracture to unstable brittle fracture at lower temperatures occurring by cleavage on specific crystallographic planes over a narrow range of temperature with the fracture toughness being suddenly reduced by a factor of 5 or more. As a consequence, in most applications the stability of the ductile fracture performance is eliminated and the fracture process becomes unstable and catastrophic. The temperature at which this transition occurs is strongly dependent on the rate of loading in the crack-tip region, and is also strongly dependent on details of the crack-tip field not characterized fully in the usually dominant first-order singularity term. This dramatic transition exhibits three primary regions of fracture toughness: lower shelf, ductile-to-brittle transition and upper shelf. Correspondingly, they must be characterized by a lower shelf fracture toughness value, an upper shelf fracture toughness value and a transition temperature. On the lower shelf, the single-point toughness K_c is used to characterize brittle fracture. On the upper shelf, the single-point toughness, J_{Ic}, and the J–R curve are used to describe ductile fracture. In the ductile-to-brittle transition region, the single-point toughness K_{Jc} converted from J_c can be used to describe cleavage fracture. Since the onset of cleavage depends on a "weakest link" trigger and the cleavage micromechanism of fracture, it generally results in unstable crack extension and highly variable initiation toughness [177–179], and thus a statistical analysis must be performed. Sorem et al. [180] showed that shallow crack specimens exhibited increased toughness at the initiation of ductile tearing and a decreased ductile-to-brittle transition temperature. MacLennan and Hancock [181] showed the effect of the loss of constraint on lower shelf toughness and in the ductile–brittle transition. In order to understand the experimental scatter, more stringent size requirements for obtaining a size and geometry independent J_c value were studied by Anderson and Dodds [182], and different constraint parameters such as the T-stress and Q-stress were proposed to show a measurable effect on the J_c values (see Section 6). However, the nature of cleavage toughness scatter remained unexplained and a method to quantify the scatter was needed.

Based on the weakest link theory [178,183] and the Weibull statistics theory [184], Wallin proposed a master curve method with a corresponding reference temperature [185] to provide a description of the statistical scatter, statistical size effects and temperature dependence of cleavage toughness in the transition region and on the lower shelf. The master curve method is not applicable on the upper shelf and Weibull statistics are used to provide the confidence bounds on the temperature above which cleavage fracture is unlikely to exist. The temperature at which the lower shelf, cleavage dominated fracture transitions to the much higher toughness ductile fracture regime depends on loading rate, specimen geometry and crack-tip constraint. The Wallin method utilizes a statistical analysis procedure to establish a "master curve" relationship between the elastic–plastic equivalent critical stress intensity factor K_{Jc} versus temperature through the ductile-to-brittle transition. The parameter K_{Jc} is derived from individual J_c test data at the onset of cleavage fracture using the relationship:

$$K_{Jc} = \sqrt{\frac{EJ_c}{(1 - v^2)}} \tag{55}$$

where J_c is calculated at the cleavage instability point using Eq. (23) according to the basic procedure of ASTM E1820 in plane strain conditions.

4.2. Weibull statistical model

Based on weakest link statistics and using the parameter J_c, Landes and Shaffer [177] first developed a statistical model using the two-parameter Weibull function, and Landes and McCabe [186] used the three-parameter Weibull function to describe the scatter of J_c data. Similarly, Wallin [178] and Wallin et al. [187] obtained a useful engineering statistical model using the parameter K_{Jc}, and showed that the cumulative probability of failure by cleavage fracture for structural steels at a specific temperature can be well characterized by the three-parameter Weibull distribution:

$$P_f = 1 - \exp\left\{-\left(\frac{K_{Jc} - K_{min}}{K_0 - K_{min}}\right)^\beta\right\} \tag{56}$$

where K_{Jc} is the fracture toughness obtained from Eq. (55) via individual J_c test data, P_f is the cumulative failure probability, K_0 is a scale parameter equal to the fracture toughness corresponding to 63.2% failure probability, K_{min} is the lower bound (threshold) fracture toughness, and β is the Weibull shape parameter. In principal, these three parameters (K_0, K_{min}, β) should be obtained by a best fit method for each set of toughness data. Application of Eq. (56) to a wide range of existing data available for ferritic steels [178,185] showed that unless very large data sets were developed it was best to assume two of the three parameters in Eq. (56) since the cumulative probability distribution of fracture toughness has nearly the same shape, and is independent of specimen size and test temperature. Technical arguments led to the assumption of $\beta = 4$ and $K_{min} = 20$ MPa $\sqrt{m}$ in plane strain, small-scale yielding conditions. As such, the only fitting parameter of the Weibull distribution to the K_{Jc} data is K_0, and this parameter can be defined using a relatively small number of specimens. The evaluation can be done as a graphical fit as often utilized in Weibull statistics. However, it can also be determined from the maximum likelihood statistical method. In this procedure, a small number of fracture toughness test results are required at a given temperature, and the scale parameter K_0 is calculated by:

$$K_0 = \left[\sum_{i=1}^{N} \frac{(K_{Jc(i)} - 20)}{N}\right]^{1/4} + 20 \; (\text{MPa } \sqrt{m}) \tag{57}$$

where $K_{Jc(i)}$ is measured fracture toughness of the tested specimen, and N is the number of K_{Jc} values. Occasional specimens can cleave at elevated toughness levels exceeding the small-scale yielding conditions at the crack tip. Rather than ignore these data, they are censored instead, recognizing that the data point exists but the value is unknown except that it exceeds a $K_{Jc(limit)}$ value given by:

$$K_{Jc(\text{limit})} = \sqrt{Eb_0\sigma_{ys}/M} \tag{58}$$

where σ_{ys} is the 0.2% offset yield strength at the test temperature, b_0 is the original ligament and M is a parameter between 30 and 200. Specimens can also be censored if ductile crack extension is observed before the attainment of cleavage initiation in an individual test, and in this case $K_{Jc(\text{limit})}$ is taken to be K_{Jc}.

In order to directly compare toughness data obtained from different thickness specimens, a statistical size correction is employed to equilibrate the highly stressed material volume sampled at the crack tip by cleavage. Each value of toughness K_{Jc} data measured for a particular specimen thickness is converted to an equivalent value for a reference 1 T specimen with thickness $B_{1T} = 25$ mm using the following equation [188]:

$$K_{Jc(1T)} = K_{min} + (K_{Jc(X)} - K_{min})\left(\frac{B_X}{B_{1T}}\right)^{1/4} \tag{59}$$

where B_X refers to the nominal thickness of the tested specimen in millimeters, regardless of side grooves. $K_{min} = 20$ MPa $\sqrt{m}$, $K_{Jc(1T)}$ denotes the equivalent toughness of the 1 T specimen, and $K_{Jc(X)}$ is measured fracture toughness of the tested specimen other than 1 T size. Note that the test data conversion is often performed first using Eq. (59) to calculate the equivalent $K_{Jc(1T)}$ values, and then using Eq. (57) to obtain the equivalent $K_{0(1T)}$ value that is needed to determine an 1 T-size equivalent median toughness $K_{Jc(med)1T}$, as discussed next. Care must be taken in a structural application to incorporate an equivalent form of this statistical size correction if the structural crack length is large compared to 25 mm.

4.3. Master curve method

Motivated by the ASME K_{Ic} design curve for describing transition fracture failure [189], Wallin [190–192] at the Technical Research Center of Finland (VTT) proposed the master curve concept and defined a temperature dependence for cleavage fracture toughness to be the master curve of median toughness for 1 T specimens over the transition range for ferritic steels in the following form:

$$K_{Jc(med)1\,T} = 30 + 70\exp[0.019(T - T_0)] \tag{60}$$

where $K_{Jc(med)1T}$ represents an equivalent median toughness for test specimens other than 1 T size and has units in MPa $\sqrt{m}$, T is test temperature in degree C, and T_0 is a reference temperature at which $K_{Jc(med)1T}$ is set to be 100 MPa $\sqrt{m}$. If T_0 is known for a material, the master curve in Eq. (60) or fracture toughness over temperature in the transition region is determined completely. This master curve method assumes that the toughness versus temperature relationship in Eq. (60) is universal for all ferritic steels [193].

From the equivalent scale parameter $K_{0(1T)}$ obtained from Eq. (57) using the $K_{Jc(1T)}$ values, the equivalent median toughness $K_{Jc(med)1T}$ result of a data population that corresponds to the 50% cumulative failure probability is calculated by:

$$K_{Jc(med)1\,T} = K_{min} + (K_{0(1T)} - K_{min})\{\ln(2)\}^{1/4} \tag{61}$$

There are two approaches available for estimating the master curve reference temperature T_0. The first one is used when data are measured at a single test temperature, with T_0 determined from the equivalent median toughness $K_{Jc(med)1T}$ value and test temperature T using Eq. (60) in the form of:

$$T_0 = T - \frac{1}{0.019} \ln \left(\frac{K_{Jc(med)1T} - 30}{70} \right) \tag{62}$$

The second approach is used when data are measured at more than one test temperature, with T_0 determined from the size adjusted $K_{Jc(1T)}$ data using a multi-temperature randomly censored maximum likelihood expression [193,194]:

$$\sum_{i=1}^{N} \frac{\delta_i \exp\{0.019(T_i - T_0)\}}{11 + 77 \exp\{0.019(T_i - T_0)\}} - \sum_{i=1}^{N} \frac{(K_{Jc(i)} - 20)^4 \exp\{0.019(T_i - T_0)\}}{(11 + 77 \exp\{0.019(T_i - T_0)\})^5} = 0 \tag{63}$$

where N is the number of tested specimens, T_i is the test temperature corresponding to $K_{Jc(i)}$, δ_i is 1 if the datum is valid, or 0 if it is invalid. Eq. (63) is solved iteratively to determine T_0. Merkle et al. [193] showed that the multi-temperature procedure results in a T_0 value equivalent to the single temperature procedure.

With the T_0 value, the master curve function in Eq. (60) is fully determined, and then the lower and upper tolerance bounds of the master curve can be calculated from the following equation:

$$K_{Jc(0.xx)} = 20 + \left[\ln \left(\frac{1}{1 - 0.xx} \right) \right]^{1/4} \{11 + 77 \exp[0.019(T - T_0)]\} \tag{64}$$

where 0.xx represents the selected cumulative probability level; for example, 0.xx = 0.95 implies a 95% confidence of survival to that K_{Jc} level at the temperature T. Based on Eq. (64), different tolerance bounds for the toughness distribution can be constructed as needed. An example of a master curve with 95% upper bound and 5% lower bound is given in Fig. 12, where the test data of K_{Jc} was obtained using 1/2 T CT specimens at −75 °C for A533B steel.

4.4. ASTM E1921 development

ASTM E399 and E1820 basically infer normal statistics and imply at least that two or three test results can be averaged to give a toughness measurement, and the statistical analysis can be used to obtain standard deviation for applications. ASTM E399 could be used on the lower shelf to obtain some K_c values, but testing on the lower shelf is insensitive to temperature and cannot be used to measure T_0. ASTM E1820 provides the procedure to obtain K_{Jc} values, but characterizing the results requires the statistical analysis as prescribed in the master curve method. Therefore, a new ASTM standard entitled Standard Test Method for Determining of Reference Temperature T_0 for Ferritic Steels in The Transition Range was published in 1997 with designation as E1921–97 [195]. The present version is ASTM E1921–11 [18]. This standard is based on the master curve method developed primarily by Wallin [178,188,190–192,194] as described above, and provides the procedures for determination of the reference temperature T_0 to characterize the fracture toughness K_{Jc} of ferritic steels that experience onset of cleavage cracking at elastic or elastic–plastic instabilities in the ductile-to-brittle transition region. The specific types of ferritic steels have the yield strengths from 275 to 825 MPa. The recommended specimens are fatigue-precracked SE(B), C(T) and DC(T) specimens, and precracked Charpy size SE(B) specimens are allowed. The suggested crack aspect ratio a/W is 0.5 nominally for all specimens and the target loading rate is 1 MPa $\sqrt{m}$/s. Specimen width in compact specimens is two times the thickness. In bend bars, specimen width can be either one or two times the thickness. A technical support doc-
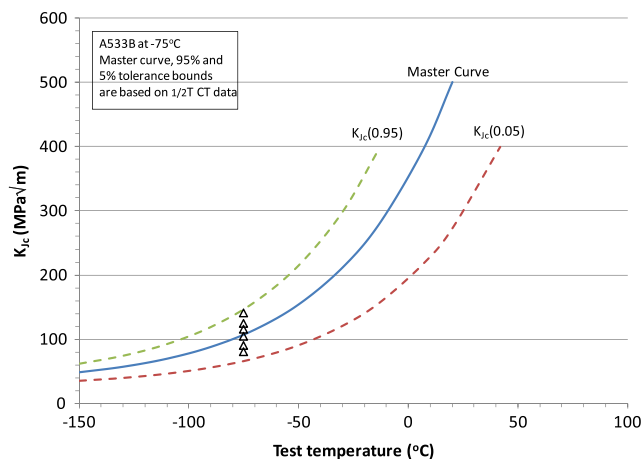

Fig. 12. A master curve of ductile-to-brittle fracture toughness for A533B steel with 95% upper and 5% lower tolerance bounds.

ument for ASTM E1921–97 prepared by Merkle et al. [193] includes much of the rationale behind the requirements of this new standard. A large database of applicable historical testing provided by Kirk et al. [196] also supports much of the basis for this standard. Joyce and Tregoning [197] evaluated this standard using toughness data obtained from precracked Charpy specimens for determining the reference temperature T_0 for different steels. Other relevant investigations can be found in the manual of the master curve method by McCabe et al. [185].

At least six tests are required in ASTM E1921 for estimating the median K_{Jc} of the Weibull distribution of the measured data population and for determining a valid reference temperature T_0. The test temperature range limits within $-50\,°C < T - T_0 < 50\,°C$ to ensure that the tests are performed in the transition region where the fracture probability is governed by the weakest link failure. There are two validity criteria for quantification of toughness K_{Jc} data. The first one sets the maximum K_{Jc} capacity of the specimen using the $K_{Jc(limit)}$ criterion in Eq. (58) with $M = 30$. The other one limits the maximum stable, ductile crack growth to be the smaller of:

$$\Delta a_{max} = 0.05(W - a_0) \quad \text{or} \quad \Delta a_{max} = 1.00 \text{ mm} \tag{65}$$

If a specimen exceeds the $K_{Jc(limit)}$ criterion, the measured K_{Jc} value is invalid and shall be replaced by $K_{Jc(limit)}$ for the specimen size used in the data censoring procedure. If the maximum crack growth criterion is violated, the K_{Jc} value also shall be regarded as invalid and replaced with the highest valid K_{Jc} in the data set for any specimen size in the censoring procedure.

The $K_{Jc(limit)}$ requirement used in ASTM E1921 is intended to denote the maximum allowable toughness at which the calculated T_0 value is unaffected by constraint loss. Presently, $M = 30$ is used in Eq. (58) to define $K_{Jc(limit)}$ for C(T), SE(B) and precracked Charpy specimen geometries. However, Joyce and Tregoning [198] showed that this single limit is likely to result in specimen geometry-dependent estimates of the master curve reference temperature T_0. These authors suggested that $M_{limit} = 30$ be adequate for the compact specimen, but $M_{limit} = 150$ should be required for the bend specimen. It was thus recommended that C(T) specimens be used when a geometry-insensitive T_0 value and the associated master curve are desired. Constraint correction procedures have been proposed by several authors as discussed in Section 6, but have not yet been considered into ASTM E1921.

The first version of ASTM E1921–97 [195] incorporated loading rate limits directly from the quasi-static loading sections of E1820 that have been developed for measurement of elastic–plastic fracture toughness on the upper shelf using the J–R curve method. The experimental data of Joyce et al. [199] supported the loading rate range allowed by the present version ASTM E1921–11 [18]. The change results in a reduction of the original allowed dK/dt range from approximately 100 (0.1– 10 MPa $\sqrt{\text{m}}$/s) to 20 (0.1–2.0 MPa $\sqrt{\text{m}}$/s), with a targeted $dK/dt = 1.0$ MPa $\sqrt{\text{m}}$/s. This corresponds to an allowed rate effect on the T_0 measurement of 10 °C or less. The previously allowed range of loading rate adopted from the quasi-static sections of E1820 did not recognize the sensitivity of the reference temperature T_0 to loading rate in the ductile-to-brittle transition. Loading rate effects can be correlated using the analysis of Wallin [200] if loading rates are more rapid than this quasi-static range in the application of interest.

5. CTOD and CTOA-based fracture testing

5.1. CTOD concept and estimation

In addition to the K and J concepts described above, another important fracture mechanics parameter is the crack-tip opening displacement (CTOD) first proposed by Wells [3] at the British Welding Institute. Initially, Wells referred to this quantity as the crack opening displacement (COD), but more recently the name has been changed to CTOD to distinguish the quantity from the crack mouth opening displacement (CMOD), a physical crack opening displacement measured across the crack mouth at the specimen surface. Wells developed the CTOD approach in order to extend the elastic stress intensity factor approach into elastic–plastic yielding conditions. Using the Irwin's estimate of plastic zone size and the elastic displacement solutions for a center-cracked infinite plate, the CTOD (δ) was approximated as:

$$\delta = \frac{4}{\pi} \frac{K_I^2}{E\sigma_{ys}} \tag{66}$$

Wells recognized that the factor $4/\pi$ is inconsistent with the energy balance approach (which would require a factor of unity), and subsequently omitted this factor. The CTOD criterion assumes that fracture occurs when a critical δ_c measured in a specimen configuration is met or exceeded: that is $\delta \geqslant \delta_c$ in the structural application. From Eq. (66), this displacement criterion is equivalent to the K criterion for a linear elastic crack.

By means of the plane stress strip yield model proposed by Dugdale [30] for perfectly plastic materials, Goodier and Field [201] and Burdekin and Stone [202] obtained a more accurate expression of CTOD for the center-cracked infinite plate in tension:

$$\delta = \frac{8\sigma_{ys}a}{\pi E} \ln \sec \left(\frac{\pi}{2} \frac{\sigma}{\sigma_{ys}} \right) \tag{67}$$

For applied stresses far less than the yield stress, i.e., $\sigma \ll \sigma_{ys}$, Eq. (67) reduces to:

$$\delta = \frac{K_I^2}{E\sigma_{ys}} \tag{68}$$

This equation is the same as Eq. (66) if the factor $4/\pi$ is omitted. The development of CTOD and the relationship in Eq. (67) preceded the development of the J-integral by several years, and thus obtained extensive applications in elastic–plastic fracture mechanics analysis during the 1960s. For instance, based on a series of wide-plate tests, Harrison et al. [203] in The British Welding Institute proposed the "COD Design Curve" approach, and developed its application procedure for various engineering structures including offshore rigs, oil and gas pipelines, pressure vessels.

Applying the J-integral to the Dugdale model, Rice and Rosengren [91] obtained the following general relationship between J and CTOD:

$$J = m\sigma_{ys}\delta \tag{69}$$

where $m = 1$ for plane stress conditions. For actual stress states, the constraint factor m has values between 1 and 2, as shown by Hollstein and Blauel [204]. Eqs. (68) and (69), taken together with Eq. (3), show the equivalence of the fracture mechanics parameters (G, K, J and δ) under linear elastic conditions. The work of Dawes [205] showed that the two fracture parameters CTOD and J are linearly related in elastic–plastic conditions so that they are equally useful as fracture characterizing parameters. Detailed elastic–plastic finite element results of Shih and German [94] showed that the unique J–δ relationship in Eq. (69) applies well beyond linear elastic fracture mechanics. To consider the strain hardening effect, the yield stress σ_{ys} in Eq. (69) is commonly replaced by the effective yield stress σ_Y that is the average of σ_{ys} and σ_{ts}. Different expressions of the constraint factor m have been formulated as functions of crack aspect ratios from extensive elastic–plastic finite element analyses by Kirk and Wang [206] and Wang et al. [207] for SE(B) specimens and by Panontin et al. [208] for C(T) specimens. Wilson and Landes [209] pointed out that the plastic hinge model used in ASTM E1290 at the time was inconsistent with the converted results from the J calculation procedure in ASTM E813.

The use of CTOD criterion requires a laboratory measurement of a critical CTOD value, δ_c, usually associated with the onset of cleavage fracture under plane strain conditions. Such a measurement near the vicinity of the blunting crack tip is difficult and subjective. Initial measurements were made using injection and removal of dental implant compound. The early approaches for CTOD measurements were reviewed by Burdekin [210]. The subsequent measurements were estimated using geometrical models inputting displacement measurements made remotely from the crack tip. In particular, a plastic hinge model was developed by Hollstein and Blauel [204] to determine CTOD by assuming that two arms of the specimen rotate rigidly about a plastic hinge point in the uncracked ligament. In order to apply the plastic hinge model to both elastic and elastic–plastic conditions, the total δ is separated into elastic and plastic components, just like the J separation. The plastic component δ_{pl} is determined from the plastic CMOD in terms of the plastic hinge model, and the elastic component δ_{el} is calculated from the applied stress intensity factor K. Hellmann and Schwalbe [211] at GKSS in Germany proposed a general estimate of CTOD:

$$\delta = \frac{K^2(1-v^2)}{2\sigma_{ys}E} + \frac{\lfloor r_p(W-a) + \Delta a\rfloor V_{pl}}{\lfloor r_p(W-a) + a + Z\rfloor} \tag{70}$$

where a is the crack length, Δa is the crack extension, V_{pl} is the plastic component of CMOD, Z is the distance of knife edge measurement point from the front face of specimen, $r_p(W-a)$ denotes the distance of the plastic hinge point from the crack tip, and r_p is the plastic rotation factor that was obtained from the limit load analysis as given by Wu et al. [212,213]. It was accepted that $r_p \approx 0.44$ for deep-cracked SE(B) specimens, and $r_p \approx 0.46$ for C(T) specimens. It was latter realized that the factor r_p is not a constant, but depends on the a/W ratio and material properties, and this has given a renewed stimulus to efforts to obtain δ from J-integral measurements. Eq. (70) was proposed for the critical δ_c testing with $\Delta a = 0$, but can also be used for δ-based crack growth resistance curve evaluation. Note that δ was used as an important toughness parameter in the pipeline and offshore industry during the development of North Sea oil field, and it continues to be important in the industry worldwide.

5.2. CTOD testing and ASTM E1290 (E1820) development

The details of early CTOD testing practice were documented in Burdekin [210] and Nichols [214]. The first CTOD test standard is BS 5762 [215] that was developed by the British Standards Institution (BSI) and published in 1979. In this CTOD standard, the plastic hinge model in Eq. (70) was adopted for estimating the critical δ_c from CMOD measurements. The plastic hinge model remains in use in the latest unified Britain Standard BS 7448–1991 [216]. A similar CTOD test standard using the plastic hinge model was published by ASTM with designation E1290–89 [217] in 1989, and then incorporated into the three-parameter K, J, δ combined standard ASTM E1820–96 [169] in 1996. As a result, the CTOD test methods in ASTM E1290 and ASTM E1820 are similar. The former focuses only on the critical δ_c at the onset of cleavage, while the latter includes a basic procedure for obtaining the critical δ_c value, a ductile initiation value δ_i similar to J_{Ic}, and a resistance curve procedure for generating a δ–R curve, similar to J–R testing. The test method in E1290 is comparable to the basic procedure in E1820, and essentially evaluates critical CTOD values, δ_c and δ_u corresponding to the onset of cleavage fracture without and with significant prior slow stable crack extension.

From its earliest development by The Welding Institute (TWI) the CTOD approach was directed to the fracture testing of welds and to the assurance that the weld of interest, tested in ASTM E1290 in "the full section of interest" would not cleave in the structural application. Since the weld microstructure of interest was often close to the test sample surface (or structure surface) it was felt important to extend this standard to shallow crack geometries. The geometrical approach to evaluate CTOD was found to be strongly dependent on crack length for $a/W < 0.45$ as well as a function of strain hardening. Rather than develop rotation factor relationships for these cases it was felt that obtaining CTOD from the J-integral, using the CMOD-based J relationship which had be demonstrated to be insensitive to strain hardening was a better approach. Using the improved expressions for m obtained by Wang et al. [207] for SE(B) specimens and Panontin et al. [208] for C(T) specimens from elastic–plastic finite element calculations, an accurate CTOD estimate becomes possible directly from the J value using Eq. (69). In 2002, ASTM E1290 discarded the plastic hinge model, and adopted the J conversion Eq. (69) to determine the critical δ_c value. Correspondingly, ASTM E1820 revised the CTOD calculation method in 2005. The recommended specimens in these two standards are fatigue-precracked SE(B), C(T) and A(B) specimens with nominal crack aspect ratios of $0.45 \leqslant a_0/W \leqslant 0.70$. The development of a shallow crack annex to E1820 is viewed as the final step to obtaining δ_c and J_c values for shallow crack configurations, and this is presently available in a draft format. The lower constraint present in these configurations will elevate the apparent fracture toughness, but if the microstructure of interest is found only at the shallow crack location, the test must be conducted with the shallow crack configuration and the interpretation of the test done accurately and consistently.

In the present ASTM E1820–11 [15], CTOD is calculated using Eq. (69) in the form of:

$$\delta = \frac{J}{m\sigma_Y} = \frac{1}{m\sigma_Y}\left[\frac{K^2(1-v^2)}{E} + J_{pl}\right] \tag{71}$$

where the plastic component J_{pl} is calculated using Eq. (23) or (41) adopted in the basic procedure and using Eq. (33) adopted in the resistance curve procedure, and m is a function of crack size and material properties:

$$m = A_0 - A_1\left(\frac{\sigma_{ys}}{\sigma_{ts}}\right) + A_2\left(\frac{\sigma_{ys}}{\sigma_{ts}}\right)^2 - A_3\left(\frac{\sigma_{ys}}{\sigma_{ts}}\right)^3 \tag{72}$$

with

$$A_0 = 3.18 - 0.22\left(\frac{a_0}{W}\right), \quad A_1 = 4.32 - 2.23\left(\frac{a_0}{W}\right),$$
$$A_2 = 4.44 - 2.29\left(\frac{a_0}{W}\right), \quad A_4 = 2.05 - 1.06\left(\frac{a_0}{W}\right) \tag{73}$$

for SE(B) specimens and

$$A_0 = 3.62, \quad A_1 = 4.21, \quad A_2 = 4.33, \quad A_3 = 2.00 \tag{74}$$

for C(T) specimens. The calculation of CTOD using Eq. (71) requires $\sigma_{ys}/\sigma_{ts} \geqslant 0.5$.

In the present ASTM E1290–08e1 [16], the CTOD determination is similar to the basic procedure in E1820–11 and is calculated using:

$$\delta = \frac{1}{m\sigma_Y}\left[\frac{K^2(1-v^2)}{E} + \frac{\eta_{CMOD}A_{CMOD}^{pl}}{B(W-a_0)\{1 + Z/(0.8a_0 + 0.2W)\}}\right] \tag{75}$$

where Z is the distance of the knife edge measurement point from the front face of SE(B) specimens, the expression of m is the same as Eq. (72) with the same coefficients in Eqs. (73) and (74). Comparison of Eqs. (75) and (41) shows that the Z term is used in Eq. (75) and thus E1290. In addition, ASTM E1290 has withdrawn the use of inaccurate expression of η_{CMOD} in Eq. (42), but uses the more accurate equation, (47a). Recently, Tagawa et al. [218] found that ASTM E1290–08e1 tends to give a smaller value of δ_c than BS 7448. Thus, further investigations are needed to resolve the differences between these two standards.

5.3. CTOA testing and ASTM E2472 development

The crack tip opening angle (CTOA) is defined as the average angle of the two crack surfaces measured at a point 1 mm behind the crack tip. Note that the CTOD corresponding to the CTOA definition here is different from that used in ASTM E1290 and E1820, but takes the value of crack-opening displacement at an arbitrary 1 mm point back from the crack tip. The CTOA fracture mechanics method was developed primarily to characterize the stable crack extension behavior for thin-walled materials in low constraint conditions. The early experimental work and FEA results of Kanninen et al. [219] showed that after a short initiation phase the CTOA attains a steady state condition which means that the crack propagates with a nearly constant operation angle over a wide range of crack extension. Most applications of the CTOA criterion are made for thin-walled or sheet metals as used in aircraft engineering and pipeline industry. Research has shown that the CTOA parameter can be used as a material property for an efficient characterization of large amounts of crack extension

when the crack extension exceeds the material thickness dimension. Therefore, experiments were conducted to determine a constant critical CTOA value for use as a fracture property.

During the last decade, extensive numerical studies have been undertaken applying the CTOA concept to ductile fracture analysis, as reviewed by Newman et al. [220], Zerbst et al. [221] and Horsley [222]. As a result, the CTOA-based fracture mechanics method has become mature, and a standard test method for the critical CTOA testing was developed recently by ASTM with a designation as E2472–06e1 [17]. This newer standard uses C(T) and M(T) specimens made from thin-sheet materials in order to achieve low constraint conditions at the crack tip. The standard was validated by Heerens and Schodel [223] using a comprehensive data set on the stable crack extension in an aluminum sheet material with a thickness of 3 mm. The CTOA fracture criterion now becomes one of the most promising fracture criterion used for characterizing the stable tearing in thin metallic materials 224. Note that use of the CTOA criterion must combine with the FEA simulation for applications involving ductile crack growth making application of the method both complex and expensive. This limits the practical application of the CTOA fracture mechanics method.

In addition, ASTM E2472 also provides the test methods and procedures for another fracture parameter, crack-opening displacement δ_5 developed mainly at GKSS [73]. δ_5 denotes relative displacement of the crack surfaces normal to the original un-deformed crack plane at the tip of the fatigue pre-cracked size. In the standard E2472, the fracture parameter δ_5 is measured at the original crack size location over a gage length of 5-mm as the crack stably tears. A δ_5–R curve is determined as the variation of δ_5 with crack extension. The critical δ_5 value and the δ_5–R curve are utilized as alternatives to describe the resistance of ductile sheet materials to stable crack extension under low-constraint conditions. More detailed discussions on this topic were given recently by Heerens and Schodel [223].

6. Constraint effect on fracture toughness

6.1. Experimental observations on fracture constraint effect

Application of fracture mechanics methods to engineering design and structural integrity assessment requires fracture toughness values be transferred from the laboratory test to a structural application. Experiments have shown that the crack depth, section thickness, specimen size, crack geometry and loading configuration all can have a strong effect on the fracture toughness measurements (K, G, J and δ). These effects are referred to as "constraint effect." ASTM standards intentionally choose specimen configurations that maximize crack-tip constraint by using deeply cracked, relatively thick or side-grooved, predominantly bend loaded specimens to obtain conservative measurements of fracture toughness properties. In structural applications the cracks are often small relative to other dimensions, often three dimensional in shape and the loading can be predominantly tensile. These differences, alone or in combination, result in effectively tougher behavior, causing the direct application of ASTM fracture toughness measurements to structures to be conservative. Often engineers accept the conservatism and use the laboratory toughness measurements directly in structural applications. Alternatively, the engineer can obtain a second parameter that is an estimate of the constraint in the structure relative to that of the laboratory sample, and adjust the structure design accordingly. Note that the CTOA parameter is generally used to characterize fracture toughness in the stable crack extension for thin-sheet materials in low constraint conditions, and thus it has less in-plane geometry and size effect.

For cracks dominated by linear elastic deformation, as mentioned previously in Section 2.2, Irwin et al. [28] demonstrated in the 1950s that the specimen thickness has considerable effect on the apparent toughness G_c and K_c values that were
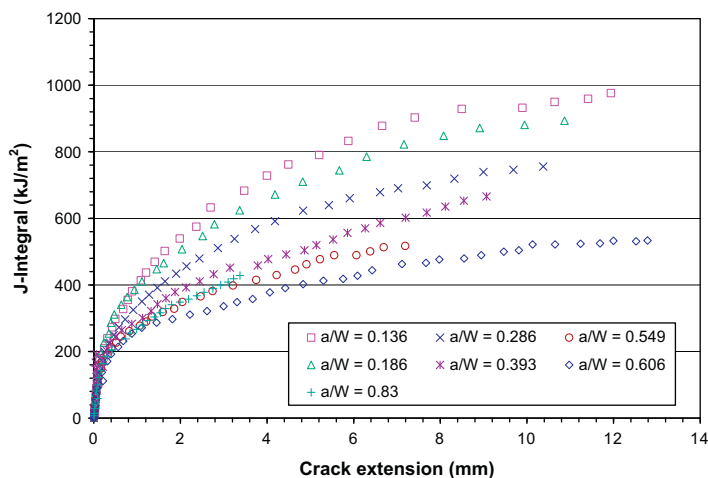

Fig. 13. J–R curves of HY80 steel obtained by Zhu and Joyce [153] using SE(B) specimens and normalization method.

measured in the laboratory. As shown in Fig. 4, the apparent toughness K_c decreases dramatically with thickness until a plateau value of the plane strain fracture toughness K_{Ic} is reached. It was also recognized that K_{Ic} is thickness-independent if the size requirements as suggested in ASTM E399 are satisfied. On the other hand, for thin-sheet specimens the stress intensity factor K-based resistance curves (K–R curves) have less crack size or in-plane geometry dependence, as reviewed in Section 2.4 and demonstrated experimentally in [67–74]. As a result, for thin-section specimens, K–R curves are nearly independent of in-plane geometry if the remaining ligament is predominantly elastic as prescribed in ASTM E561.

For cracks dominated by plastic deformation, the linear elastic fracture mechanics or the K-factor theory become invalid, and thus the elastic–plastic fracture mechanics or the J-integral theory are used to describe the fracture resistance of materials using J_c, J_{Ic}, or J–R curves. For plane stress or thin-section specimens, a size-independent J–R curve can be obtained and is equivalent to the corresponding K–R curve for aluminum alloys, as shown by Zhu and Leis [88]. For plane strain or thick-section specimens, however, experiments have shown that the constraint effect caused by both specimen geometry and loading mode can considerably affect the J-integral resistance curves, although relatively small effects on the initiation toughness were observed. Garwood [225] was among the first and showed that an experimental J–R curve derived from the center-cracked panel was appreciably steeper than one obtained from a three-point bend specimen, but the initiation toughness values were essentially identical for these two geometries. Similar constraint effects on J–R curves for ductile materials under plane strain conditions were observed widely by many other investigators, including McCabe et al. [226], Towers and Garwood [227], Eisele et al. [228], Hancock et al. [229], Joyce et al. [230–232], Wardle [233], Lam et al. [234], Neimitz et al. [235], and Shen et al. [236]. All experimental results showed that deeply cracked, bending loaded standard specimens result in lower J–R curves, and shallow cracked, predominantly tensile loaded nonstandard specimens lead to higher J–R curves, with the plane strain initiation toughness J_{Ic} being nearly independent of these specimen geometry and loading mode effects. The observed effects were large with dramatically smaller crack extensions corresponding to a J integral value beyond crack initiation for a shallow cracked, tensile loaded test geometry in comparison to the deeply cracked, bending loaded ASTM standard geometry.

Joyce and Link [231,232] showed that three-point bend SE(B) specimens can be tested over a wide range of a/W ratios with the resulting J–R curves demonstrating a wide range of effective toughness. Since this geometry is a relatively easy one to test, SE(B) specimens with various a/W ratios are often used to investigate the constraint effect on J–R curves for ductile materials, with the fracture tests following the procedures specified in ASTM E1820, except for the much larger range in a/W ratios utilized. Fig. 13 shows the constraint-dependent J–R curves of HY80 steel obtained by Zhu and Joyce [237] using SE(B) specimens with different crack sizes and the normalization method. As evident in this figure, significant differences exist between the J–R curves for deep and shallow cracks. The SE(B) specimens valid according to ASTM E1820 with a/W between 0.45 and 0.70 define the lower and more consistent J–R curve behavior, while the specimens with either deeper cracks or more shallow cracks result in more elevated J–R curve behavior with shallow cracks, i.e. $a/W < 0.28$, providing the most elevated toughness behavior. For this reason, ASTM E1820 bending specimens with $0.45 \leqslant a/W \leqslant 0.70$ are used for the standard J–R curve evaluation so as to determine a lower bound, relatively crack size insensitive J-integral resistance curve for ductile materials.

In order to minimize the constraint effect on the laboratory measured toughness, all ASTM fracture standards including E399, E561, E1290, E1820 and E1921 prescribe strict size requirements for valid tests with the objective of obtaining conservative fracture toughness measurements. While some variation will still result due to the range of specimen types, specimen sizes and crack length ratios allowed, the variations will be small compared to those implicit in applying the laboratory results to structural applications. Since the crack-tip constraint effect is the root cause of the transferability issue, quantifying the intrinsic constraint presenting in laboratory specimens and in cracked structural components can allow the fracture analyst to estimate the magnitude of the conservatism implicit in the direct use of the conservative E1820 J–R curve result for a particular application. Therefore, the analysis and quantification of constraint effect on fracture toughness, particularly for J-integral resistance curves for ductile materials or for the master curve and reference temperature T_o, are of practical importance. A non-mandatory appendix was added to E1820 in 2011 prescribing testing techniques for shallow cracked SE(B) specimens with $0.05 \leqslant a/W \leqslant 0.45$ which should aid in the understanding of the magnitude of the constraint effect of fracture toughness in structural materials. Different fracture constraint theories and constraint analysis technologies have been developed, as reviewed in the following sections.

In addition, in the 1980s, the size dependence of J–R curves was not fully understood and it was suggested that the J-integral was incapable of describing fracture resistance of ductile materials at large crack extensions. In order to obtain a geometry-independent resistance curve, Ernst [238,239] suggested a modified J-integral parameter, J_M, for use in characterization of fracture resistance at large crack extensions beyond the limits of deformation J–R curves, and showed that J_M–R curves were consistent at the early stages with the J_M versus tearing modulus curves correlated closely for C(T) specimens. However, further experimental investigations of Joyce et al. [240] showed that J_M–R curves for different C(T) specimen geometries can be very size-dependent beyond 30% crack extension except for very high toughness materials. In contrast, evaluating deformation J values using Eq. (33) results in J–R curves that are consistent to more than 30% crack extensions which was three times the maximum crack extension limitation prescribed at the time in ASTM E1152 (i.e., the maximum crack extension is 10% of the original crack ligament, $\Delta a_{max} = 0.1 b_0$). Similar experimental observations were reported by Wilkowski et al. [241], Link et al. [242], Hiser [243] and others. As a result, the deformation J, corrected for crack growth continues to be used in E1820 J–R curves up to the present day.

6.2. Fracture constraint theories

The characterization of crack-tip stress and strain fields is fundamental to fracture mechanics. As reviewed previously in Sections 2.1 and 3.1, the elastic crack-tip field in Eq. (1) with the K-factor and the elastic–plastic crack-tip field in Eq. (11) with the J-integral led to the establishment and development of the linear elastic fracture mechanics and the elastic–plastic fracture mechanics, respectively. Both K and J parameters describe the intensity of the singular crack-tip stress fields, but when large changes are made in crack depth, crack geometry, or the mode of loading, non-singular terms can result in measureable differences in the effective fracture toughness. In fact, the slip-line field solutions of McClintock [92] for plane strain mode-I cracks in ideally plastic materials already showed that different crack-tip stresses and strains exist at the crack tip for bending and center-cracked tension geometries. This is a typical example of crack-tip constraint effect due to specimen geometry and loading mode. Extensive research has been devoted to quantifying the effect of constraint on standard specimen geometries and on typical cracked structural configurations. The proposed remedy in both the elastic and elastic–plastic cases has been to define a second parameter, used in concert with K or J, that is related to the non-singular stress expansions that quantifies and can thus be used to correct for the variation in crack tip constraint. Over the years, several second parameters and corresponding two-parameter crack-tip field solutions were developed to improve the single-parameter elastic K field or the elastic–plastic HRR field. The K–T (or J–T) approach, J–Q theory and J–A_2 three-term solution are three examples, with the parameters T, Q and A_2 being used to quantify the constraint effect on the crack-tip field and on the fracture toughness in an elastic or elastic–plastic condition. The following sections give a brief description of these three proposed constraint characterizations.

6.2.1. The J–T approach

For a linear elastic material, the elastic singular stress field in Eq. (1) is the leading term of the series of expansion proposed by Williams [27]. Larsson and Carlsson [244] were the first to point out that the second, non-singular term in the Williams' expansion has a significant effect on the shape and size of the plastic zone near the crack tip under small-scale yielding (SSY) conditions, even within the rather small range of plastic yield zone sizes allowed by the ASTM limits for fracture test in terms of K values. Rice [245] further studied the limitations of the SSY approximation, and rewrote the first two terms of the William's series expansion as:

$$\sigma_{ij} = \frac{K_I}{\sqrt{2\pi r}} f_{ij}(\theta) + T\delta_{1i}\delta_{1j} \tag{75}$$

where the first term of the above equation is the singular elastic K field of Eq. (1) with K_I being the stress intensity factor, the second term is nonsingular with magnitude denoted by a parameter T, and δ_{ij} is the Kronecker delta. Since T represents the tensile stress acting parallel to the crack plane, this parameter is simply called T-stress. Eq. (75) shows clearly that the second term or T-stress has an effect on the crack-tip field, and if an applied T-stress varies at a constant K, the plastic zone will vary in size and in shape.

Different analytical and numerical methods including the higher-order weight function [246], the Green's function [247], the stress difference [248] and the FEA calculation [249,250] were developed to determine the T-stress for a variety of fracture specimens and geometries. In reference to the T-stress and K-factor, Leevers and Radon [251] introduced a biaxiality ratio parameter, $B = T\sqrt{\pi a}/K_I$, that is widely used. For example, a through-thickness crack in an infinite plate subjected to a remote tensile stress σ has the biaxiality ratio of $B = T/\sigma = -1$, and thus the remote stress σ induces a compressive T-stress equal in magnitude to the remote tensile stress in the direction parallel to the crack plane in the plate. Sherry et al. [252] compiled the T-stress solutions available at that time via the biaxiality ratio B for a variety of crack geometries, including the conventional M(T), SE(B) and C(T) specimens with a full range of a/W ratios. The results showed that for the M(T) specimen the biaxiality ratio is insensitive to a/W and very negative at about -1.0, for the C(T) specimen the biaxiality ratio is between 0.5 and 0.6 in the ASTM allowed range of $0.45 \leqslant a/W \leqslant 0.70$ but then falls to nearly zero for $a/W < 0.4$, while for the SE(B) specimen the biaxiality ratio varies with a/W rather linearly from -0.1 to 0.5 over the ASTM allowed a/W range but continues to larger negative values for shallow crack geometries. Thus, the biaxiality ratio or the T-stress corresponds to the observed experimental trends, and is a qualitative index of the relative crack-tip constraint levels for various geometries with a positive value representing a high level of constraint and a negative value denoting a low level of constraint.

The elastic–plastic FEA results of Dodds et al. [253] have shown that for any two cracks having the same K (or J) at their crack tips the crack-tip stress and strain fields can be different if the constraint levels are different. Bilby et al. [254] showed that the T-stress can dramatically affect the magnitude of hydrostatic triaxiality in the immediate vicinity of the crack tip. Under the SSY conditions, the two parameter K–T solution in Eq. (75) can describe the crack-tip field. Because deeply-cracked SE(B) and C(T) specimens have positive T-stresses and high triaxiality near the crack tip, experiments have not been able to measure differences in K_{Ic} between these two types of specimens, and so the constraint has not become an issue for K_{Ic} testing using ASTM E399. However, if one measured K_{Ic} on low constraint specimens like shallow-cracked SE(B) specimens or M(T) specimens even without plasticity, the constraint effect would be expected because of the negative T-stress. For cleavage fracture of ferritic steels, the constraint effect on the ductile to brittle transition can be large as shown Joyce and Tregoning [255].

For elastic–plastic materials under large plastic deformation, the J-integral parameter and the HRR solutions are used to characterize the crack-tip behavior. The J-dominance analyses from extensive FEA calculations [93–97] have shown that the HRR solution can reasonably describe the actual crack-tip fields for deeply-cracked bending specimens in SSY conditions, and that the single J parameter can accurately describe the intensity of the crack-tip stress field for the high constraint specimens, but breaks down for low constraint specimens or for large-scale yielding (LSY). To investigate the constraint effect on the crack-tip field under the LSY conditions, Betegon and Hancock [256] and Du and Hancock [257] at the University of Glasgow in Scotland developed a FEA model using a modified boundary layer formulation with the displacement boundary conditions corresponding to the two-parameter elastic crack-tip stress field in Eq. (75). Their results showed that the elastic crack-tip stress field can be characterized using the K factor and the T-stress, and the elastic–plastic crack-tip field can be characterized by J and T into full plasticity. For geometries with positive T-stresses, the J-integral dominates the crack-tip field, and the HRR solution holds; while for geometries with negative T-stresses, the J-dominance is lost, and the crack-tip behavior is characterized by the two parameters, J and T. This technology, proposed for quantifying the crack-tip constraint effect, is often referred to as the J–T approach. The parameter T has been successfully used to quantify the constraint effect on fracture toughness K_c and J_c for various fracture specimens and crack geometries [229,258,259].

6.2.2. The J–Q theory

The J–T approach has limitation, however, because the T-stress is an elastic parameter, and becomes less meaningful as the plastic zone expands at the crack tip. To address this limitation, a new second parameter Q was studied for an elastic–plastic crack under the SSY and LSY conditions. O'Dowd and Shih [260–263] at Brown University performed a series of detailed elastic–plastic FEA calculations for various geometries based on the theory of deformation plasticity, and developed a J–Q theory (actually, it is a numerical solution) to describe the elastic–plastic crack-tip field. By means of the full-field FEA results, they found that the difference field between the full-field numerical solution, σ_{ij}, and the HRR field $(\sigma_{ij})_{HRR}$, is approximately a uniform hydrostatic stress ahead of the crack tip. Accordingly, the following two-term crack-tip stress field was proposed:

$$\sigma_{ij} = (\sigma_{ij})_{HRR} + Q\sigma_0\delta_{ij}, \quad \text{for} \quad r > J/\sigma_0 \quad \text{and} \quad |\theta| \leqslant \pi/2 \tag{76}$$

where $(\sigma_{ij})_{HRR}$ is the HRR field in Eq. (11), σ_0 is the yield stress, and Q is a stress triaxiality parameter to reflect the hydrostatic stress level at the crack tip. From the FEA result of crack opening stress $(\sigma_{\theta\theta})_{FEA}$, the parameter Q was defined by:

$$Q = \frac{(\sigma_{\theta\theta})_{FEA} - (\sigma_{\theta\theta})_{HRR}}{\sigma_0}, \text{ at } r = \frac{2J}{\sigma_0} \quad \text{and} \quad \theta = 0 \tag{77}$$

The distance r from the crack tip that was chosen for the definition of Q above lies just outside the finite strain blunting zone so that Q obtained from a small or finite strain analysis should be nearly the same. In addition, O'Dowd and Shih [262] and O'Dowd [263] suggested an alternative reference stress field to replace the HRR solution in Eq. (76) using the SSY stress field $(\sigma_{ij})_{SSY}$ with $T = 0$, where $(\sigma_{ij})_{SSY}$ needs to be determined by FEA using the modified boundary layer model. Accordingly, the two reference stress fields result in two formats of Q definition. O'Dowd [263] discussed the difference in Q caused by these two reference stress fields. Cautions should be paid to ensure a consistent choice of a reference stress field and the corresponding Q definition when using the J–Q theory. In general, the theoretical HRR field is suggested be used as the reference stress field as utilized in Eqs. (76) and (77) to reduce the finite element calculations required by the SSY reference stress field.

Various FEA results [260–263] indicated that the J–Q solution holds approximately in the region of interest ($1 \leqslant r/(J/\sigma_0) \leqslant 5$) for most fracture specimens up to reasonable deformation levels. Under the SSY conditions, the modified boundary layer analysis showed that the J–Q solution is equivalent to the J–T approach under conditions where they both apply. However, these authors also showed that the equivalence of these two approaches does not hold under LSY or fully yielding conditions. Faleskog [264] showed that the parameter Q varies on a J–R curve during ductile crack growth. Thus this parameter is not appropriate to describe the constraint effect on a crack growth resistance curve. In general, the parameter Q can effectively describe the constraint effect on the crack-tip field for different geometries under a variety of deformation levels. Accordingly, Q has been used extensively to quantify the constraint effect on the fracture toughness parameters J_c and J_{Ic}, see O'Dowd and Shih [262], Nevalainen and Dodds [265], Joyce and Link [231,232], and Gao and Dodds [266].

6.2.3. The J − A₂ three-term solution

As presented above, the so-called J–Q theory is actually a numerical solution that was developed on the basis of FEA results. A rigorous theoretical analysis was performed by Yang [267], Yang et al. [268] and Chao et al. [269] at the University of South Carolina who developed the higher-order crack-tip field for an elastic–plastic, power-law hardening material. Using the theory of deformation plasticity under plane strain conditions, these authors found that the first three terms of the stress asymptotic expansion can be described by only two parameters: the J-integral and a second parameter they defined as A_2. This asymptotic three-term solution can be expressed as:

$$\frac{\sigma_{ij}}{\sigma_0} = A_1\left[\left(\frac{r}{L}\right)^{s_1}\tilde{\sigma}_{ij}^{(1)}(\theta) + A_2\left(\frac{r}{L}\right)^{s_2}\tilde{\sigma}_{ij}^{(2)}(\theta) + A_2^2\left(\frac{r}{L}\right)^{s_3}\tilde{\sigma}_{ij}^{(3)}(\theta)\right] \tag{78}$$

where the stress angular functions $\tilde{\sigma}_{ij}^{(k)}(\theta)$ ($k = 1, 2, 3$) and the stress power exponents s_k ($s_1 < s_2 < s_3 = 2s_2 - s_1$) depend only on the strain hardening exponent n, and L is a characteristic length parameter that is often taken as $L = 1$ mm. The parameters A_1 and s_1 are related to the HRR field by $A_1 = (J/\alpha\varepsilon_0\sigma_0 I_n L)^{-s_1}$ and $s_1 = -1/(1 + n)$. Thus, the first term of Eq. (78) is the singular HHR field, and the other two are higher-order terms, both having amplitudes described in terms of the constraint parameter A_2. This parameter A_2 can be determined using a simple point matching method [268,269] at $r = 2J/\sigma_0$ and $\theta = 0$ as used in Eq. (77) for the Q definition. Alternatively, a more accurate A_2 can be determined using a least square fitting procedure [270], or a simple weight average technique [271].

Yang [267] numerically showed that the parameter A_2 becomes constant under the LSY or fully plastic conditions when the applied load is larger than 1.2 times the limit load for three-point bending specimens or single edge-notched tension specimens. Later, Chao and Zhu [271] provided a rigorous theoretical proof that the parameter A_2 is independent of the applied J under LSY or fully plastic deformation. This load-independence makes A_2 more useful because its value determined at a ductile crack initiation load characterized by J_i may remain constant for an applied J larger than J_i. As a result, A_2 is an appropriate parameter to describe the constraint effect on both fracture toughness parameter J_c or J_{Ic}, and J–R curve during ductile crack tearing. In contrast, the parameter Q is nearly independent of the applied J only in SSY or intermediate yielding, but becomes strongly load-dependent in LSY, as shown in [261,272,273] for a variety of fracture specimens. This suggests that Q cannot be used directly to describe the constraint effect on a J–R curve because its value varies on the resistance curve, as shown by Faleskog [264]. Accordingly, the $J - A_2$ three-term solution was used to characterize the elastic–plastic crack-tip fields for two- and three-dimensional geometries [274–277], and the parameter A_2 was used to quantify the constraint effect on the fracture toughness J_c, J_{Ic} and J–R curves for ductile materials [278,271,234,279].

6.2.4. Consideration of the global bending influence

For bending dominated specimens, such as C(T) and SE(B) specimens, various numerical results showed that the global bending moment can significantly impinge the crack-tip stress field under the LSY or fully plastic conditions [262,274,280]. As a consequence, the J–T approach, the J–Q theory and the $J - A_2$ three-term solution all may lose the validity to describe the crack-tip field for bending geometries at large plastic deformation. To eliminate the global bending influence on the crack-tip field, Zhu and Leis [281] recently proposed a bending modified J–Q solution through introducing an additional term to reflect the global bending stress. For tension dominated geometries or SSY-controlled bending bodies, the global bending influence is very small, and the original J–Q solution can be used. For bending specimens in LSY or fully plasticity, the FEA results showed that the original parameter Q defined in Eq. (77) depends strongly on the applied J, while the modified parameter Q that Zhu and Leis proposed trends to be constant. Moreover, the original Q may be strongly distance-dependent over $1 \leqslant r/(J/\sigma_0) \leqslant 5$, while the modified Q is constant over the same distance and at the same loading conditions. As such, the modified parameter Q can be used to characterize the constraint effect not only on the fracture toughness J_c or J_{Ic}, but also on J–R curves for ductile crack growth.

Using a procedure similar to that used for eliminating the global bending influence on the J–Q theory, Chao et al. [282] and Zhu and Chao [283] proposed a bending modified $J - A_2$ solution. Their results showed that the bending modified $J - A_2$ solution can match the FEA stress field, and the modified A_2 is nearly independent of the distance over the region of interest for deeply cracked SE(B) specimens at deformation levels ranging from SSY to LSY. Therefore, the bending modified parameters Q and A_2 are both distance and loading independent, and can be used equivalently to quantify the constraint effect on fracture toughness J_c, J_{Ic}, and J–R curves for SE(B) and C(T) specimens with any crack sizes, as detailed in Section 6.3.

In addition, Zhu and Chao [283] conducted a detailed constraint analysis using the bending modified $J - A_2$ solution and FEA calculations for a set of SE(B) specimens with various a/W ratios for different strain hardening materials from high to low, and obtained the critical size requirements for two-parameter (J and A_2) fracture toughness testing as:

$$(B, a, b) > 6J/\sigma_0 \tag{79}$$

Comparison of Eq. (79) with Eq. (51) indicates that the size requirements for the two-parameter fracture testing are much more relaxed than those prescribed by ASTM E1820 for the single-parameter fracture testing. Zhu and Chao [283] showed that a set of J–R curve test data for A285 steel SE(B) specimens are invalid if using ASTM E1820 specified size requirements and the maximum J criterion, while the same data becomes valid if using the new size requirements in Eq. (79). Therefore, the new size requirements may allow people to obtain more valid and usable fracture resistance curve data to meet the needs of practical applications.

6.3. Constraint correction approaches

Finite element analysis combined with experimental data have shown that high crack-tip constraint leads to the higher crack-tip stresses and lower resistance curves, whereas low crack-tip constraint tends to promote more crack-tip yielding that lowers crack-tip stresses and results in higher resistance curves for ductile fracture. Therefore, the parameter T, Q or A_2 reviewed above can be used directly to quantify the constraint effect on fracture toughness at ductile initiation or cleavage instability using the two-parameter stress field and the critical stress model (or RKR model) proposed by Ritchie et al. [284]. Based on this model, Shih et al. [285] determined the J_c–Q relationship for cleavage fracture, Chao and Ji [278] obtained the K_c–T relationship for brittle fracture, and Chao and Zhang [286] obtained the $J_c - A_2$ relationship for cleavage fracture. Since the T-stress concept is based on the elastic K field, and thus it is adequate to use T to quantify the constraint effect on cleav-

age fracture toughness in ductile-to-brittle transition, as demonstrated by Joyce and Tregoning [198], Gao and Dodds [287], Wallin [288] and Huh et al. [289].

For ductile crack growth, fracture constraint has a much significant effect on the resistance curves at the upper shelf. The bending modified constraint parameters Q and A_2 can be both loading and distance independent in LSY, and thus both are applicable for use to quantify the constraint effect on J–R curves measured using SE(B) or C(T) specimens, where the constraint parameter determined at the initiation load can remain constant for the larger loads during the crack growth. Since the RKR model is not applicable to growing cracks, a new methodology has been developed to relate a constant value of Q or A_2 to each resistance curve. The first author and his coworkers [234,271,279,281,290,291] have proposed a unique technique for correcting constraint effect on J–R curves using the parameter Q or A_2. By assuming an analytic power-law function, a family of constraint-dependent J–R curves can be constructed for ductile crack growth, in conjunction with use of at least three typical experimental J–R curve data and numerical results of the constraint parameter determined at the loading level of initiation toughness. As such, each experimental J–R curve is correlated by a specific value of the constraint parameter. In general, a constraint-corrected J–R curve is a function of crack extension and the constraint parameter, and can be expressed in a power-law function as:

$$J(\Delta a, Q) = C_1(Q)\left(\frac{\Delta a}{1mm}\right)^{C_2(Q)} \tag{80}$$

if the constraint parameter Q is used. A similar expression to Eq. (80) can be obtained if the constraint parameter A_2 is used to replace Q. Note that this constraint correction technique is valid only for the conditions of J–Q or $J - A_2$ controlled crack growth, and not for crack extensions beyond the fracture theory controlled area.

In terms of the constraint parameter Q, Zhu and Jang [290] and Zhu and Leis [291] determined constraint-corrected J–R curves for different ductile metals. In reference to the constraint parameter A_2, Chao and Zhu [271], Lam et al. [234] and Zhu and Leis [291] obtained constraint-corrected J–R curves for various ductile materials. For example, Fig. 14 depicts the experimental and predicted constraint-dependent J–R curves for X80 pipeline steel using SE(B) specimens with different crack sizes, as determined by Zhu and Leis [281] using the parameter Q. In this figure, the predicted resistance curves were obtained from the following constraint-corrected J–R curve by Q:

$$J(\Delta a, Q) = (-1225Q + 645)\left(\frac{\Delta a}{1\ mm}\right)^{(-0.066Q+0.637)} \tag{81}$$

where Δa is in mm, and J has units of kJ/m^2. Similarly, Fig. 15 shows the same experimental data as shown in Fig. 14, compared this time with the predicted results obtained by Zhu and Leis [279] using the parameter A_2. In Fig. 15, the predicted resistance curves were obtained from the constraint-corrected J–R curve by A_2:

$$J(\Delta a, A_2) = -4417.1A_2\left(\frac{\Delta a}{1\ mm}\right)^{0.668} \tag{82}$$

where Δa is in mm, and J has units of kJ/m^2. Hence either Q or A_2 can be used in closed-from expressions to obtain constraint-corrected J–R curves corresponding to the experimental data of constraint-dependent resistance curves. In addition, Zhou et al. [292,293] recently applied the constraint correction procedure to determine constrain-corrected J–R curves for HY100 steel using all three constraint parameter Q, A_2 and T. Therefore, these studies demonstrated that the constraint correction technique can be used reliably to predict a constraint-dependent J–R curve for a structural crack provided that either
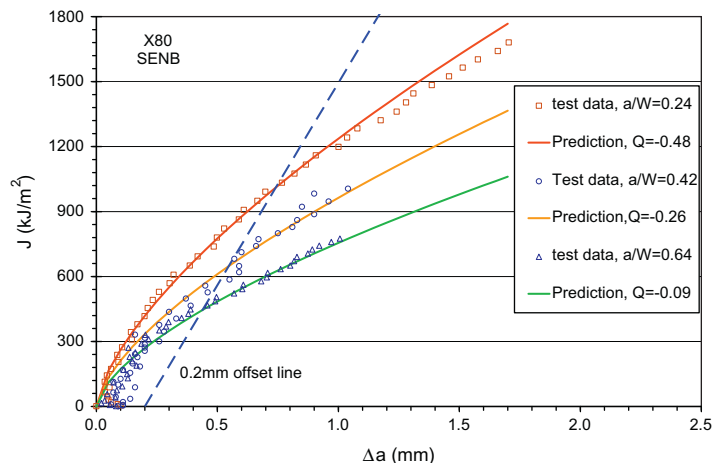

Fig. 14. Experimental J–R curves of X80 pipeline steel and the corresponding predictions obtained by Zhu and Leis [281] using the constraint parameter Q.
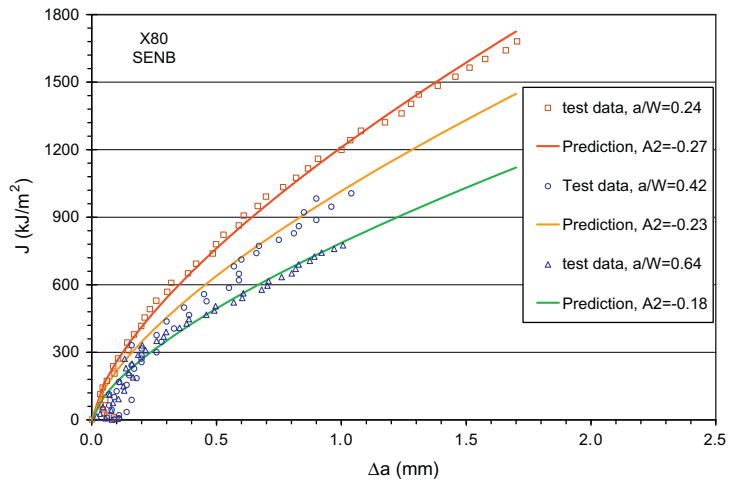
Fig. 15. Experimental J–R curves of X80 pipeline steel and the corresponding predictions obtained by Zhu and Leis [279] using the constraint parameter A_2.

Q or A_2 is evaluated a priori for that crack configuration. As a result, the constraint correction technique provides an effective compliment to the experimental measurements of ASTM E1820, and can serve as a vital tool to transfer laboratory measured fracture toughness to engineering applications.

7. Discussions and conclusions

This paper gave a systematic technical review of fracture toughness testing, experimental evaluation, test methods and standardization for metallic materials in reference to both the linear elastic fracture mechanics and the elastic–plastic fracture mechanics. This review described the most important fracture parameters of the elastic energy release rate G, the stress intensity factor K, the J-integral, the crack-tip opening displacement δ, and the crack-tip opening angle (CTOA) and presented, basically in the chronological order, the historic and state-of-the-art developments of these fracture parameter test and evaluation methods. The basic concept, definition, experimental estimation, early fracture test practice, test method, recent development, critical point-value toughness evaluation, and resistance curve testing as well as ASTM standardization effort of fracture test methods were described in detail for each fracture parameter of K (or G), J, CTOD, and CTOA. The effects of loading rate, temperature, crack-tip constraint and fracture instability on fracture toughness measurements were also reviewed. Three typical fracture mechanics constraint theories, i.e. the J–T approach, the J–Q theory and the $J - A_2$ three-term solution and their applications to quantifying the constraint effect on fracture toughness were briefly reviewed.

ASTM standardization has been a key part of fracture toughness testing and evaluation by providing a forum for fracture mechanics development and by providing consistent experimental procedures for measuring fracture toughness parameters. Both early and more recent fracture toughness test standards were reviewed, including ASTM standards E399 for the plane strain fracture toughness K_{Ic} testing, E561 for the K–R curve testing, E813 for the plane strain fracture toughness J_{Ic} testing, E1152 for the J–R curve testing, E1737 for the J_{Ic} and J–R curve testing, E1290 for the δ_c testing, E2472 for the CTOA testing, the combined test standard E1820 for three fracture parameter (K, J, δ) testing, and E1921 for defining the ductile-to-brittle transition reference temperature T_0 and a master curve for ferritic steels. The adoptions of specimen geometry, crack size, side groove, allowed load capacity, crack extension limitation, fracture initiation definition, size requirement, and validity criterion were described, and some improvements presently being developed were also discussed for each standard. While ASTM E813, E1152 and E1737 have withdrawn, all other standards have undergone a series of revisions up to the present versions of ASTM E399–09e2, E561–10, E1290–08e1, E1820–11, E1921–11, and E2472–06e1. These six current ASTM standards should be used appropriately for the K_{Ic} testing, K–R curve testing, δ_c testing, J_{Ic} and J–R curve testing or δ_{Ic} and δ–R curve testing, critical CTOA testing, as well as for the reference temperature T_0 and K_{Jc} master curve determination. Guidelines were discussed on selection of a proper parameter to characterize fracture toughness for the material in consideration, use of an appropriate test standard to measure the fracture toughness, and limitation of each test method and fracture parameter in practice.

This review indicates that fracture toughness testing, experimental evaluation and standardization for metallic materials have experienced a long history of more than 50 years in the development of fracture mechanics theory. Different fracture toughness parameters have been proposed, and various fracture toughness test methods and experimental technologies have been developed and revised incrementally over the years. In the 1950s and 1960s, the experimental fracture mechanics analysis was focused on linear elastic materials testing using the energy release rate G and the stress intensity factor K. In the 1970s and 1980s, fracture toughness testing and analysis was concentrated on the J-integral and on the CTOD testing for elastic–plastic materials. In the 1990s, the ductile to brittle transition of ferritic steels became the central research topic

leading to the development of a master curve of cleavage toughness K_{Jc} for ferric steels over the range of ductile-to-brittle transition temperatures. In the 2000s, the attention was paid to CTOA testing for stable crack extension of thin-walled materials in low-constraint conditions. In this new century progress has also been made on the conversion of high constraint fracture mechanics data developed according to ASTM standards to lower constraint applications generally found in structural applications. So far, significant progress has been achieved for both linear elastic and elastic–plastic fracture toughness testing in providing the practicing engineer the means to quantify the crack-tip constraint in common laboratory test geometries and in structural applications where the crack is complex in shape and subjected to combined tensile, bending and pressure loadings. More comprehensive discussions on fracture toughness estimation and application for engineering materials were recently detailed in two new books of Wallin [294] and Zehnder [295].

The development of fracture toughness test standards has been a concentrated effort by many researchers and scientists worldwide for more than a half century. The work to improve test procedures has been a constant topic of interest, debate and incremental research, and this process is still continuing. This is shown by the progress of the ASTM fracture toughness test standards that grew step by step, such as E399, E561, E813, E1152, E1737, E1290, E1820, E1921, E2472 and their different updated versions. The present versions of ASTM E399–09e2, E561–10, E1290–08e1, E1820–11, E1921–11, and E2472–06e1 have been developed and improved over the years to provide consistent and economical procedures to measure estimates of fracture toughness designated as K_{Ic}, K–R curve, J_{Ic}, J–R curve, δ_{Ic}, CTOA, δ–R curve, and K_{Jc} master curve to meet the needs of practical engineering applications. Now the test procedures in these standards have been further simplified, the experimental measurements become more accurate, the validity requirements are more relaxed, the test conditions are broadened, the experimental costs are more efficient, and the test results are more reliable in quality. This progress would not have been achieved without the contributions made by hundreds and thousands of researchers and scientists around the world. Although many technical articles and publications are available from a variety of resources, only the documents considered most relevant by the authors were cited in this review, and the most important equations and relationships were presented. It is expected that this review can serve as a summarized technical document for tracing the historic development of fracture toughness testing and evaluation, for better understanding and using proper fracture parameters and fracture toughness test methods, and for further improving ASTM fracture test standards in the future.

References

[1] Irwin GR. Analysis of stresses and strains near the end of a crack traversing a plate. J Appl Mech 1957;24:361–64.
[2] Rice JR. A path independent integral and the approximate analysis of strain concentration by notches and cracks. J Appl Mech 1968;35:379–86.
[3] Wells AA. Application of fracture mechanics at and beyond general yielding. Br Weld J 1963;10:563–70.
[4] Broek D. Elementary engineering fracture mechanics. Leyden: Noordhoff International Publishing; 1974.
[5] Kanninen MF, Popelar CH. Advanced fracture mechanics. New York: Oxford University Press; 1985.
[6] Hertzberg RW. Deformation and fracture mechanics of engineering materials. 4th ed. New York: John Wiley & Sons; 1995.
[7] Anderson TL. Fracture mechanics – fundamentals and applications. 3rd ed. Boca Raton: CRC Press; 2005.
[8] Irwin GR, DeWit R. A summary of fracture mechanics concepts. J Test Evaluat 1983;11:56–65.
[9] Erdogan F. Fracture mechanics. Int J Solids Struct 2000;37:171–83.
[10] Cotterell B. The past, present and future of fracture mechanics. Engng Fract Mech 2002;69:533–53.
[11] Milne I, Ritchie RO, Karihaloo B. Comprehensive structural integrity, vols 1–10 (print version). Elsevier; 2003; or vols. 1-11 (online version), Elsevier; 2007.
[12] ASTM E1823-10a. Standard terminology relating to fatigue and fracture testing. American Society for Testing and Materials; 2011.
[13] ASTM E399-09e2. Standard test method for linear-elastic plane strain fracture toughness K$_{Ic}$ of metallic materials. American Society for Testing and Materials; 2011.
[14] ASTM E561-10. Standard test method for K–R curve determination. American Society for Testing and Materials; 2011.
[15] ASTM E1820-11. Standard test method for measurement of fracture toughness. American Society for Testing and Materials; 2011.
[16] ASTM E1290-08e1. Standard test method for crack-tip opening displacement (CTOD) fracture toughness measurement. American Society for Testing and Materials; 2011.
[17] ASTM E2472-06e1. Standard test method for determination of resistance to stable crack extension under low-constraint conditions. American Society for Testing and Materials; 2011.
[18] ASTM E1921-11. Standard test method for determining of reference temperature T$_0$ for ferritic steels in the transition range. American Society for Testing and Materials; 2011.
[19] Heyer RH. Crack growth resistance curves (R-curves) – literature review. In: Fracture toughness evaluation by R-curve methods. ASTM STP 527. American Society for Testing and Materials; 1973. p. 3–16.
[20] Barsom JM. In: Fracture mechanics retrospective – early classic papers (1913 to 1965). ASTM RPS1. American Society for Testing and Materials; 1987.
[21] Joyce JA. Manual on elastic–plastic fracture: laboratory test procedures. ASTM Manual Series: MNL27; 1996.
[22] Landes JD. Elastic–plastic fracture mechanics: where has it been? Where is it going? In: Fatigue and fracture mechanics. ASTM STP 1360, vol. 30. American Society for Testing and Materials; 2000. p. 3–18.
[23] Landes JD. Fracture toughness testing and estimations. In: Milne I, Ritchie RO, Karihaloo B, editors. Comprehensive structural integrity, vol. Elsevier; 2003 [Chapter 7.02].
[24] Schwalbe KH, Landes JD, Heerens J. Classic fracture mechanics methods. In: Milne I, Ritchie RO, Karihaloo B, editors. Comprehensive structural integrity, vol. 11. Elsevier; 2007.
[25] Zhu XK. J-integral resistance curve testing and evaluation. J Zhejiang Univ Sci A 2009;10:1541–60.
[26] Zhu XK. Advances in development of J-integral experimental estimation, testing and standardization. In: Proceedings of ASME 2011 pressure vessels and piping conference, Baltimore, Maryland, July 17–21, 2011.
[27] Williams ML. On the stress distribution at the base of a stationary crack. J Appl Mech 1957;24:109–14.
[28] Irwin GR, Kies JA, Smith HL. Fracture strengths relative to onset and arrest of crack propagation. Proc Am Soc Test Mater 1958;58:640–60.
[29] Irwin GR. Plastic zone near a crack and fracture toughness. In: Proceedings of the 7th sagamore ordnance materials conference; 1960. p. 463–78.
[30] Dugdale DS. Yielding of steel sheets containing slits. J Mech Phys Solids 1960;8:100–8.
[31] Griffith AA. The phenomena of rupture and flow in solids. Philos Trans Roy Soc Lond, Ser A 1920;221:163–97.
[32] Tada H, Paris PC, Irwin GR. The stress analysis of cracks handbook. 3rd ed. New York: ASME Press; 2000.
[33] Murakami Y. Stress intensity factors handbook. Oxford: Pergamon Press; 1987.

[34] Rooke DP, Cartwright DJ. Compendium of stress intensity factors. London: Her Majesty's Stationery Office; 1976.
[35] Gallagher JP. Damage tolerant design handbook. Wright-Patterson Air Force Base (OH): Air Force Materials Laboratory; 1983.
[36] Irwin GR. Fracture dynamics. In: Fracturing of metals, symposium of American Society for Metals. Transaction ASM 40A; 1948. p. 147–66.
[37] Orowan E. Fracture and strength of solids. Rep Prog Phys 1949;12:185–232.
[38] Irwin GR. Onset of fast crack propagation in high strength steel and aluminum alloys. In: Proceedings of the second sagamore ordnance materials conference, vol. 2; 1956. p. 289–305.
[39] Irwin GR, Kies JA. Critical energy rate analysis for fracture strength. Weld J Res Suppl. 1954;19:193–8.
[40] Irwin GR. Fracture testing of high-strength sheet materials under conditions appropriate for stress analysis. Report 5486, Naval Research Laboratory, July 27, 1960.
[41] Anon. ASTM special committee on fracture testing of high strength materials. ASTM Bulletin, January 1960. p. 29–40.
[42] Krafft JM, Sullivan AM, Boyle RW. Effect of dimensions on fast fracture instability of notched sheets. In: Cranfield symposium, vol. I; 1961. p. 8–28.
[43] Srawley JE, Brown WF. Fracture toughness testing methods. In: Fracture toughness testing and its applications. ASTM STP 381. American Society for Testing and Materials; 1965. p. 133–96.
[44] Kaufman JG. Progress in fracture testing of metallic materials. In: Review of developments in plane strain fracture toughness testing. ASTM STP 463. American Society for Testing and Materials; 1970. p. 3–21.
[45] Anon. The slow growth and rapid propagation of cracks. Mater Res Stand 1961;1:389–93.
[46] Anon. Proposed method of test for plane-strain fracture toughness of metallic materials. ASTM STP 410. American Society for Testing and Materials; 1966. p. 130–45.
[47] Brown WF, Srawley JE. In: Plane strain crack toughness testing of high strength metallic materials. ASTM STP 410. American Society for Testing and Materials; 1966. p. 1–65.
[48] ASTM E399-70T. Tentative method of test for plane strain fracture toughness of metallic materials. In: Review of developments in plane strain fracture toughness testing, ASTM STP 463. American Society for Testing and Materials; 1970. p. 249–69.
[49] Newman JC. Stress analysis of the compact specimens including the effects of pin loading. In: Fracture analysis. ASTM STP 560. American Society for Testing and Materials; 1974. p. 105–21.
[50] Srawley JE. Wide range stress intensity factor expressions for ASTM E399 standard fracture toughness specimens. Int J Fract 1976;12:475–6.
[51] Freese CE, Baratta FI. Single edge-crack stress intensity factor solutions. Engng Fract Mech 2006;73:616–25.
[52] Srawley JE, Jones MH, Brown WF. Determination of plane strain fracture toughness. Material research and standards, vol. 7. American Society for Testing and Materials; 1967. p. 261–6.
[53] Heyer RH, McCabe DE. Evaluation of a test method for plane-strain fracture toughness using a bend specimen. In: Review of developments in plane strain fracture toughness testing. ASTM STP 463. American Society for Testing and Materials; 1970. p. 22–41.
[54] McCabe DE. Evaluation of the compact tension specimen for determining plane-strain fracture toughness of high strength materials. J Mater 1972;7:449–542.
[55] Underwood JH, Kendall DP. Cooperative plane strain fracture toughness tests with C-shaped specimens. J Test Evaluat 1978;6:296–300.
[56] Wallin KRW. Critical assessment of the standard ASTM E399. J ASTM Int 2005;2:JAI12051.
[57] Joyce JA, Smudz R. Evaluation of elastic intensity using J-integral specimen geometries. J Test Evaluat 1992;20:1–5.
[58] Joyce JA. Experimental justification for proposed changes to the measurement of K_{Ic} using ASTM E399. J Test Evaluat 1998;26:455–62.
[59] Irwin GR. Crack toughness testing of strain rate sensitive materials. J Engng Power Transmiss 1964;86:444–50.
[60] Irwin GR. Basic concepts for dynamic fracture testing. J Basic Engng 1969;91:519–24.
[61] Madison RB, Irwin GR. Dynamic K_c testing of structural steel. J Struct Div 1974;7:1331–49.
[62] Shoemaker AK, Seeley RR. Summary report of round robin testing by the ASTM Task Group E24.01.06 on rapid loading plane-strain fracture toughness K_{Ic} testing. J Test Evaluat 1983;11:261–72.
[63] Feddersen CE. Evaluation and prediction of the residual strength of center cracked tension panels. In: Damage tolerance in aircraft structures. ASTM STP 486. American Society for Testing and Materials; 1971. p. 50–78.
[64] Feddersen CE, Simonen FA, Hulbert LE, Hyler WS. An experimental and theoretical investigation of plane-stress fracture of 2024-T351 aluminum alloy. NASA CR-1678. National Aeronautics and Space Administration, Washington, DC, September 1970.
[65] Orange TW, Sullivan TL, Calfo FD. Fracture of thin sections containing through and part-through cracks. NASA TN-6305. National Aeronautics and Space Administration, Washington, DC, April 1971.
[66] Schwalbe KH, Newman JC, Shannon JL. Fracture mechanics testing on specimens with low constraint – standardisation activities within ISO and ASTM. Engng Fract Mech 2005;72:557–76.
[67] McCabe DE, Heyer RH. R-curve determination using a crack-line-wedge-loaded (CLWL) specimen. In: Fracture toughness evaluation by R-curve methods. ASTM STP 527. American Society for Testing and Materials; 1973. p. 17–35.
[68] Sullivan AM, Freed CN, Stoop J. Comparison of R-curves determined from different specimen types. In: Fracture toughness evaluation by R-curve methods. ASTM STP 527. American Society for Testing and Materials; 1973. p. 85–104.
[69] Heyer RH, McCabe DE. Plane-stress fracture toughness testing using a crack-line-loaded specimen. Engng Fract Mech 1972;4:395–412.
[70] Heyer RH, McCabe DE. Crack growth resistance in plane-stress fracture testing. Engng Fract Mech 1972;4:413–30.
[71] Wang DY, McCabe DE. Investigation of R-curve using comparative tests with center-cracked-tension and crack-line-wedged-loaded specimens. In: Mechanics of crack growth. ASTM STP 590. American Society for Testing and Materials; 1976. p. 169–93.
[72] Schwalbe KH, Setz W. R curve and fracture toughness of thin sheet materials. J Test Evaluat 1981;9:182–94.
[73] Hellmann D, Schwalbe KH. Geometry and size effects on J–R and δ-R curves under plane stress conditions. In: Fracture mechanics: fifteen symposium. ASTM STP 833. American Society for Testing and Materials; 1984. p. 557–605.
[74] Putatunda SK, Rigsbee JM, Corten HT. Effect of size on elastic–plastic fracture toughness parameters. J Test Evaluat 1985;13:181–90.
[75] Chao YJ. On a single parameter controlled fracture of solids under plane stress conditions. Int J Fract 1993;62:R7–R10.
[76] Yan C, Mai YW. Numerical investigation on stable crack growth in plane stress. Int J Fract 1998;91:117–30.
[77] Feddersen CE. Discussion. Plane strain crack toughness testing of high strength metallic materials. ASTM STP, vol. 410. American Society for Testing and Materials; 1966. p. 77–79.
[78] Newman JC, Haines MJ. Verification of stress-intensity factors for various middle-crack tension test specimens. Engng Fract Mech 2005;72:1113–8.
[79] Dawicke DS, Newman JC, Starnes JH, Rose CA, Young RD, Seshadri BR. Residual strength analysis methodology: laboratory coupons to structural components. In: The third joint FAA/DoD/NASA conference on aging aircraft, Albuquerque, New Mexico, September 20–23, 1999.
[80] Pearson HS, McCabe DE. R-curve round-robin program for ASTM recommended practice for R-curve determination (E561). J Test Evaluat 1986;14:191–9.
[81] McCabe DE, Ernst HA. A perspective on R-curves and instability theory. In: Fracture mechanics: fourteen symposium. Theory and analysis, ASTM STP 791, vol. I. American Society for Testing and Materials; 1983. p. I-561–84.
[82] Newman JC. An evaluation of fracture analysis methods. In: Elastic–plastic fracture mechanics technology. ASTM STP 896. American Society for Testing and Materials; 1985. p. 5–96.
[83] Reynolds AP. Comparison of R-curve methodologies for ranking the toughness of aluminum alloys. J Test Evaluat 1996;24:406–10.
[84] Pearson HS. Evaluation of plane stress fracture testing methods. J Test Evaluat 1986;14:224–6.
[85] McCabe DE, Schwalbe KH. Prediction of instability using K_R-curve approach. In: Elastic–plastic fracture mechanics technology. ASTM STP 896. American Society for Testing and Materials; 1985. p. 99–113.

[86] McCabe DE, Landes JD. *J–R* curve testing of large compact specimens. In: Elastic–plastic fracture mechanics. ASTM STP 803, vol. II. American Society of Testing and Materials; 1983. p. II-353–71.
[87] Haynes MT, Gangloff RP. High resolution R-curve characterization of the fracture toughness of thin sheet aluminum alloys. J Test Evaluat 1997;25:82–98.
[88] Zhu XK, Leis BN. Revisit of ASTM round robin test data for determining R curves of thin sheet materials. J ASTM Int 2009 [paper ID JAI102510].
[89] Kobayashi AS, Chiu ST, Beeuwkes R. A numerical and experimental investigation on the use of J-integral. Engng Fract Mech 1973;5:293–305.
[90] Hutchinson JW. Singular behavior at the end of a tensile crack in a hardening material. J Mech Phys Solids 1968;16:13–31.
[91] Rice JR, Rosengren GF. Plane Strain deformation near a crack tip in a power law hardening material. J Mech Phys Solids 1968;16:1–12.
[92] McClintock FA. Plasticity aspect of fracture. In: Liebowitz H, editor. Fracture: an advanced treatise, vol. 3. London: Academic press; 1971. p. 47–225.
[93] McMeeking RM, Parks DM. On criteria for J-dominance of crack-tip fields in large-scale yielding. In: Elastic–plastic fracture. ASTM STP 668. American Society for Testing and Materials; 1979. p. 175–94.
[94] Shih CF, German MD. Requirements for a one parameter characterization of crack tip fields by the HRR singularity. Int J Fract 1981;17:27–43.
[95] Rice JR, McMeeking RM, Parks DM, Sorensen EP. Recent finite element studies in plasticity and fracture mechanics. Comput Meth Appl Mech Engng 1979;17/18:411–42.
[96] Al-Ani AM, Hancock SW. J-dominance of short cracks in tension and bending. J Mech Phys Solids 1991;39:23–43.
[97] Parks DM. Three-dimensional aspects of HRR-dominance. In: Proceedings of the conference of european symposium on elastic–plastic fracture mechanics: defect assessment in components—fundamentals and applications, Freiburg, Germany, October 9–12, 1989. p. 205–31.
[98] Kumar V, German MD, Shih CF. An engineering approach for elastic–plastic fracture analysis. EPRI report # NP-1931, Electric Power Research Institute; 1981.
[99] Begley JA, Landes JD. The J-integral as a fracture criterion. In: Fracture mechanics. ASTM STP 514. American Society for Testing and Materials; 1972. p. 1–23.
[100] Landes JD, Begley JA. The effect of specimen geometry on J_{Ic}. In: Fracture mechanics. ASTM STP 514. American Society for Testing and Materials; 1972. p. 24–39.
[101] Rice JR, Paris PC, Merkle JG. Some further results of J-integral analysis and estimates. In: Progress in flaw growth and fracture toughness testing. ASTM STP 536. American Society for Testing and Materials; 1973. p. 231–45.
[102] Landes JD, Walker H, Clarke GA. Evaluation of estimation procedures used in J-integral testing. In: Elastic–plastic fracture. ASTM STP 668. American Society for Testing and Materials; 1979. p. 266–87.
[103] Merkle JG, Corten HT. A J integral analysis for the compact specimen considering axial force as well as bending effects. J Press Ves Technol 1974;96:286–92.
[104] Srawley JE. On the relationship of J_I to work done per unit uncracked area: 'total' or component 'due to crack'. Int J Fract 1976;12:470–4.
[105] Sumpter JDG, Turner CE. Method for laboratory determination of J_C (contour integral for fracture analysis). In: Cracks and fracture. ASTM STP 601. American Society for Testing and Materials; 1976.
[106] Turner CE. The ubiquitous η factor. In: Fracture mechanics: twelfth conference. ASTM STP 700. American Society for Testing and Materials; 1980. p. 314–37.
[107] Roos E, Eisele U, Silcher H. A procedure for the experimental assessment of the J-integral by means of specimen of different geometries. Int J Press Ves Pip 1986;23:81–93.
[108] Turner CE. Fracture toughness and specific energy: a reanalysis of results. Mater Sci Engng 1973;11:275–82.
[109] Clarke GA, Landes JD. Evaluation of the J-integral for the compact specimen. J Test Evaluat 1979;7:264–9.
[110] Sumpter JDG. J_C determination for shallow notch welded bend specimens. Fatigue Fract Engng Mater Struct 1987;10:479–93.
[111] Kirk MT, Dodds RH. *J* and CTOD estimation equations for shallow cracks in single edge notched bend specimens. J Test Evaluat 1993;21:228–38.
[112] Nevalainen M, Dodds RH. Numerical investigation of 3-D constraint effect on brittle fracture in SE(B) and C(T) specimens. Int J Fract 1995;74:131–61.
[113] Paris PC, Ernst HA, Turner CE. A J-integral approach to the development of η factors. In: Fracture mechanics: twelfth conference. ASTM STP 700. American Society for Testing and Materials; 1980. p. 251–338.
[114] Ernst HA, Paris PC, Rossow M, Hutchinson JW. Analysis of load–displacement relationships to determine *J–R* curve and tearing instability material properties. In: Fracture mechanics. ASTM STP 677. American Society for Testing and Materials; 1979. p. 581–99.
[115] Sharobeam MH, Landes JD. The load separation criterion and methodology in ductile fracture mechanics. Int J Fract 1991;47:81–104.
[116] Sharobeam MH, Landes JD. The load separation and η_{pl} development in precracked specimen test records. Int J Fract 1993;59:213–26.
[117] Joyce JA. On the mechanisms and mechanics of plastic flow and fracture. Sc.D. thesis, Massachusetts Institute of Technology, May 1974.
[118] Towers OL, Garwood SJ. Maximum load toughness. Int J Fract 1980;16:R85–90.
[119] Landes JD, Begley JA. Test results from J-integral studies: an attempt to establish a J_{Ic} testing procedure. In: Fracture analysis. ASTM STP 560. American Society for Testing and Materials; 1974. p. 170–86.
[120] Hutchinson JW, Paris PC. Stability analysis of J-controlled crack growth. In: Elastic–plastic fracture. ASTM STP 668. American Society for Testing and Materials; 1979. p. 37–64.
[121] Clarke GA, Andrews WR, Paris PC, Schmidt DW. Single specimen tests for J_{Ic} determination. In: Mechanics of crack growth. ASTM STP 590. American Society for Testing and Materials; 1976. p. 27–42.
[122] Garwood SJ, Robinson JN, Turner CE. The measurement of crack growth resistance curves (R-curves) using the J integral. Int J Fract 1975;11:528–30.
[123] Etemad MR, Turner CE. An experimental investigation of slow stable crack growth using HY130 steel. J Strain Anal 1985;20:201–8.
[124] Etemad MR, John SJ, Turner CE. Elastic–elastic R-curves for large amounts of crack growth. In: Fracture mechanics: eighteenth symposium. ASTM STP 945. American Society for Testing and Materials; 1988. p. 986–1004.
[125] Ernst HA, Paris PC, Landes JD. Estimations on J-integral and tearing modulus T from a single specimen test record. In: Fracture mechanics: thirteenth conference. ASTM STP 743. American Society for Testing and Materials; 1981. p. 476–502.
[126] Joyce JA. Application of the key curve method to determining *J–R* curve for A533B steel. Nuclear regulatory commission report, NUREG/CR-1290, February 1980.
[127] Zhu XK, Joyce JA. More accurate formulation of J-integral equation for evaluating fracture resistance curves. J ASTM Int 2009;7(1) [paper ID JAI102505].
[128] Joyce JA, Gudas JP. Computer interactive J_{Ic} testing of navy alloys. In: Elastic–plastic fracture. ASTM STP 668. American Society for Testing and Materials; 1979. p. 451–68.
[129] Neimitz A. The jump-like crack growth model, the estimation of fracture energy and J_R curve. Engng Fract Mech 2008;75:236–52.
[130] Kroon M, Faleskog J, Oberg H. A probabilistic model for cleavage fracture with a length scale – parameter estimation and predictions of growing crack experiments. Engng Fract Mech 2008;75:2398–417.
[131] Johnson HH. Calibrating the electric potential method for studying slow crack growth. Mater Res Stand 1965;5:442–5.
[132] Schwalbe KH, Hellmann D. Application of the electrical potential method of crack length measurement using Johnson's formula. J Test Evaluat 1981;9:218–21.
[133] Bakker A. A DC potential drop procedure for crack initiation and R-curve measurements during ductile fracture tests. In: Elastic–plastic fracture test methods: the user's experience. ASTM STP 586. American Society for Testing and Materials; 1985. p. 394–410.
[134] Roos E, Eisele U. Determination of material characteristic values in elastic–plastic fracture mechanics by means of J-integral crack resistance curves. J Test Evaluat 1988;16:1–11.
[135] Eisele U, Roos E. Evaluation of different fracture mechanical J-integral initiation values with regard to their usability in the safety assessment of components. Nucl Engng Des 1991;130:237–47.

[136] Paris PC, Tada H, Zahoor A, Ernst H. The theory of instability of the tearing mode of elastic–plastic crack growth. In: Elastic–plastic fracture. ASTM STP 668. American Society for Testing and Materials; 1979. p. 5–36.
[137] Morrison J, Karisallen KJ. An experimental comparison of J and CTOD estimation formulas. Engng Fract Mech 1995;51:145–9.
[138] Wang YY, Reemsnyder HS, Kirk MT. Inference equations for fracture toughness testing: numerical analysis and experimental verification. In: Fatigue and fracture mechanics. ASTM STP 1321, vol. 28. American Society for Testing and Materials; 1997. p. 469–84.
[139] Wallin K, Laukkanen A. Improved crack growth corrections for *J–R* curve testing. Engng Fract Mech 2004;71:1601–14.
[140] Zhu XK, Leis BN, Joyce JA. Experimental estimation of *J–R* curve from load–CMOD records for SE(B) specimens. J ASTM Int 2008;5(5) [paper ID JAI101532].
[141] Cravero S, Ruggieri C. Further developments in J evaluation procedure for growing cracks based on LLD and CMOD data. Int J Fract 2007;148:387–400.
[142] Zhu XK, Joyce JA. Revised incremental J-integral procedure for ASTM E1820 using crack mouth opening displacement. J Test Evaluat 2009;37:205–14.
[143] Zhu XK, Leis BN. Experimental determination of *J–R* curves using SENB specimen and P-CMOD data. In: Proceedings of ASME pressure vessel and piping conference, Chicago, Illinois, USA, July 27–31, 2008.
[144] Joyce JA, Ernst HA, Paris PC. Direct *J–R* curve analysis: a guide to the methodology. In: Fracture mechanics: twelfth national symposium. ASTM STP 700. American Society for Testing and Materials; 1980. p. 222–36.
[145] Herrera R, Landes JD. Direct *J–R* curve analysis of fracture toughness test. J Test Evaluat 1988;16:427–49.
[146] Joyce JA. *J*-resistance curve testing of short crack bend specimens using unloading compliance. In: Fracture mechanics: twenty-second symposium. ASTM STP 1131, vol. I. American Society for Testing and Materials; 1992. p. 904–24.
[147] Herrera R, Landes JD. Direct *J–R* curve analysis: a guide to the methodology. In: Fracture mechanics: twenty-first symposium. ASTM STP 1074. American Society for Testing and Materials; 1990. p. 24–43.
[148] Orange TW. Methods and models for R-curve instability calculations. In: Fracture mechanics: twenty-first symposium. ASTM STP 1074. American Society for Testing and Materials; 1990. p. 545–59.
[149] Landes JD, Zhou Z, Lee K, Herrera R. Normalization method for developing *J–R* curves with the LMN function. J Test Evaluat 1991;19:305–11.
[150] Joyce JA. Analysis of a high rate round robin based on proposed annexes to ASTM E 1820. J Test Evaluat 2001;29:329–51.
[151] Oh YJ, Hwang IS, Joyce JA. Round robin test on normalization method under static loading condition. J Test Evaluat 2006;34:537–61.
[152] Dzugan J, Viehrig HW. Application of the normalization method for the determination of *J–R* curves. Mater Sci Engng A 2004;387–389:307–11.
[153] Zhu XK, Joyce JA. J-resistance curve testing of HY80 steel using SE(B) specimens and normalization method. Engng Fract Mech 2007;74:2263–81.
[154] Zhu XK, Leis BN. Fracture resistance curve testing of X80 pipeline steel using SENB specimen and normalization method. J Pipeline Engng 2008;7:126–36.
[155] Zhu XK, Lam PS, Chao YJ. Applications of normalization method to experimental measurement of fracture toughness for A285 carbon steel. J Press Ves Pip 2009;86:669–76.
[156] Clarke GA, Andrews WR, Begley JA, Donald JK, Embley GT, Landes JD, et al. A procedure for the determination of ductile fracture toughness values using J integral techniques. J Test Evaluats 1979;7:49–56.
[157] Paris PC. A written discussion of Begley and Landes (1972). In: Fracture toughness. ASTM STP 514. American Society for Testing and Materials; 1972. p. 21–2.
[158] Landes JD, Begley JA. Recent developments in J$_{Ic}$ testing. In: Development in fracture mechanics test methods standardization. ASTM STP 632. American Society for Testing and Materials; 1977. p. 57–81.
[159] Clarke GA. Evaluation of the J$_{Ic}$ testing procedure by round robin tests on A533B class 1 pressure vessel steel. J Test Evaluat 1980;8:213–20.
[160] Clarke GA, Landes JD, Begley JA. Results of an ASTM cooperative test program on the J$_{Ic}$ determination of HY130 steel. J Test Evaluat 1980;8:221–32.
[161] ASTM E813-81. Standard test method for J$_{Ic}$, a measure of fracture toughness. American Society for Testing and Materials; 1982.
[162] Hiser AL, Loss FJ, Menke BH. *J–R* Curve characterization of irradiated low upper shelf welds. NUREG/CR-3506; 1984.
[163] Jablonski DA. Computerized single-specimen *J–R* curve determination for compact tension and three-point bend specimens. In: Automated test methods for fracture and fatigue crack growth. ASTM STP 877. American Society for Testing and Materials; 1985. p. 269–97.
[164] ASTM E1152-82. Standard test method for determining *J–R* curves. American Society for Testing and Materials; 1982.
[165] Albrecht P, Andrews WR, Gudas JP, Joyce JA, Loss FJ, McCabe DE, et al. Tentative test procedure for determining the plane strain J$_I$–R curve. J Test Evaluat 1982;10:245–51.
[166] Gudas JP, Davis DA. Evaluation of the tentative J$_I$–R curve testing procedure by round robin tests of HY130 steel. J Test Evaluat 1982;10:252–62.
[167] ASTM E1737-96. Standard test method for J-integral characterization of fracture toughness. American Society for Testing and Materials; 1996.
[168] ASTM E1290-90. Standard test method for crack-tip opening displacement (CTOD) fracture toughness measurement. American Society for Testing and Materials; 1998.
[169] ASTM E1820-96. Standard test method for measurement of fracture toughness. American Society for Testing and Materials; 1996.
[170] Landes JD, Brown KH. Results from a round robin on a standard method for measurement of fracture toughness – ASTME1820-96. In: Filed in the ASTM archives. American Society for Testing and Materials; 1997.
[171] Landes JD, Brown K. Results from a round robin on a standard method for measurement of fracture toughness. J Test Evaluat 1998;26:396–403.
[172] Anon. Standard method for measurement of fracture toughness, draft 10. American Society for Testing and Materials, December 1990.
[173] Joyce JA, Davis DA, Hackett EM, Hays, application of the J-integral and modified J integral to cases of large crack extension. NUREG/CR-5143, USNRC, 1988.
[174] Joyce JA, Hackett EM. Development of an engineering definition of the extent of J singularity controlled crack growth. NUREG/CR-5238, USNRC, 1989.
[175] Landes JD. Evaluation of the ASTM J initiation procedure using the EURO fracture toughness data set. J Test Evaluat 2006;34:200–10.
[176] Wallin K. Specimen size limitation in *J–R* curve testing – standards versus reality. J ASTM Int 2007;4(9) [paper ID: JAI100978].
[177] Landes JD, Shaffer DH. Statistical characterization of fracture in the transition region. In: Fracture mechanics: twelfth conference. ASTM STP 700. American Society for Testing and Materials; 1980. p. 368–82.
[178] Wallin K. The scatter in K$_{Ic}$ results. Engng Fract Mech 1984;19:1085–93.
[179] Anderson TL, Stienstra D. A model to predict the sources and magnitude of scatter in toughness data in the transition region. J Test Evaluat 1989;17:46–53.
[180] Sorem WA, Dodds RH, Rolfe ST. Effect of crack depth on elastic plastic fracture toughness. Int J Fract 1991;47:105–26.
[181] MacLennan IJ, Hancock JW. The effect of constraint on the ductile–brittle transition. In: in Shallow crack fracture mechanics, toughness tests and applications: TWI international conference. Cambridge, UK, 23–24 September, 2002. p. 21/1–9.
[182] Anderson TL, Dodds RH. Specimen size requirements for fracture toughness testing in the transition region. J Test Evaluat 1991;19:123–34.
[183] Anderson TL, Stienstra D, Dodds RH. A theoretical framework to addressing fracture in the ductile-to-brittle region. In: Fracture mechanics. ASTM STP 1207, 24. American Society for Testing and Materials; 1994. p. 86–214.
[184] Weibull W. A statistical distribution function of wide applicability. J Appl Mech 1951;18:293–7.
[185] McCabe DE, Merkle JG, Wallin K. In: An introduction to the development and use of the master curve method. ASTM MNL52. American Society for Testing and Materials; 2005.
[186] Landes JD, McCabe DE. Effect of section size on transition temperature behavior of structural steels. In: Fracture mechanics: fifteenth symposium. ASTM STP 833. American Society for Testing and Materials; 1984. p. 78–392.
[187] Wallin K, Saario T, Torronen K. Statistical model for carbide induced brittle fracture in steel. Metals Sci 1984;18:13–6.
[188] Wallin K. The size effect in K$_{Ic}$ results. Engng Fract Mech 1985;22:149–63.
[189] Anon. PVRC recommendation on toughness requirements for ferritic materials. WRC Bulletin 175, Welding Research Council; August 1972.

[190] Wallin K. A simple theoretical Charpy V-K_{Ic} correlation for irradiation embrittlement. In: Proceedings of 1989 ASME pressure vessel and piping conference – innovative approaches to irradiation damage and fracture analysis, PVP, vol. 170. American Society for Mechanical Engineers; July 1989.

[191] Wallin K. Fracture toughness transition curve shape for ferritic structural steels. In: Teoh ST, Lee KH, editors. Fracture of engineering materials and structures. London: Elsevier; 1991. p. 3–88.

[192] Wallin K. Irradiation damage effects on the fracture toughness transition curve shape for reactor pressure vessel steels. Int J Press Ves Pip 1993;55:61–79.

[193] Merkle JG, Wallin K, McCabe DE. Technical basis for an ASTM standard on determining the characterization temperature, T_0, for ferritic steels in the transition range. NUREG/CR-5504, US Nuclear Regulatory Commission, Washington, DC, November 1998.

[194] Wallin K. Validity of small specimen fracture toughness estimates neglecting constrain corrections. In: Constraint effects in fracture theory and applications. ASTM STP 1244, vol. 2. American Society for Testing and Materials; 1995. p. 519–37.

[195] ASTM E1921-97. Standard test method for determining of reference temperature T_0 for ferritic steels in the transition range. American Society for Testing and Materials; 1997.

[196] Kirk M, Lott R, Kim C, Server W. Empirical validation of the master curve for irradiated and unirradiated reactor pressure vessel steels. Proceedings of 1998 ASME pressure vessels and piping conference, San Diego, CA. American Society for Mechanical Engineers; 1998.

[197] Joyce JA, Tregoning RL. Development of the T_0 reference temperature from precracked Charpy specimens. Engng Fract Mech 2001;68:861–94.

[198] Joyce JA, Tregoning RL. Determination of constraint limits for cleavage initiated toughness data. Engng Fract Mech 2005;72:1559–79.

[199] Joyce JA, Tregoning RL, Roe C. On setting testing rate limitations for the master curve reference temperature T_0 of ASTM E1921. J Test Evaluat 2006;34(2) [paper ID: JTE14108].

[200] Wallin K. Effect of strain rate on the fracture toughness reference temperature T_0 for ferritic steels. In: Mahidhara RK et al., editors. Recent advances in fracture. The Minerals, Metals and Materials Society; 1997. p. 171–82.

[201] Goodier JN, Field FA. Plastic energy dissipation in crack propagation. In: Drucker DC, Gilman JJ, editors. Fracture of solids. New York: Wiley; 1963. p. 103–18.

[202] Burdekin FM, Stone DEW. The crack opening displacement approach to fracture mechanics in yielding materials. J Strain Anal 1966;1:145–53.

[203] Harrison JD, Dawes MG, Archer GL, Kamath MS. The COD approach and its application to welded structures. In: Elastic–plastic fracture. ASTM STP 668. American Society for Testing and Materials; 1979. p. 606–31.

[204] Hollstein T, Blauel JG. On the relation of the crack opening displacement to the J-integral. Int J Fract 1977;13:385–90.

[205] Daves MG. Elastic–plastic fracture toughness based on the COD and J-contour integral concepts. In: Elastic–plastic fracture. ASTM STP 668. American Society for Testing and Materials; 1979. p. 307–33.

[206] Kirk MT, Wang YY. Wide range CTOD estimation formulae for SE(B) specimens. In: Fatigue and fracture mechanics. ASTM STP 1256, vol. 26. American Society for Testing and Materials; 1995. p. 126–41.

[207] Wang YY, Reemsnyder HS, Kirk MT. Inference equations for fracture toughness testing: numerical analysis and experimental verification. In: Fatigue and fracture mechanics. ASTM STP 1321, vol. 28. American Society for Testing and Materials; 1997. p. 469–84.

[208] Panontin TL, Makino A, Williams JF. Crack tip opening displacement estimation formulae for C(T) specimens. Engng Fract Mech 2000;67:293–301.

[209] Wilson CD, Landes JD. Inconsistencies between CTOD and J calculations. J Test Evaluat 1994;22:505–11.

[210] Burdekin MF. Crack opening displacement: a review of principles and methods. In: Proceedings of symposium on fracture toughness concepts for weldable structural steel; 1969. p. C1–12.

[211] Hellmann D, Schwalbe KH. On the experimental determination of CTOD based R-curves. In: Schwalbe KH, editor. The crack tip opening displacement in elastic–plastic fracture mechanics (proceedings of the workshop of the CTOD methodology). Berlin: Springer; 1986. p. 115–32.

[212] Wu SX, Mai YW, Cotterell B. Plastic rotation factors of three-point bend and compact tension specimens. J Test Evaluat 1988;16:555–7.

[213] Wu SX, Cotterell B, Mai YW. Slip-line field solutions for three-point notch bend specimens. Int J Fract 1988;37:13–29.

[214] Nichols RW, Cowan A, Ingham T, Burdekin MF, Elliot D. The use of critical COD techniques for the selection of fracture resistant materials. In: Proceedings of symposium on fracture toughness concepts for weldable structural steel; 1969. p. F1–113.

[215] BS 5762. Methods for crack opening displacement (COD) testing. London: British Standards Institute; 1979.

[216] BS 7448: Part 1. Fracture mechanics toughness tests: Part 1 – Method for determining of K_{Ic}, critical CTOD and critical J values of metallic materials. London: British Standards Institute; 1991.

[217] ASTM E1290-89. Standard test method for crack-tip opening displacement (CTOD) fracture toughness measurement. American Society for Testing and Materials; 1989.

[218] Tagawa T, Kayamori Y, Ohata M. Comparison of CTOD standards: BS 7448 – Part 1 and revised ASTM 1290. Engng Fract Mech 2010;77:327–36.

[219] Kanninen MF, Rybicki EF, Stonesifer RB, Broek D, Rosenfied AR, Marschall CW, et al. Elastic–plastic fracture mechanics for two-dimensional stable crack growth and instability problems. In: Elastic–plastic fracture. ASTM STP 668. American Society for Testing and Materials; 1979. p. 121–50.

[220] Newman JC, James MA, Zerbst U. A review of the CTOA/CTOD fracture criterion. Engng Fract Mech 2003;70:371–85.

[221] Zerbst U, Heinimann M, Donne CD, Steglich D. Fracture and damage mechanics modeling of thin-walled structures – an overview. Engng Fract Mech 2009;76:5–43.

[222] Horsley DJ. Background to the use of CTOA for prediction of dynamic ductile fracture arrest in pipelines. Engng Fract Mech 2003;70:547–52.

[223] Heerens J, Schodel M. Characterization of stable crack extension in aluminum sheet material using the crack tip opening angle determined optically and by the δ_5 clip guage technique. Engng Fract Mech 2009;76:101–13.

[224] Sakhalkar A, Frink E, Mahmoud S, Lease K. Crack tip opening angle measurement methods and crack tunneling in 2024-T351 aluminum. Strain – Int J Exp Mech 2011;47:e130–41.

[225] Garwood SJ. Effect of specimen geometry on crack growth resistance. In: Fracture mechanics. ASTM STP 677. American Society for Testing and Materials; 1979. p. 11–532.

[226] McCabe DE, Landes JD, Ernst HA. An evaluation of the J_R-curve method for fracture toughness characterization. In: Elastic–plastic fracture. Fracture resistance curves and engineering applications. ASTM STP803, vol. II. American Society for Testing and Materials; 1983. p. I-562–II-581.

[227] Towers OL, Garwood SJ. Influence of crack depth on resistance curves for three-point bend specimens in HY130. In: Fracture mechanics. ASTM STP 905, vol. 7. American Society for Testing and Materials; 1986. p. 454–84.

[228] Eisele U, Roos E, Seidenfuss M, Silcher H. Determination of J-integral-based crack resistance curves and initiation values for the assessment of cracked large-scale specimens. In: Fracture mechanics: twenty-second symposium. ASTM STP 1131, vol. I. American Society for Testing and Materials; 1992. p. 37–59.

[229] Hancock JW, Reuter WG, Parks DM. Constraint and toughness parameterized by T. In: Constraint effects in fracture. ASTM STP 1171. American Society for Testing and Materials; 1993. p. 1–40.

[230] Joyce JA, Hackett EM, Roe C. Effect of crack depth and mode of loading on the J–R curve behavior of a high-strength steel. In: Constraint effects in fracture. ASTM STP 1171. American Society for Testing and Materials; 1993. p. 239–63.

[231] Joyce JA, Link RE. Effects of constraint on upper shelf fracture toughness. In: Fatigue and fracture mechanics. ASTM STP 1256, vol. 26. American Society for Testing and Materials; 1995. p. 142–77.

[232] Joyce JA, Link RE. Application of two parameter elastic–plastic fracture mechanics to analysis of structures. Engng Fract Mech 1997;57:431–46.

[233] Wardle G. A study of specimen size effects on the initiation toughness and tearing resistance of an A533B-1 steel. In: Small specimen test techniques. ASTM STP 1418. American Society for Testing and Materials; 2002. p. 48–66.

[234] Lam PS, Chao YJ, Zhu XK, Kim Y, Sindelar RL. Determination of constraint-modified J–R curves for carbon steel storage tanks. J Press Ves Technol 2003;125:136–43.

[235] Neimitz A, Dzioba I, Galkiewicz J, Molasy R. A study of stable crack growth using experimental methods, finite elements and fractography. Engng Fract Mech 2004;71:1325–55.
[236] Shen G, Tyson WR, Glover A, Horsley D. Constraint effects on linepipe toughness. In: Proceedings of the 4th international conference on pipeline technology, vol. 2, May 9–13, 2004, Ostend, Belgium. p. 703–20.
[237] Zhu XK, Joyce JA. J-resistance curve testing of HY80 steel using SE(B) specimens and normalization method. Engng Fract Mech 2007;74:2263–81.
[238] Ernst HA. Material resistance and instability beyond J controlled crack growth. In: Elastic plastic fracture: second symposium, nonlinear crack analysis. ASTM STP 803, vol. I. American Society for Testing and Materials; 1983. p. I-191–213.
[239] Ernst HA, Landes JD. Elastic–plastic fracture mechanics methodology using the modified J, J$_M$, resistance curve approach. J Press Ves Technol 1986;108:50–6.
[240] Joyce JA, Davis DA, Hackett EM, Hays RA. Application of J-integral and modified J-integral to cases of large crack extension. In: Fracture mechanics: twenty-first symposium. ASTM STP 1074. American Society for Testing and Materials; 1990. p. 85–105.
[241] Wilkowski GM, Marschall CM, Landow MP. Extrapolation of C(T) specimen *J–R* curves. In fracture mechanics: twenty-first symposium, ASTM STP 1074; 1990. p. 56–84.
[242] Link RE, Landes JD, Herrera R, Zhou Z. Something new on size and constraint effects for *J–R* curves. In: defect assessment in components – fundamentals and applications, ESIS/EGF9; 1991. p. 707–21.
[243] Hiser AL. Specimen size effects on *J–R* curves for RPV steels. In: Constraint effects in fracture, ASTM STP 1171; 1993. p. 195–238.
[244] Larsson SG, Carlsson AJ. Influence of non-singular stress terms and specimen geometry on small-scale yielding at crack tips in elastic–plastic material. J Mech Phys Solids 1973;21:263–78.
[245] Rice JR. Limitations to the small scale yielding approximation for crack tip plasticity. J Mech Phys Solids 1974;22:17–26.
[246] Sham TL. The determination of the elastic T-term using higher order weight functions. Int J Fract 1991;48:81–102.
[247] Fett T. A Green's function for T-stresses in an edge-cracked rectangular plate. Engng Fract Mech 1997;57:365–73.
[248] Yang B, Ravi-Chandar. Evaluation of elastic T-stress using the stress difference method. Engng Fract Mech 1999;64:589–605.
[249] Wang X. Elastic T-stress for cracks in test specimens subjected to non-uniform stress distributions. Engng Fract Mech 2002;69:1339–52.
[250] Wang X. Elastic T-stress solutions for semi-elliptical surface cracks in finite thickness plates. Engng Fract Mech 2003;70:731–56.
[251] Leevers PS, Radon JC. Inherent stress biaxiality in various fracture specimen geometries. Int J Fract 1983;19:311–25.
[252] Sherry AH, France CC, Goldthorpe MR. Compendium of T-stress solutions for two and three dimensional geometries. Fatigue Fract Engng Mater Struct 1995;18:141–55.
[253] Dodds RH, Anderson TL, Kirk MT. A framework to correlate *a/W* ratio effects on elastic–plastic fracture toughness (J$_c$). Int J Fract 1991;48:1–22.
[254] Bilby BA, Cardew GE, Goldthorpe MR, Howard IC. A finite element investigation of the effect of specimen geometry on the fields of stress and strain at the tips of stationary cracks. In: Size effects in fracture. London: Mechanical Engineering Publications Limited; 1986. p. 37–46.
[255] Joyce JA, Tregoning RL. Quantification of specimen geometry effects on the master curve and T$_o$ reference temperature. In: Proceedings of the 13th European conference on fracture (ECF-13), San Sebastian, Spain, September 6–9, 2000.
[256] Betegon C, Hancock JW. Two-parameter characterization of elastic–plastic crack-tip fields. J Appl Mech 1991;58:104–10.
[257] Du ZZ, Hancock JW. The effect of non-singular stresses on crack-tip constraint. J Mech Phys Solids 1991;39:555–67.
[258] Sumpter JDG. An experimental investigation of the T-stress approach. In: Constraint effect in fracture. ASTM STP 1171. American Society for Testing and Materials; 1993. p. 492–502.
[259] Tregoning RL, Joyce JA. Application of T-stress based constraint correction to A533B steel fracture toughness data. In: Fatigue and fracture mechanics. ASTM STP 1417, Vol. 33. American Society for Testing and Materials; 2002. p. 307–27.
[260] O'Dowd NP, Shih C F. Family of crack-tip fields characterized by a triaxiality parameter – I: Structure of fields. J Mech Phys Solids 1991;39:989–1015.
[261] O'Dowd NP, Shih CF. Family of crack-tip fields characterized by a triaxiality parameter – II: Fracture applications. J Mech Phys Solids 1992;40:939–63.
[262] O'Dowd NP, Shih CF. Two-parameter fracture mechanics: theory and applications. In: Fracture mechanics. ASTM STP 1207, 24. American Society for Testing and Materials; 2002. p. 21–47.
[263] O'Dowd NP. Application of two parameter approaches in elastic–plastic fracture mechanics. Engng Fract Mech 1995;52:445–65.
[264] Faleskog J. Effects of local constraint along three-dimensional crack fronts – a numerical and experimental investigation. J Mech Phys Solids 1995;43:447–93.
[265] Nevalainen M, Dodds RH. Numerical investigation of 3D constraint effects on brittle fracture in SE(B) and C(T) specimens. Int J Fract 1995;74:131–61.
[266] Gao X, Dodds RH. An engineering approach to assess constraint effects on cleavage fracture toughness. Engng Fract Mech 2001;68:263–84.
[267] Yang S. Higher order asymptotic crack-tip fields in a power-law hardening material. Ph.D. Dissertation, University of South Carolina, Columbia, South Carolina, 1993.
[268] Yang S, Chao YJ, Sutton MA. Higher-order asymptotic fields in a power-law hardening material. Engng Fract Mech 1993;45:1–20.
[269] Chao YJ, Yang S, Sutton MA. On the fracture of solids characterized by one or two parameters: theory and practice. J Mech Phys Solids 1994;42:629–47.
[270] NIkishkov GP, Bruckner-Foit A, Munz D. Calculation of the second fracture parameter for finite cracked bodies using a three-term elastic–plastic asymptotic expansion. Engng Fract Mech 1995;52:685–701.
[271] Chao YJ, Zhu XK. Constraint-modified *J–R* curves and its applications to ductile crack growth. Int J Fract 2000;106:135–60.
[272] Cravero S, Ruggieri C. Correlation of fracture behavior in high pressure pipelines with axial flaws using constraint designed test specimens – Part I: Plane strain analyses. Engng Fract Mech 2005;72:1344–60.
[273] Silva LAL, Cravero S, Ruggieri C. Correlation of fracture behavior in high pressure pipelines with axial flaws using constraint designed test specimens – Part II: 3-D effects on constraint. Engng Fract Mech 2006;73:2123–38.
[274] Chao YJ, Zhu XK. *J – A$_2$* characterization of crack-tip fields: extent and size requirements. Int J Fract 1998;89:285–307.
[275] Zhu XK, Chao YJ. Characterization of constraint of crack-tip fields in non-hardening materials by the three-term solution. Int J Solids Struct 1999;36:4497–517.
[276] Kim Y, Chao YJ, Zhu XK. Effect of size and crack depth on 3D crack-front constraint for SENB specimens. Int J Solids Struct 2003;40:6267–84.
[277] Labbe F. Three-term asymptotic stress field expansion for analysis of surface cracked elbows in nuclear pressure vessels. J Mater Engng Perform 2007;16:220–3.
[278] Chao YJ, Ji W. Constraint effect on cleavage fracture by J and A$_2$. In: Constraint effect in fracture theory and applications. ASTM STP 1244, 2. American Society for Testing and Materials; 2002. p. 3–20.
[279] Zhu XK, Leis BN. Application of constraint-corrected *J–R* curve to fracture analysis of pipelines. J Press Ves Technol 2006;128:581–9.
[280] Wang YY, Parks DM. Limits of *J–T* characterization of elastic–plastic tip fields. In: Constraints in fracture theory and applications. ASTM STP 1244, 2. Philadelphia: American Society for Testing and Materials; 2002. p. 43–67.
[281] Zhu XK, Leis BN. Bending modified *J–Q* theory and crack-tip constraint quantification. Int J Fract 2006;141:115–34.
[282] Chao YJ, Zhu XK, Kim Y, Lam PS, Pechersky MJ, Morgan MJ. Characterization of crack-tip field and constraint for bending specimens under large-scale yielding. Int J Fract 2004;127:283–302.
[283] Zhu XK, Chao YJ. Specimen size requirements for two-parameter fracture toughness testing. Int J Fract 2005;135:117–36.
[284] Ritchie RO, Knott JF, Rice JR. On the relationship between critical tensile stress and fracture toughness in mild steel. J Mech Phys Solids 1973;21:395–410.
[285] Shih CF, O'Dowd NP, Kirk MT. A framework for quantifying crack tip constraint. In: Constraint effect in fracture. ASTM STP 1171. American Society for Testing and Materials; 2002. p. 2–20.

[286] Chao YJ, Zhang XH. Constraint effect on brittle fracture. In: Fatigue and fracture mechanics: 27th symposium. ASTM STP 1296. American Society for Testing and Materials; 2002. p. 41–60.
[287] Gao X, Dodds RH. Constraint effects on the ductile-to-brittle transition temperature of ferritic steels: a Weibull stress model. Int J Fract 2000;102:43–69.
[288] Wallin K. Quantifying T_{stress} controlled constraint by the master curve transition temperature T_0. Engng Fract Mech 2001;68:303–28.
[289] Huh NS, Stumptrack L, Schuler X, Roos E. Quantification of crack-tip constraint effect on master curve reference temperature based on two-parameter approach. Solid State Phenom (Trans Tech Publication, Switzerland) 2006;110:89–96.
[290] Zhu XK, Jang SK. J–R curves corrected by load independent parameter in ductile crack growth. Engng Fract Mech 2001;68:285–301.
[291] Zhu XK, Leis BN. Constraint corrected J–R curve and its applications for X80 pipeline steel. J ASTM Int 2006;3(6) [paper ID JAI13209].
[292] Zhou DW, Xu WG, Smith SD. R-curve modeling with constraint effect. In: Proceeding of the 12th international conference on fracture, Ottawa, Canada, July 12–17, 2009.
[293] Zhou DW. Measurement and modeling of R-curves for low-constraint specimens. Engng Fract Mech 2011;78:605–22.
[294] Wallin K. Fracture toughness of engineering materials – estimation and application. Warrington, UK: EMAS Publishing Co.; 2011.
[295] Zehnder AT. Fracture Mechanics. London: Springer; 2012.